RICE UNIVERSITY

The Role of Base Modification on Tyrosyl-tRNA Structure, Stability, and Function in *Bacillus subtilis* and *Bacillus anthracis*

By

Andria Pearlen Denmon

A THESIS SUBMITTED
IN PARTIAL FULFILLMENT OF THE
REQUIREMENTS FOR THE DEGREE

Doctor of Philosophy

APPROVED, THESIS COMMITTEE

Edward P. Nikonowicz, Associate Professor
Biochemistry and Cell Biology

George N. Bennett, E. Dell Butcher Professor
Biochemistry and Cell Biology

Bonnie Bartel, Ralph and Dorothy Looney Professor
Biochemistry and Cell Biology

Jonathan Silberg, Associate Professor
Biochemistry and Cell Biology

Laura Segatori, Assistant Professor
Chemical and Biomolecular Engineering

HOUSTON, TEXAS
MAY 2013

ABSTRACT

The Role of Base Modification on Tyrosyl-tRNA Structure, Stability, and Function in *Bacillus subtilis* and *Bacillus anthracis*

By

Andria Pearlen Denmon

tRNA molecules contain more than 80 chemically unique nucleotide base modifications that contribute to the chemical and physical diversity of RNAs as well as add to the overall fitness of the cell. For instance, base modifications have been shown to play a critical role in tRNA molecules by improving the fidelity and efficiency of translation. Most of this work has been carried out in Gram-negative bacteria, however, the role of modified bases in tRNAs as they relate to structure, stability, and transcriptional regulation in Gram-positive bacteria, such as *Bacillus subtilis* and *Bacillus anthracis,* are not well characterized. Infections by Gram-positive bacteria that have become more resistant to established drug regiments are on the rise, making Gram-positive bacteria a serious threat to public safety.

My thesis work examined what role partial base modification of the tyrosyl-anticodon stem-loops (ASL^{Tyr}) of *B. subtilis* and *B. anthracis* have on thermostability, structure, and transcriptional regulation. The ASL^{Tyr} molecules have three modified residues which include Queuine (Q_{34}), 2-thiomethyl-N6-dimethylallyl ($ms^2i^6A_{37}$), and pseudouridine (Ψ_{39}). To examine the effects of partial base modification on ASL^{Tyr} structure, NMR spectroscopy was employed. The NMR data indicated that the unmodified ASL^{Tyr} forms a protonated C-A^+

Watson-Crick-like base pair instead of the canonical bifurcated interaction and that the loop regions of the unmodified and [Ψ_{39}]-ASL^{Tyr} molecules were well ordered. Interestingly, the [i^6A_{37}]- and [i^6A_{37}, Ψ_{39}]- ASL^{Tyr} molecules did not form a protonated C-A^+ base pair and the bases of the loop region were not well ordered. The NMR data also suggested that the unmodified and partially modified molecules do not adopt the canonical U-turn structure. The structures of the unmodified, [Ψ_{39}]-, and [i^6A_{37}, Ψ_{39}]-ASL^{Tyr} molecules did not depend on the presence of Mg^{2+}, but the structure of the [i^6A_{37}]-ASL^{Tyr} molecule did depend on the presence of multivalent cations.

Differential Scanning Calorimetry (DSC) and UV melting were employed to examine the thermodynamic effects of partial modification on ASL^{Tyr} stability. The DSC and UV data indicated that the Ψ_{39} and i^6A_{37} modifications improved the molecular stability of the ASL. Additionally, these experiments suggested that the i^6A modified hairpins were more dynamic and less ordered in the loop.

Finally, to determine the repercussions that partial modification has on physiology and tRNA mediated transcriptional regulation in *B. anthracis*, antibiotic sensitivity tests, growth curves, and quantitative real-time polymerase chain reaction (qRT-PCR) were employed. Strains deficient in ms^2 showed comparable growth to the parent strain when cultured in defined media, but Q deficient strains did not. The loss of $ms^2i^6A_{37}$ conferred resistance to spectinomycin and ciprofloxacin, whereas the loss of Q_{34} resulted in sensitivity to erythromycin. Changes in the ratio of full-length to truncated transcripts of the *tyrS1* and *tyrS2* genes were used to monitor tRNA mediated transcriptional regulation. The qRT-PCR data suggested that *tyrS1* and *tyrS2* are T-box regulated and that the loss of $ms^2i^6A_{37}$ and Q_{34} might affect the interaction of the $tRNA^{Tyr}$ molecule with the specifier sequence, which is

located in the 5'-untranscribed region (UTR) of the messenger RNA (mRNA).

AKNOWLEDGEMENTS

I would like to acknowledge Dr. Edward Nikonowicz for his assistance during my tenure at Rice. I would also like to thank the past and present members of the Nikonowicz lab for their help, support, and making the lab more interesting while I stepped outside of my comfort zone and embarked on this challenging educational endeavor. I would like to thank Dr. Sean Moran for helping me navigate the Varian software and keeping me company in the basement. Even though you could not make it to one of our official Nikonowicz Lab lunches, we always considered you one of us. To Dr. Malgorzata "Margaret" Michnicka, thank you for helping me get situated in the lab, showing me how to work with RNA, and teaching me a lot about Poland. Dr. Izabela Tworowska, thank you so much for your friendship. I certainly enjoyed all of our non-nerd science activities like going to *Great Day Houston*, music and dance performances, lunches, and hearing about your menagerie of pets. It was always a treat to walk into the lab during a holiday and see that you had decorated it. I believe that it was necessary and brightened everyone's day. I would also like to thank you for helping me assign some of my NOESY walks when I was stuck or explain certain structural motifs. I appreciate our friendship and I will miss you a lot. I would like to extend a big thank you to Dr. Jaichen Wang for always being available to answer my many questions about running calculations, modifying scripts, making structures, and uploading coordinates. Without your help, things would have moved ten times slower. I would also like to thank you for making the computer room/dungeon a much more enjoyable place. I enjoyed our conversations about your family as well as Chinese characters, food, and traditions. To my colleague Andrew Chang thanks for letting me make up a song for you and multiple remixes. Your floral hand sanitizer always made me smile. I wish you much luck and success in the future. Finally, I

would like to thank Dr. Quinn Kleerekoper, whose presence certainly made things interesting.

To my committee members Dr. George Bennett, Dr. Bonnie Bartel, and Dr. Jonathan "Joff" Silberg, thank you for being encouraging, supportive, and positive during my time at Rice. I truly appreciate your feedback and suggestions. Without your support, things would have been quite challenging. To Dr. Bennett, thank you for always having a smile and kind words as well as giving me constructive feedback after my progress reviews. To Dr. Bartel, I appreciate your support, encouragement, and light-hearted nature. It was a pleasure getting to know you through AGEP and I am glad that you were one of the first faculty members that I met. Finally, to Joff, I truly appreciate your assistance with the thesis and I appreciate you taking time out of your busy schedule to meet with me every Friday to discuss my writing and experimental progress. I will not forget that and I have taken a lot away from our meetings.

In addition to the lab and my committee members, I would also like to thank the BCB office staff, Dr. Jennifer Wilson, and Dr. Roopa Thapar. You all have been instrumental in my success and without you I know that I would not have completed this degree. To the office staff, thank you for always having a smile on your faces, a funny story to share, encouraging words and hugs, or yummy treats in the office. I always enjoyed coming into the office and seeing all of you and I can only hope that I will find such nice people the next place I go. To Dr. Wilson, thank you for all of your help on my thesis manuscript and your friendship. Your assistance was necessary and I truly appreciate all that you did to help me push things along. Finally, to Dr. Thapar, thank you for your advice, mentorship, and friendship. I am so happy that our paths crossed while I was at Rice. You have been such an

integral part to my success and I thank you for providing opportunities for me to be on papers and for encouraging me to apply to postdoctoral positions.

I would like to extend a big thank you to my friends who supported me emotionally through this whole process. There are not enough words to describe how much I appreciate and love you all. I am truly humbled by your kindness and I cannot even begin to understand what I did to deserve such beautiful people in my life. To my dear friend Rosa, thank you so much for your continued support and friendship. I feel so lucky that I found a friend like you and I truly appreciate your emotional support. I have enjoyed our conversations, shopping trips, and cupcake/coffee runs, which I think were necessary for our sanity. To my friend Anu, you were my very first friend at Rice and I am so happy that I met you. We have had many adventures during the last six years and I am grateful for them. Thanks for introducing me to Nepali cuisine and letting me come over to your place anytime. To my friend Sol, you are so funny to me and I am glad that I had the pleasure of meeting you. I loved hearing about your Peruvian adventures. I think my favorite story was the one that started out "So this one time when I used to live in the rainforest…" I also enjoyed our deep conversations over meals and our random adventures to the opera, the Peruvian Festival, and Latin poetry events. To Lisa Blinn, thank you for your friendship, support, advice, and the cats. I am so thankful that I met you and I will miss seeing you all the time, but I am certain that our paths will cross again and when they do, I will be ready. To the kind faces on the 3rd floor of Keck and in the department, thank you for the laughter, friendships, and lasting memories. Your kind words motivated me and helped propel me forward; for that I am indebted and I will never forget you all. To the beautiful people I met in AGEP, thank you for your compassion and support. I am so thankful for this group and the lasting friendships that I made. You all

were wonderful and I am glad that I had the chance to get to know you. To the lovely ladies of the Rice Owls Dance Team and the Rice Dance Theatre, thank you for cultivating a safe and welcoming space that allowed me to be creative and express myself. I love you all dearly and I am so thankful for our crazy shenanigans, which certainly made my time at Rice exciting.

Last, but certainly not least, I would like to thank my family. To my grandmother, I dedicate this degree to you. You worked tirelessly to accomplish your goals and your tenacity to achieve your dreams despite individuals attempting to hold you back truly inspired me and motivated me to keep pushing forward. You were a champion for education and inspired so many of your students to strive for excellence. I hope to be a source of positivity and motivate people as well as you did. To my mom, thanks for listening and encouraging me to keep pushing forward. To my cousins, thank you for your kind words and encouragement. I love you all so much and I thank you for inviting me over for the holidays, cookouts, and birthday parties as well as providing me with a place to sleep when I first arrived in Houston. To Jennifer Jamison and Nikki Delk, thank you for being like sisters to me. Words cannot even begin to describe how wonderful I think you ladies are. I enjoyed our outings and I will really miss you both. I look up to the both of you so much and I hope that I will be able to help someone as much as you both helped me. Finally, I would like to thank my close family friends. You all have been marvelous and I cannot even begin to think of ways to repay you. Thank you for your kind words, cards, hugs, and smiles. I will cherish everything you did for me and I will never forget your love and kindness.

TABLE OF CONTENTS

LIST OF FIGURES

LIST OF TABLES

ABBREVIATIONS

(2-thiomethyl, N^6-dimethylallyl)-adenine	ms^2i^6A
(dimethylallyl)adenosine tRNA methylthiotransferase	MiaB
1-methyadenosine	m^1A
1-methylguanosine	m^1G
2'-O-methylcytosine	C_m
2-methylthio-N6-(4-hydroxyisopentenyl) adenosine	ms^2io^6A
2-O-methylguanosine	G_m
2-thio	s^2
2-thiocytodine	s^2C
2-thioribothymidine	s^2T
2-thiouridine	s^2U
5'-nucleoside triphosphate	5'-NTP
5-methylaminomethyl	mnm^5
5-methylaminomethyl-2-thiouridine	mnm^5s^2U
7-aminomethyl-7-deazaguanine	$PreQ_1$
A_{37} (N^6-dimethylallyl)-modified anticodon stem-loop	$[i^6A_{37}]$-ASL
amino	NH_2
anticodon stem-loop	ASL
Bacillus anthracis	*B. anthracis*
Bacillus cereus	*B. cereus*
Bacillus subtilis	*B. subtilis*
Bacillus thuringiensis	*B. thuringiensis*
Clostridium beijerinckii	*C. beijerinckii*
cobalt hexamine	$Co(NH_3)_6^{3+}$
correlated spectroscopy	COSY
differential scanning calorimetry	DSC
dihydrouridine	D
dimethylallyl (Δ^2-isopentenyl) diphosphate:tRNA transferase	MiaA
dimethylallyl diphosphate	DMAPP
double quantum filtered correlated spectroscopy	DQF-COSY

enthalpy	ΔH
Escherichia coli	*E. coli*
ethylenediaminetetraacetic acid	EDTA
guanine	G
heteronuclear correlation	HetCor
heteronuclear multiple quantum coherence	HMQC
heteronuclear single quantum coherence	HSQC
histidine	His
imino	NH
inosine	I
iron	Fe
lysine	Lys
magnesium	Mg^{2+}
methylthiol	ms^2
messenger RNA	mRNA
Minimum Inhibitory Concentration	MIC
molecular dynamics	MD
N^4-Acetyl-2'-O-methylcytidine	ac^4C_m
N6-(4-hydroxyisopentenyl)-adenosine	io^6A
N6-threonylcarbamoyl-adenosine	t^6A
NOE spectroscopy	NOESY
nuclear magnetic resonance	NMR
nuclear Overhauser effect	NOE
nucleoside triphosphate	NTP
parts per million	ppm
phenylalanine	Phe
protein data bank	PDB
Pseudomonas aeruginosa	*P. aeruginosa*
pseudouridine	Ψ
queuosine	Q
restrained molecular dynamics	rMD

ribonucleic acid	RNA
ribothymidine	T
root mean square deviation	RMSD
Salmonella flexneri	*S. flexneri*
Salmonella typhimurium	*S. typhimurium*
serine	Ser
small nuclear RNA	snRNA
sulfur	S
Symbiobacterium thermophilum	*S. thermophilum*
Thermus thermophilus	*T. thermophilus*
three dimensional	3D
total COSY	TOCSY
transfer ribonucleic acid	tRNA
transition temperature	T_m
tRNA-guanine transglycosylase	TGT
two dimensional	2D
tyrosine	Tyr
ultra violet	UV
uridine	U
valine	Val
wybutosine	yW

Chapter 1

Introduction

1.1 Overview

Currently, there are limited crystal and solution structures of tRNAs available and even less information regarding base modification on tRNA structure. The most extensively characterized tRNA molecules are the yeast $tRNA^{Phe}$ and the anticodon stem loop (ASL) from the human $tRNA^{Lys}$. Surprisingly, there are no structures (free or bound) available of either the full-length or ASL of $tRNA^{Tyr}$. Even more surprising is there are no structures of tRNAs from *Bacilli*, such as *Bacillus subtilis*, which is one of the most studied Gram-positive bacteria. Aside from the limited information regarding tRNA structure (specifically $tRNA^{Tyr}$), there is even less knowledge regarding the contribution of individual base modifications on the known tRNA structures. Secondly, there are 107 known RNA base modifications known to date. Even though the structures, locations, or compositions of these modifications have been well characterized, there are limited examples of how the known modifications affect the stability of RNA molecules, especially tRNAs. Finally, even though there is a wealth of knowledge pertaining to the overall function of tRNA molecules as it relates to translation, very little is known about the role of tRNAs in transcriptional regulation in Gram-positive bacteria or how base modifications affect their ability to regulate gene expression. Therefore, the goal of my thesis is to address the above mentioned gaps in knowledge by determining what role base modifications play in the structure, stability, and function of the $tRNA^{Tyr}$ molecule in *B. subtilis* and *Bacillus anthracis*.

1.2 Nucleotide Modifications in RNA and their Relevance in the Cell

Typically RNA molecules are thought to be comprised of the four bases adenosine (A), uridine (U), cytosine (C), and guanosine (G). However, these residues can be modified, resulting in 107 different RNA bases. The expansion and diversification of the RNA genome results in different modes of RNA recognition for gene expression (Niu et al., 2013) as well as affects RNA stability and function (Pan, 2013). These posttranscriptional modifications occur in cells from all branches of life and are an important step in the maturation and functional properties of RNA molecules (Agris, 1996; Björk, 1995; Garcia and Goodenough-Lashua, 1998; Winkler, 1998). In addition to their roles in translation (Diaz et al., 1987; Ericson and Björk, 1991a; Hagervall et al., 1990), base modifications have direct roles in other cellular processes such as RNA processing (Dönmez et al., 2004; Hall and McLaughlin, 1991; Newby and Greenbaum, 2001), viral replication (Bilbille et al., 2009; Maynard et al., 2012), and antibiotic resistance (Johansen et al., 2006; Maus et al., 2005).

Pseudouridine (Ψ), which is the most widespread modification, plays an important role in mRNA splicing (Dönmez et al., 2004; Hall and McLaughlin, 1991; Newby and Greenbaum, 2001). Within the 5' end of the human U1 small nuclear RNA (sn)RNA, there are two Ψs that play an important role in recognizing the splice site in the mRNA (Reddy, 1989). In addition to being conserved in the U1 snRNA, Ψ is also conserved in the U2 snRNA, where it has been shown to be important for inducing a change in the architecture of the U2 snRNA–intron binding site and promoting splicing (Newby and Greenbaum, 2001). In addition to the three Ψs, the U2 snRNA contains a 3-methylguanine cap at the 5' terminus and five 2'O-methylation sites within the first 20 nucleotides. The Ψs, in conjunction with four of the five 2'O-methylation sites, were necessary for splicing and played an important role in supporting the formation of the early complex (Dönmez et al., 2004).

Nucleotide modifications are also integral to viral replication (Bilbille et al., 2009; Maynard et al., 2012). In *Escherichia coli*, deletion of tRNA thiolation enzymes that are Fe-S cluster-independent conferred significant resistance to lambda phage compared to the wild type strain (Maynard et al., 2012). The reduction in lambda replication was due to increased frameshifting due to the loss of the 2-thiouridine modification in the lysyl-tRNA at position 34 (Maynard et al., 2012).

In addition to their role in splicing and viral replication, modifications contribute to antibiotic resistance in cells (Gustafsson and Persson, 1998; Johansen et al., 2006; Maus et al., 2005). In *E. coli* the loss of 1-methylgunine at position 745 in 23S rRNA resulted in weak viomycin resistance, even though the modified base does not interact directly with viomycin or located proximal to the decoding center of the 30S subunit (Gustafsson and Persson, 1998). The loss of 2'-O-methylcytidine in both the 23S and 16S rRNAs, has been implicated in conferring resistance to capreomycin in *Mycobacterium tuberculosis* (Johansen et al., 2006; Maus et al., 2005).

1.2.1 Commonly Modified Residues in the Anticodon Stem-Loop of tRNA

Of the 107 base modifications known to date, more than 80 different varieties have been discovered in tRNA alone. These modifications can range in complexity from small chemically simple modifications to large and bulky hypermodified bases. Certain residues within tRNAs that are modified are synonymous for specific modifications, which have contributed to the nomenclature associated with the structure or region of the tRNA molecule. For example, the TΨC loop, which contains a conserved ribothymidine (T) and Ψ, and the D arm, which contains conserved dihydrouridines (D). Notably, the ASL contains the largest diversity of base modifications (Cantara et al., 2011) with the four most common

sites for modification being residues 32, 34, 37 and 39. In the *B. subtilis* and *B. anthracis* $tRNA^{Tyr}$ molecules, which are the RNAs that my thesis focuses on, the common sites for modification include positions 34, 37, and 39. This section highlights the common modified sites in tRNAs as well as introduces modifications that are also found in the *B. subtilis* and *B. anthracis*, but in the context of different tRNAs from other organisms.

1.1.2.1 Modifications at Residue 32

Residue 32 is located at the stem-loop junction of the ASL and plays an important role in a specialized base pairing with residue 38. In the kinetoplastid *Trypanosoma brucei*, the C at position 32 is modified to U in the nucleus of all three of the threonyl-tRNA ($tRNA^{Thr}$) species (Gaston et al., 2007). The conversion of C_{32} to U_{32} occurs before 5' end editing of tRNAs, but after 3' end editing (Gaston et al., 2007).

Residue 32 is also modified to 2-thiocytodine (s^2C) in four of the five *E. coli* arginyl-tRNA ($tRNA^{Arg1,3,4,5}$) isoacceptors and one of the seryl-tRNAs ($tRNA^{Ser,2}$) (Jühling et al., 2009). Although s^2C_{32} is one of the most rare modifications, it is found in a specific tRNA consensus sequence with s^2C_{32} or C_{32} being found in fifty-six percent of all *E. coli* sequences (Cantara et al., 2011). s^2C_{32} in $tRNA^{Arg,1}$ maintains the proper translation reading frame (Baumann et al., 1985). *In vitro* assays using a $tRNA^{Arg,1}$ deficient in s^2C at position 32 does not affect the $tRNA^{Arg,1}$ molecule's ability to decode its cognate codon, CGU, when it is in the A-site (Cantara et al., 2012). However, the presence of s^2C_{32} completely abolished the ability of $tRNA^{Arg,1}$ to decode the non-cognate, synonymous codon, CGA (Cantara et al., 2012). This negative function of s^2C_{32} may prevent $tRNA^{Arg,1}$ from incorrect binding to a wobble pair. Previous studies suggest that the s^2C modification improves translational accuracy by reducing the speed of the reaction (Jäger et al., 2004). Loss of s^2C in *Salmonella*

enterica did not affect the growth rate, but $tRNA^{Arg,3}$, which contains the s^2C_{32} modification, showed decreased selection rate when the AGG codon was in the A-site of the ribosome (Jäger et al., 2004).

1.1.2.2 Modifications at Residue 34

Residue 34, or the wobble position, plays an important role in codon recognition. Due to the degeneracy of the genetic code, the wobble position allows one tRNA to recognize multiple codon sequences that differ only at the third position. For example, tRNAs with inosine (I) at the wobble position recognize codons with a C in the third position and can wobble to either an A or a U (Crick 1966). Modification at the wobble position has also been shown to contribute to enhanced codon recognition. For example, in *E. coli* the 2'-O-methylcytosine (C_m) modification enhanced cognate codon recognition (Satoh et al., 2000).

Queuosine (Q), which is present in the *B. subtilis* and *B. anthracis* $tRNA^{Tyr}$ molecules, is derived from G and is commonly found in $tRNA^{Asp}$, $tRNA^{Asn}$, $tRNA^{His}$, and $tRNA^{Tyr}$. Q is synthesized *de novo* by bacteria, but in vertebrates, Q must be supplemented through the diet. Loss of Q_{34} in *E. coli* $tRNA^{Tyr}$ and RNA^{His} resulted in frameshifting of $tRNA^{Pro}$ or $tRNA^{Phe}$ in the P-site when the UAU (Tyr) codon was in the A-site and frameshifting of $tRNA^{Phe}$ in the P-site when the CAU (His) codon was adjacent to the A-site (Urbonavičius et al., 2001). The slippage observed by the tRNA in the P-site is most likely caused by slow entry of the hypomodified (Q_{34} deficient) tRNAs into the A-site (Urbonavičius et al., 2001). Interestingly, both hypo- and fully modified tRNAs have a bias toward codons that have a C at the end position of the codon instead of a U (Urbonavičius et al., 2001).

Another modification common to position 34 is 5-methylaminomethyl-2thiouridine

(mnm^5s^2U), which is specific to $tRNA^{Gln}$, $tRNA^{Lys}$, and $tRNA^{Glu}$. In *E. coli*, frameshifting of $tRNA^{Pro}$ in the P-site was observed in bacteria with $tRNA^{Lys}$ deficient in mnm^5 when lysine codons were in the A-site (Urbonavičius et al., 2001). A similar observation was made in cells deficient in s^2 (Urbonavičius et al., 2001). These observations indicate that both the mnm^5 and s^2 groups are necessary for decoding the lysine codons. Additionally, the mnm^5s^2U in the context of the human $tRNA^{Lys}$ promotes stacking of $mnm^5s^2U_{34}$ with residues U_{35} and U_{36}, stabilizes the stacking of the anticodon residues, and aids in the formation and stabilization of the U-turn motif (Sundaram et al., 2000). The orientation of mnm^5s^2U along with the fact that the s^2U-A bond is more stable than the s^2U-G bond (Testa et al. 1999) explains the frameshifting and codon preference observed by Urbonavičius et al.

1.1.2.3 Modifications at Residue 37

Residue 37, which is adjacent to the 3' nucleotide of the anticodon, is modified seventy-five percent of the time in tRNAs (Björk, 1998; Sprinzl et al., 1998). The modified bases i^6A_{37}, $ms^2i^6A_{37}$, io^6A_{37} and $ms^2io^6A_{37}$, often follow anticodon sequences terminated by an adenine (Motorin et al., 1997; Sprinzl et al., 1998; Xie et al. 2007). i^6A_{37} and $ms^2i^6A_{37}$, which are two of the most common modified forms of A_{37} in bacterial tRNA, occur in 10 of 46 tRNA species in *E. coli*. In *B. subtilis*, hypomodification of A_{37} to i^6A_{37} in $tRNA^{Phe}$ reduces the rate and formation of dipeptides (Hoburg et al., 1979). Interestingly, the rate of aminoacylation is not affected by hypomodification (Hoburg et al., 1979).

In *Salmonella typhimurium*, tRNAs that have suppressor activity, such as $tRNA^{Tyr}$, $tRNA^{Gln}$, and $tRNA^{Ser}$ that recognize the amber nonsense codon, contain the 2-methylthio-N^6-(4-hydroxyisopentenyl) adenosine (ms^2io^6A) modification at position 37. The ms^2io^6A modification contributes to decreased codon context sensitivity, particularly when flanked on

the 3' side by an A or a C (Ericson and Björk, 1991a). Previous studies in *S. typhimurium* have shown that suppressor tRNAs unmodified at position 37 are more likely to bind to nonsense codons when an adenosine is adjacent to the 3' side of the codon than when a C is present, resulting in readthrough of amber codons (Bossi and Ruth, 1980). When suppressor tRNAs are modified with ms^2io^6A at position 37, the codon context is no longer a determining factor of whether suppressor tRNAs bind and allow readthrough of the amber codon (Ericson and Björk, 1991a).

Other modifications that are common to position 37 include wybutosine (yW) and its precursor 1-methylguanosine (m^1G). Previous studies have shown that m^1G_{37} plays an important role in sustaining the translational reading frame, cellular growth rate, and codon recognition in the ribosome (Ashraf et al., 2000; Björk et al., 2001; Hagervall et al., 1990). Additionally, the m^1G modification in the yeast ASL^{Phe} reduces the flexibility of the loop nucleotides (Stuart et al., 2003). Similar to its precursor, yW has been shown to maintain the reading frame in rabbit reticulocytes (Carlson et al., 2001), however, its effects on ASL structure differ. Unlike its precursor m^1G, which is flipped out into solution, the yW modification stacks inside the loop (Stuart et al., 2003). Despite these differences, both modifications are important for maintaining tRNA function.

1.1.2.4 Modifications at Position 39

Position 39 is modified to Ψ in 95% of all tRNAs (Sprinzl et al., 1998). The Ψ modification is derived from U and is the most widespread RNA modification. In yeast, Pus3 is responsible for incorporating Ψ at positions 38 and 39 (Lecointe et al., 1998). Loss of $\Psi_{38/39}$ resulted in translational defects. For example, readthrough of nonsense codons by suppressor tRNAs is significantly reduced and the +1 frameshifting of the Ty1 slippery site is

decreased by 1.8-fold (Lecointe et al., 2002). Structural and thermodynamic data in the context of the yeast $tRNA^{Phe}$ has shown that Ψ_{39} increases thermal stability and maintains the structural integrity of the RNA (Agris et al., 1999).

In bacteria such as *S. typhimurium* and *E. coli*, TruA is responsible for catalyzing the U to Ψ reaction at position 39. tRNAs deficient in Ψ_{39} showed a twenty percent reduction in the rate of translation and a decrease in growth rate (Palmer et al., 1983). The loss of Ψ_{39} in the two $tRNA^{Lys}$ species in *S. typhimurium* resulted in a 3-fold increase in frameshifting (Li et al., 1997). Additionally the selection of these two $tRNA^{Lys}$ species to their cognate codons, CUG and CUA, resulted in a seventy percent decrease (Li et al., 1997), indicating that Ψ_{39} plays a critical role in tRNA function.

1.3 Effects of Base Modification on ASL Structure and Stability

Since tRNA molecules must enter the ribosome, they must share similar structural motifs. Some modifications in the ASL promote the transition from non-canonical to canonical structures, which indicates that base modifications play an integral role in altering and stabilizing the overall structure of the molecule. Characteristic tRNA structure elements include the U-turn motif, which was first identified in $tRNA^{Phe}$, and a specialized base pairing that occurs between bases 32 and 38 (Figure 1).

1.3.1 Common tRNA Structural Motifs

The U-turn motif, which is considered a canonical structural motif of the ASL in tRNA molecules, is defined by a 180-degree change in the direction of the phosphate backbone 3' at the conserved uridine at position 33. This motif is stabilized by base stacking and hydrogen bonding of the imino nitrogen of U_{33} to the phosphate between residues 35 and

36 as well as hydrogen bonding between the 2'-hydroxyl of U_{33} and residue 35 (Cabello-Villegas et al., 2004; Kim et al., 1974) (Figure 1). Modifying *E. coli* ASL^{Phe} with i^6A at position 37 caused the molecule to adopt the classic U-turn motif that was absent in the unmodified molecule (Cabello-Villegas et al., 2004). However, modification of human $tRNA^{Lys,3}$ to $[\Psi_{39}]$-$tRNA^{Lys,3}$ does not result in the canonical U-turn structure but instead promotes the formation of a tri-nucleotide loop (Durant and Davis, 1999); an indication that not all modifications contribute to the formation of classical tRNA structure.

Another conserved structural motif within tRNAs is the hydrogen bonding between residues 32 and 38 (Figure 1). This interaction assists in stabilizing the ASL and strengthening the interaction of residues 31 and 39 (Durant and Davis, 1999). Hydrogen bonding between residues 32 and 38 can take the form of a normal base pair or a bifurcated hydrogen bond. The bifurcated hydrogen bond is observed in all tRNA crystal structures reported to date and is considered a conserved interaction in all tRNA molecules (Auffinger and Westhof, 1999). Figure 1 shows the bifurcated bond involves the interaction of the amino group on the A and the carbonyl oxygen on the C (Auffinger and Westhof, 1999). Yeast $tRNA^{Phe}$, $tRNA^{Asp}$, and $tRNA^{iMet}$ along with *E. coli* $tRNA^{Cys}$ are among the tRNA molecules that contain the A_{32}-C_{38} bifurcated hydrogen bond (Auffinger and Westhof, 1999).

1.3.2 Crystal and Solution Structures of Full-Length tRNAs and ASLs

The canonical tRNA structural motifs that are specific to the ASLs of tRNA molecules are the U-turn motif and a bifurcated hydrogen bond between residues 32 and 38, which has been observed in the crystal structures of tRNA molecules (Byrne et al., 2010; Chimnaronk et al., 2009; Robertus et al., 1974). The yeast $tRNA^{Phe}$ was the first three

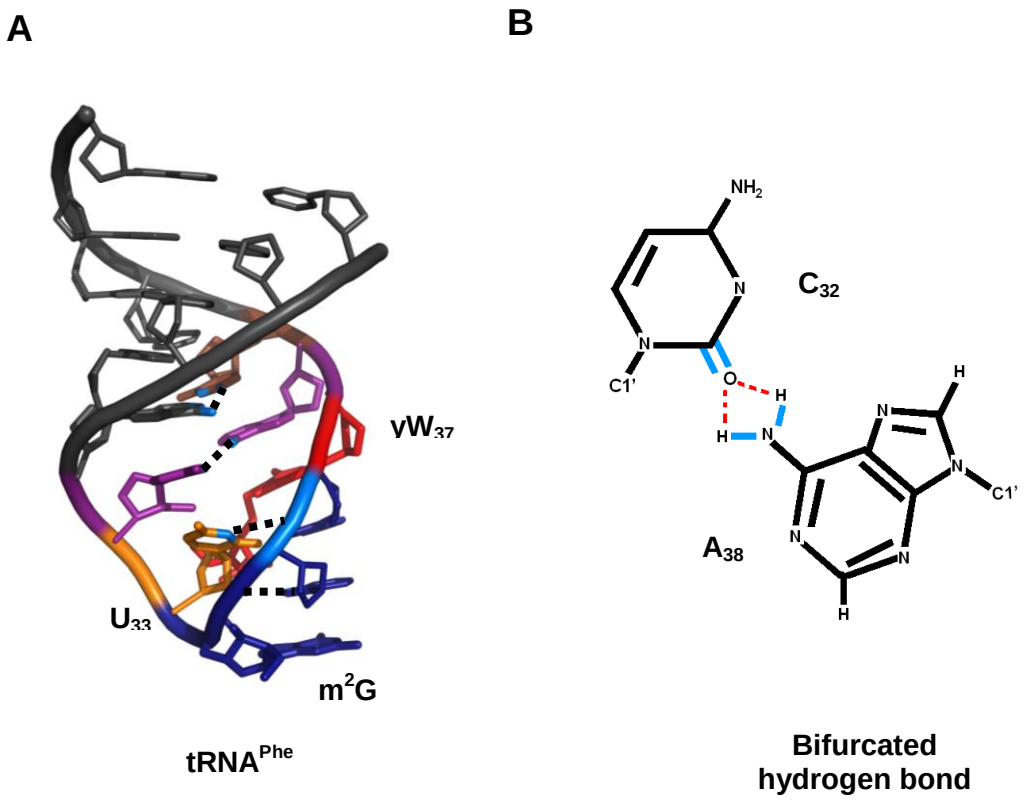

Figure 1. Conserved tRNA Structural Motifs: U turn and Bifurcated Hydrogen Bond

U-turn motif (A) is defined by a 180-degree change in the direction of the phosphate backbone 3' at the conserved uridine (gold) at position 33. The motif is stabilized by hydrogen bonding of the imino nitrogen of U_{33} to the phosphate between residues 35 and 36 as well as the 2' hydroxyl from residue U_{33} to residue 35. The bifurcated bond (B) involves hydrogen bonding of the amino group on the adenosine to the carbonyl oxygen on the cytosine. Blue, anticodon; Red, residue 37; Purple, C_{32}-A_{38} bifurcated hydrogen bond; Dashed lines, hydrogen bonding

dimensional crystal structure of a full-length tRNA molecule (Figure 2) (Kim et al., 1974; Robertus et al., 1974). The preferred conformation of the molecule revealed that the amino acid acceptor stem stacks on top of the TΨC loop, making a long A-form helix (Robertus et al., 1974). Unlike the acceptor stem and the TΨC loop, the D stem and the anticodon stems do not form a long helix. Instead, they are slightly angled from each other (by 20°), promoting an L-shape conformation (Robertus et al., 1974). Finally, the ASL is hinged slightly to the right of the D stem and the loop residues of the ASL are stacked on the 3' side of the molecule. The residues of the anticodon are flipped outward, whereas residues 32 and 33 are stacked and facing the inside of the molecule. This conformation is supported by a U-turn in the phosphate backbone (Robertus et al., 1974).

Using the yeast $tRNA^{Phe}$ crystal structure as a model, other full-length tRNAs were crystallized and their structures solved. Recently, the unmodified *E. coli* $tRNA^{Phe}$ was solved by X-ray crystallography (Byrne et al., 2010). Interestingly, the overall fold of the molecule was similar to the fully modified and mature $tRNA^{Phe}$ but there were a few slight differences. Even though the molecule has an L-shape conformation, the contacts and base pairing of the residues in the center of the molecule were significantly different from those observed in the mature yeast $tRNA^{Phe}$ (Byrne et al., 2010). Similar to the modified yeast $tRNA^{Phe}$, the electron density of the D loop suggests that the unmodified *E. coli* $tRNA^{Phe}$ is also flexible. It has been proposed that the D in the D loop is what lends the flexibility to this region of the molecule; however, the flexibility that is observed in the unmodified *E. coli* $tRNA^{Phe}$ is most likely caused by a lack of crystal contacts and not the modification (Byrne et al., 2010; Jovine et al., 2000). Additionally, the ASL of the unmodified tRNA adopts the canonical U-turn motif, which is often attributed to base modifications. The appearance of the U-turn

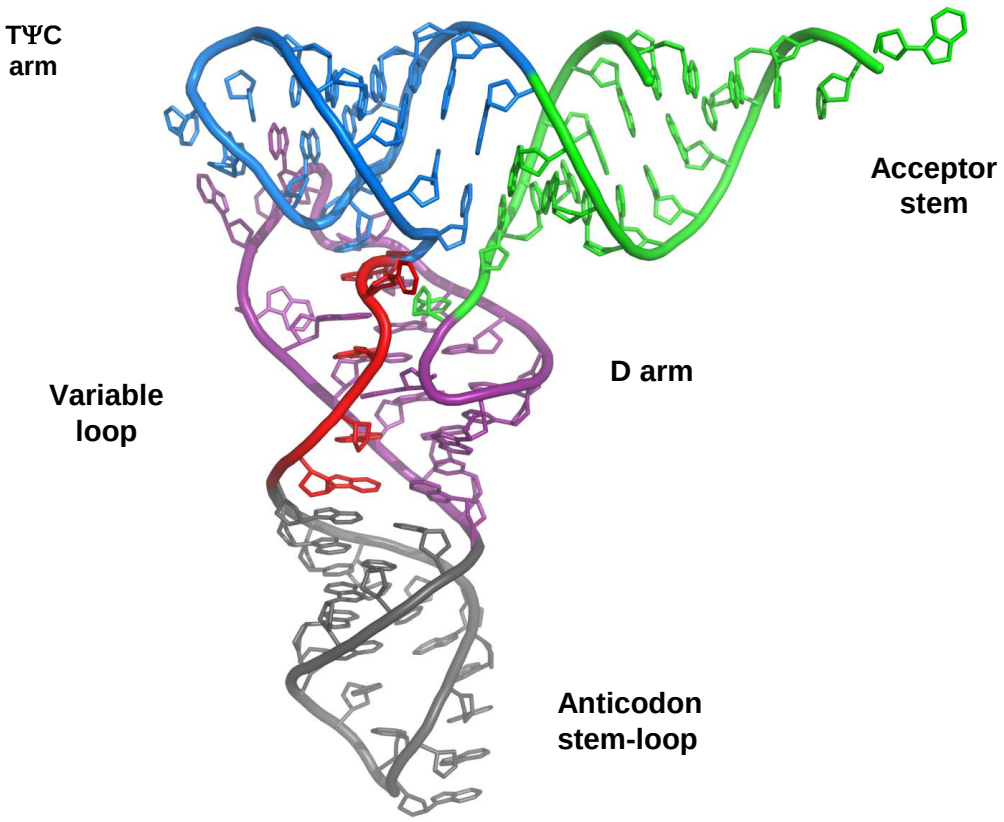

Figure 2. Canonical Structure of Full-Length tRNA: Crystal Structure of $tRNA^{Phe}$

The tertiary contacts of the full-length molecule form an L-shaped conformation. The residues of the anticodon are flipped outward, whereas residues 32 and 33 are stacked and facing the inside of the molecule. This conformation is supported by a kink (U-turn) in the phosphate backbone. Silver, anticodon stem-loop; Red, variable loop; Purple, D arm; Turquoise, TΨC arm; Lime, acceptor stem (PDB Code 1EHZ).

motif in the unmodified tRNA may actually be driven by crystal packing interactions (Byrne et al., 2010).

Although crystallographic structures provide useful information regarding the preferred conformation of a molecule under conditions that promote crystal formation, it does not allow the molecule to sample multiple conformations under more physiological conditions as a solution structure would. The solution environment provides information regarding the dynamic nature of the molecule. When the unmodified ASL from the *E. coli* $tRNA^{Phe}$ was solved in solution, the loop nucleotides adopted a tri-loop conformation (Cabello-Villegas et al., 2002). However, the conversion of A_{37} to N^6-dimethylallyl (i^6A_{37}) disrupts the tri-loop and facilitates formation of the U-turn motif (Cabello-Villegas et al., 2002). A similar effect was also observed for the anticodon arm of the human $tRNA^{Lys,\ 3}$, which also has a tri-loop that is disrupted by the addition of the threonyl-6-adenine modification at position 37 (Stuart et al., 2000). Both cases suggest that modification to the ASL may contribute to the formation of the canonical U-turn motif.

In addition to the U-turn archetype, crystallographic data indicates that several tRNAs possess a bifurcated hydrogen bond between the first (residue 32) and last (residue 38) nucleotides of the anticodon loop (Auffinger and Westhof, 1999). The bifurcated bond involves the interaction of the amino group on the adenosine and the carbonyl oxygen on the cytosine (Auffinger and Westhof, 1999). However, in the known solution structures of unmodified and partially modified ASLs, the bifurcated hydrogen bond is not observed and instead a Watson-Crick-like base paring is noted. For example, the unmodified and [Ψ_{39}]-$ASL^{Lys,3}$ molecules form a protonated C_{32}-A^+_{38} base pair, which improves the thermal stability of the stem (Durant and Davis, 1999). Additionally, the presence of the C_{32}-A^+_{38}

base pair disrupted the seven nucleotide loop normally observed and instead initiated a dynamic U_{33}-A_{37} base pairing that resulted in a three nucleotide loop (Durant and Davis, 1999). The Watson-Crick-like base pairing between residues 32 and 38 was also observed in the partially modified *E. coli* $tRNA^{Phe}$ (Cabello-Villegas and Nikonowicz, 2005). Although the single hydrogen bond has not been observed in the crystal structures of unbound tRNA molecules, it was observed in yeast $tRNA^{Asp}$ when bound to its cognate tRNA synthetase (Auffinger and Westhof, 1999).

1.3.3 Effects of Base Modification on RNA Stability

Although it has been shown that various forces, such as electrostatic, hydrophobic, and dispersion properties are important for stabilizing nucleic acids (Friedman and Honig, 1995), modified bases also seem to play a critical role in nucleic acid stabilization. The individual stabilizing or destabilizing properties of base modifications, especially in RNA hairpins, appear to contribute to the structural and functional properties of the molecule. Depending on the location in the molecule, a base modification can increase or decrease the stability of a hairpin by 3-5 ºC, often corresponding to either a more flexible or rigid molecule. Of the 107 base modifications known to date, more than 80 different varieties have been discovered in tRNA alone, with the ASL containing the largest diversity of base modifications. These modifications range in complexity from a simple isomerization or methylation, to large and bulky hypermodified bases.

Methylations are one of the most chemically simple modifications that often disrupt hydrogen bonding between nucleotides. Interestingly, the same nucleotide methylation can have different stabilizing properties when located within a nucleotide helix. For example, the addition of 1-methyadenosine (m^1A) at position 9 of the acceptor stem in the human

mitochondrial $tRNA^{Lys}$ resulted in a significant structural change and conferred increased stability of 3-4 kJ/mol from the unmodified tRNA in the presence of Mg^{2+} ion (Kobitski et al., 2008). However, the addition of m^1A into the helical structure of DNA resulted in a loss of stability corresponding to 6.5 kJ/mol due to the loss of hydrogen bonding and the formation of a Hoogsteen base pair (Yang and Lam, 2009). Another example of the differing properties observed due to nucleotide methylation can be seen in the yeast $tRNA^{Phe}$ hairpin. The 1-methylpseudouridine modification was shown to increase the thermal stability of the molecule, whereas 3-methylpseudouridine and 5,6-dimethyluridine had destabilizing properties (Agris et al., 1999).

Ψ, which is another chemically simple modification and the most frequently found modification in RNA, is an isomer of U that contains a C1'-C5 glycosidic bond. Ψ is often located in a helical stem where it confers additional stability to the helix by forming a water-mediated hydrogen bond to the phosphate backbone through the N1 NH group. For example, the addition of Ψ at position 39 of the human $tRNA^{Lys}$ and *E. coli* $tRNA^{Phe}$ (loop-stem junction) led to an increase in the thermal stability by ~5 °C and improved base stacking in the anticodon arm at the stem-loop junction (Cabello-Villegas and Nikonowicz, 2005; Durant and Davis, 1999). However, when Ψ is located in the loop region of a stem-loop, which is the case for Ψ at position 32 in the *E. coli* ASL^{Phe}, there is a modest increase in the melting temperature (T_m) by 3.5ºC (Cabello-Villegas and Nikonowicz, 2005). This suggests that a Ψ at the stem-loop junction confers greater stability than when located in the loop. Additionally, the increased stability conferred by Ψ at position 39 (stem-loop junction) may enhance translation efficiency and improve growth rate (Charette and Gray, 2000; Lecointe et al., 2002).

Although chemically simple modifications play an important role in large conformational changes, such as restructuring tRNAs and improving their stability, simple modifications such as methylation, pseudouridinylation, and thiolation can also promote subtle conformational changes (e.g., changes in sugar pucker) that contribute greatly to the stabilization of RNA. For example, methylation of the sugar 2'-OH group and pseudouridinylation or thiolation of a pyrimidine O2 atom promotes a 3'-endo sugar pucker, which increases the stabilization of a helical formation (Kawai et al., 1992; Lee and Tinoco, 1977; Watanabe et al., 1979). Not only does the 3'-endo conformation improve stability of helical regions, it also protects RNAs from catalytic degradation (Motorin and Helm, 2010; Wakeman and Winkler, 2009). Additionally, these chemically simple modifications play an important role in protecting RNA from catalytic degradation and stabilize RNA at high temperatures. For example, 2-O-methylguanosine (G_m), N^4-Acetyl-2'-O-methylcytidine (ac^4C_m), and m^1A are induced at high temperatures in thermophilic organisms, yielding increased thermal stability (Kowalak et al., 1994; Kumagai et al., 1980).

Although chemically simple modifications contribute significantly to tRNA and RNA stability, hypermodified bases also play significant roles. The hypermodified base 2-thioribothymidine (s^2T), which is induced at high temperatures, makes a significant contribution to the thermal stability of tRNA. In the $tRNA^{Ile}$ from *Thermus thermophilus*, the addition of the 2-thio (s^2) group to ribothymidine (T) at position 54 resulted in a 3°C increase in thermal stability (Horie et al., 1985; Watanabe et al., 1979). Two residues that are often hypermodified in tRNA are the adenosine located at position 37 and the guanosine at position 34. The most common modification found at this position is N^6-dimethylallyl adenosine (i^6A) and 2-methylthio-N^6-dimethylallyl (ms^2i^6A). In the context of the *E. coli* ASL^{Phe}, the i^6A

modification has a destabilizing effect on the molecule (Cabello-Villegas et al., 2002). However, in the *E. coli* ASL^{Trp} the i^6A modification had a stabilizing effect resulting in a ΔG° of –7.54 kcal/mol, whereas the unmodified molecule had a ΔG° –5.05 kcal/mol (Kierzek and Kierzek, 2003). Moreover, the addition of the fully hypermodified base, ms^2i^6A, in the context of the *E. coli* ASL^{Tyr} provided additional stability (ΔG° = –8.46 kcal/mol) to the molecule (Kierzek and Kierzek, 2003). Notably, the addition of i^6A or ms^2i^6A into the interior of an RNA duplex results in the destabilization of the molecule, which is most likely due to steric hindrance (Kierzek and Kierzek, 2001, 2003). The second most modified residue in tRNA is the G at position 34, which is modified to Q at the wobble position. Although there is limited information about the stabilizing properties of Q, the bulky base introduces three additional hydrogen bond donors and the stability of the Q-U and Q-C wobble pairs are more stable than the G-U wobble pair (Meier et al., 1985).

1.4 *B. subtilis* and *B. anthracis* ASL^{Tyr} Contains Four Base Modifications: i^6A_{37}, ms^2A_{37}, Ψ_{39}, and Q_{34}

tRNA molecules contain a large and diverse pool of modified nucleotide bases with the greatest variety concentrated in the anticodon arm (Cantara et al., 2011). The anticodon arm of $tRNA^{Tyr}$ reflects this diversity and contains modified nucleotide bases at three positions (Figure 3). The most extensively modified residue in ASL^{Tyr} is located at position 37 and is adjacent to the 3' nucleotide of the anticodon (Björk, 1998). This modified base, i^6A_{37}, or variants that include $ms^2i^6A_{37}$ and io^6A_{37}, often follows anticodon sequences terminated by an A (Motorin et al., 1997; Sprinzl et al., 1998). i^6A_{37}, which is added by the enzyme MiaA, and $ms^2i^6A_{37}$, which is formed by the addition of ms^2 by MiaB, are two of the most common modified forms of A_{37} in bacterial tRNA. The most common tRNA

modification, Ψ, which is added by the enzyme TruA, is found at position 39 in the ASL^{Tyr}. Interestingly, anticodon arms of nearly all cellular tRNA molecules contain the Ψ modification at residues 38, 39, or 40 as well as other positions throughout the tRNA molecule (Sprinzl et al., 1998). Lastly, the enzyme TGT is involved in the early steps of converting G_{34} to Q. The bulky Q modification introduces three additional hydrogen bond donors and is found at the wobble position of $tRNA^{His}$, $tRNA^{Asn}$, $tRNA^{Asp}$, and $tRNA^{Tyr}$.

1.4.1 MiaA Converts A_{37} to i^6A_{37}

The enzyme dimethylallyl (Δ^2-isopentenyl) diphosphate:tRNA transferase, or MiaA, catalyzes the addition of the dimethylallyl unit from dimethylallyl diphosphate (DMAPP) to the exocyclic amino nitrogen (N6) of A_{37}, to form i^6A_{37} (Figure 4). MiaA consists of two domains that contain a catalytic core and an α-helical domain (Chimnaronk et al., 2009). Binding of MiaA distorts the phosphate backbone, resulting in a loss of the canonical U-turn motif (Chimnaronk et al., 2009). Once the tRNA is bound, MiaA binds DMAPP and modifies the tRNA (Chimnaronk et al., 2009). The loss of this modification in *E. coli* and *Salmonella typhimurium*, which are both Gram-negative bacteria, caused defects in translation, including reduced rates of polypeptide chain elongation (Diaz et al., 1987; Ericson and Björk, 1991b; Hagervall et al., 1990), and decreased efficiency of translation (Hagervall et al., 1990). Additionally, the loss of i^6A_{37} results in increased codon context sensitivity and decreased function of suppressor tRNA species (Björnsson and Isaksson, 1993; Bouadloun et al., 1986; Connolly and Winkler, 1989) as well as increased translation misread error rates for the first codon position (Harrington et al. 1993). This latter defect leads to incorrect amino acid incorporation and decreased translation misreading error rates

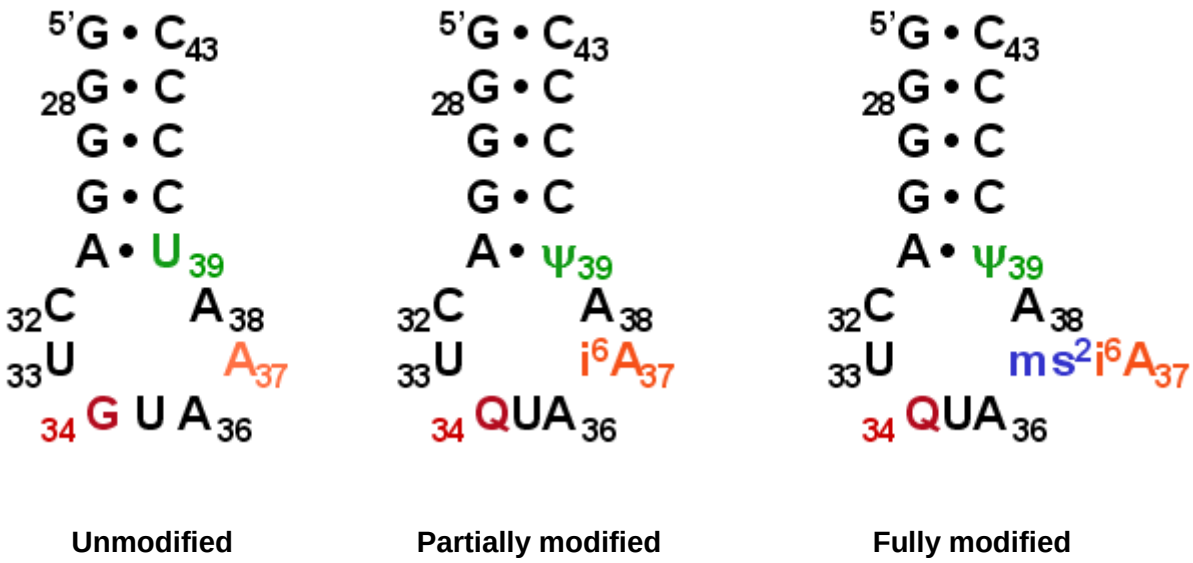

Figure 3. Modified and Unmodified States of ASL^{Tyr} from *B. subtilis* and *B. anthracis*

In *B. subtilis*, tRNA^{Tyr} is found in two modified states. The first form, which is the predominate species during exponential growth, is hypomodified with i^{6}A. The second species, which is the hypermodified form (ms^{2}i^{6}A$_{37}$), is the predominant form during stationary phase.

at the third codon position resulting in reduced wobble function (Björnsson and Isaksson, 1993; Bouadloun et al., 1986).

1.4.2 MiaB Converts i^6A_{37} to ms^2A_{37}

The importance of the dimethylallyl modification at residue A_{37} for tRNA function has been studied extensively in *E. coli* (Bouadloun et al., 1986; Connolly and Winkler, 1989; Diaz et al., 1987; Ericson and Björk, 1991b; Hagervall et al., 1990). This research has revealed that modification of A_{37} to i^6A_{37} by MiaA is a prerequisite to forming the hypermodified base, $ms^2i^6A_{37}$ through the activity of MiaB (Figure 4) (Björk, 1998). MiaB is a radical-*S*-adenosylmethionine enzyme that contains two [4Fe-4S] clusters that are necessary to catalyze the methylation and thiolation of tRNA molecules (Hernández et al., 2007; Pierrel et al., 2004). *In vivo,* the reaction is dependent on iron, cysteine and *S*-adenosylmethionine, which result in the conversion of the aromatic C-H bond to a C-S bond (Buck and Griffiths, 1982; Gefter, 1969; Pierrel et al., 2004; Rosenberg and Gefter, 1969). In *B. subtilis*, which is closely related to *B. anthracis*, the $tRNA^{Tyr}$ molecule exists in two forms, the modified i^6A_{37} form and the hypermodified $ms^2i^6A_{37}$ form (Buu et al., 1981; Menichi and Heyman, 1976; Vold, 1978). In stationary-phase cells, the hypermodified form predominates, whereas in exponential growth phase cells, the i^6A single-modified form of $tRNA^{Tyr}$ is the dominant form (Menichi and Heyman, 1976). *In vitro* ribosome binding experiments revealed that the fully hypermodified form is better able to decode the UAC tyrosine-specific codon (Menichi and Heyman, 1976). Aside from improving codon recognition, the presence of the thiomethyl modification in $ms^2i^6A_{37}$ correlates with the onset of sporulation (Buu et al., 1981).

E. coli and *S. typhimurium* that lack a functional copy of *miaB* contain the i^6A

modification but do not have $ms^2i^6A_{37}$, indicating that only MiaB is responsible for methylthiolation (Esberg et al., 1999). Without the $ms^2i^6A_{37}$ modification, there is a decrease in translational efficiency and an increase in mutated proteins (Pierrel et al., 2002). Additionally, loss of *miaB* in *S. typhimurium* causes suppressor $tRNA^{Tyr}$ to have decreased effectiveness and results in decreased suppression of translation (Esberg et al., 1999). Enzymatic studies have provided direct evidence that MiaB alone is responsible for adding the methylthiol (ms^2) group to i^6A_{37}, resulting in the fully modified base, $ms^2i^6A_{37}$ (Esberg et al., 1999). Figure 4 illustrates how the methylthiolation occurs at position 2 of the base.

1.4.3 TruA Converts U_{39} to Ψ_{39}

One of the most common modifications found in tRNA molecules is the Ψ modification. In *E. coli*, the pseudouridine synthase TruA catalyzes the isomerzation of uridines 38, 39, and 40 in the ASL of 17 different tRNAs (Sprinzl et al., 1998). The isomerization reaction leads to the formation of a $C_{1'}$-C_5 glycosidic bond within the ribose of the U and the introduction of an additional NH functional group in the base (Hur and Stroud, 2007) (Figure 5). To catalyze the reaction, the tRNA to be modified binds distal to the active site of the homodimer (Hur and Stroud, 2007). Once in position, residues 38 through 40 are positioned near the catalytic aspartic acid and the tRNA bends (Hur and Stroud, 2007). Although residues 38-40 remain stacked upon docking to TruA, the U to be modified is flipped-out into the active site (Hur and Stroud, 2007). Disruption of *truA* in Gram-negative bacteria result in reduced polypetide elongation rates and reduced translational fidelity (Björk, 1995). Additionally, TruA-associated defects in *Pseudomonas aeruginosa*, a Gram-negative bacterium, cause reduced growth rates (Björk, 1995) and loss of virulence (Connolly and Winkler, 1989). This phenotype is thought to arise because *P. aeruginosa* has

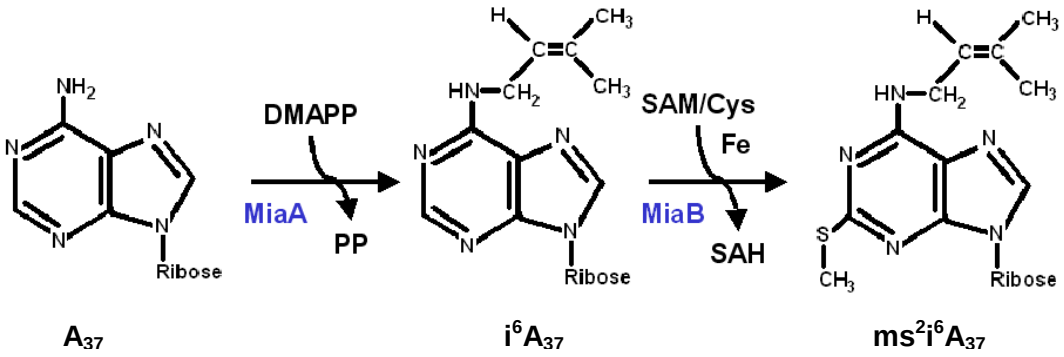

A_{37} i^6A_{37} $ms^2i^6A_{37}$

Figure 4. MiaA and MiaB Convert A_{37} to $ms^2i^6A_{37}$

The first step of the synthesis of $ms^2i^6A_{37}$ involves the addition of an isopentyl group to the N^6 position of the adenosine by MiaA. The second step involves the methylthiolation of the C^2 position by MiaB.

a defect in its expression of functional type III secretion genes (Ahn et al., 2004). In *Saccharomyces cerevisiae*, loss of Ψ at positions 38 or 39 in $tRNA^{Tyr}$, $tRNA^{Lys}$, and $tRNA^{Trp}$ impairs decoding of the amber UAG stop codon. Lack of this modification also decreases read-through efficiency during translation, resulting in decreased growth rate (Lecointe et al., 2002).

1.4.4 TGT Converts G_{34} to Q_{34}

tRNA-guanine transglycosylase (TGT) recognizes tRNA molecules that contain $U_{33}G_{34}U_{35}$ in the ASL ($tRNA^{His}$, $tRNA^{Asp}$, $tRNA^{Asn}$, and $tRNA^{Tyr}$) (Xie et al., 2003) and exchanges the G at position 34 for 7-aminomethyl-7-deazaguanine (PreQ). In most prokaryotes the hypermodification of G to Q takes place in several steps, with the first involving the conversion of a free GTP to $PreQ_1$ (Figure 6) (Romier et al., 1996). In eukaryotes, the Q base is a dietary requirement that replaces G_{34} in one enzymatic step (Romier et al., 1996; Xie et al., 2003). In *Salmonella flexniri*, TGT is essential for virulence (Durand et al., 1994), and in *E. coli*, Q_{34} has been shown to confer fitness (Dineshkumar et al., 2002). Interestingly, *tgt*$^-$ strains grow more rapidly than *tgt*$^+$ control strains; however, when grown at non-ideal temperatures, the *tgt*$^-$ strain does not grow as well as the control (*tgt*$^+$) strain (Dineshkumar et al., 2002). In the specific case of $tRNA^{Tyr}$, the absence of Q leads to amber suppressor activity (Kersten, 1988).

1.5 Transcriptional Regulation Mechanisms in Bacteria

There are multiple mechanisms that bacterial cells use to regulate gene expression, which can be characterized as either intrinsic or factor dependent transcriptional termination

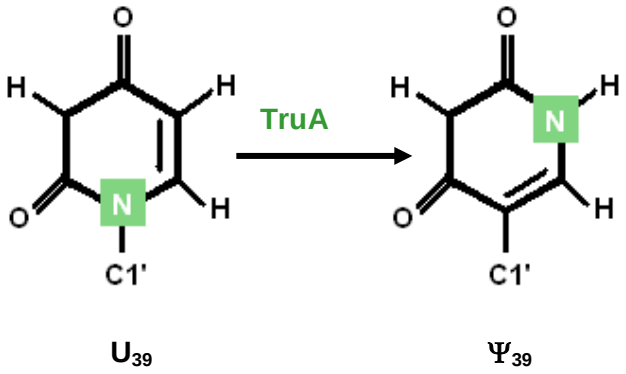

Figure 5. TruA Converts U_{39} to Ψ_{39}

TruA adds the Ψ to the uridine at position 39 in $tRNA^{Tyr}$. This modification adds an additional hydrogen bond donor at position 5 and results in a C-C glycosidic bond.

(Grundy and Henkin, 1993; Henkin and Yanofsky, 2002; Krishna et al., 2013). The mRNA of genes that are regulated intrinsically often form a hairpin structure, which results in the RNA polymerase staling on the transcript (Henkin and Yanofsky, 2002). Conversely, in factor dependent mechanisms, the mRNA acts as a receptor for a metabolite, protein, or tRNA (Babitzke, 2004; Grundy et al., 2000; Miranda-Ríos et al., 2001). The binding of the factor to the RNA results in either the promotion or termination of transcription (Babitzke, 2004; Grundy et al., 1994; Miranda-Ríos et al., 2001). Depending on the requirements of the cell, multiple mechanisms can take place at any given time.

1.5.1 Transcriptional Regulation through Alternative RNA Structures

Bacteria utilize numerous mechanisms to regulate gene expression. Although factor dependent DNA-binding mechanisms are common, bacteria also employ other mechanisms to regulate transcription and subsequently translation through the formation of alternative RNA structures in the 5' untranslated region. These RNA structures, which display ligand-dependent conformational changes, have been termed riboswitches. Genes often regulated by RNA-mediated transcriptional regulation are found in Gram-positive and Gram-negative bacteria. In *Firmicutes* such as Gram-positive *B. subtilis* and *B. anthracis*, diverse amino acid biosyntheses genes are regulated by riboswitches. These include, but are not limited to the S box, which regulates genes involved in methionine and cysteine synthesis (Grundy and Henkin, 1998); the L-box, which is involved in the lysine biosynthesis pathway needed for protein production and cell wall synthesis (Grundy et al., 2003; Rosner, 1975); the RFN element involved in riboflavin biosynthesis (Gelfand et al., 1999; Mack et al., 1998; Winkler et al., 2002); and the T box, which is commonly involved in the regulation of tRNA synthestase genes. Read-through by RNA polymerase of genes regulated by the T box

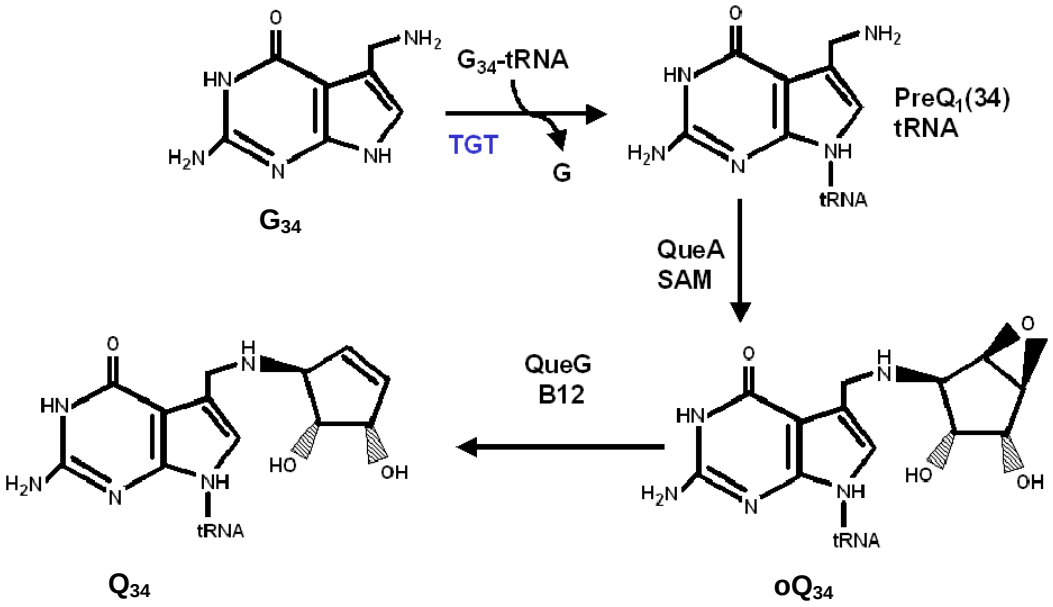

Figure 6. TGT Converts G_{34} to Q_{34}

Free GTP is converted to PreQ, which TGT uses to replace G_{34}. $PreQ_1$, 7-aminomethyl-7deazaguanine; oQ, epoxyquine; Q, 7-{[(4,5-*cis*-dihydroxy-2-cyclopentene-1-yl)-amino]-methyl}-7-deazaguanine.

mechanism is dependent on the formation of either an antiterminator or a terminator structure (Figure 7).

1.5.2 Conserved Features of the T Box Mechanism

The most common mechanism used by *Firmicutes* to regulate amino acid biosynthesis genes and their respective operons is the T box transcriptional regulatory system that acts as a riboswitch (Grundy et al., 1997, 2000; Vitreschak et al., 2008; Wels et al., 2008). The T box mechanism, which is located in the 5'-UTR of the leader in specific mRNAs, contains two mutually exclusive stem-loop secondary structures (Figure 7). The mRNA leader (5'-UTR) contains many conserved regions that aid the leader in forming the terminator or antiterminator structure, as well as facilitating the interaction of specific tRNA molecules with the appropriate leader sequences. The length of the RNA leader ranges between 180 and 300 nucleotides and contains a 14 bp sequence termed the T box sequence (Yousef et al., 2005). The leaders typically contain three stem-loop secondary structure motifs, which are identified as stem-loops I, II, and III (Grundy et al., 2002, 2005; Luo et al., 1998). Many leaders contain a stem IIA/B pseudoknot. To date, only the *glyQS* leader from *B. subtilis* has been found to lack Stem II or the Stem IIA/B pseudoknot motifs (Yousef et al., 2005). Additionally, the mRNA leaders include an AGAGA conserved sequence termed the GA box, which is found within Stem I as well as a specifier domain that contains the specifier codon, which is complementary to the tRNA anticodon (Grundy et al., 1994; Yousef et al., 2005).

The terminator and antiterminator hairpins are responsible for pre-mature transcription termination and transcription read-through, respectively. T box elements bind tRNAs that are related to the function of the genes whose transcription they regulate. Read-

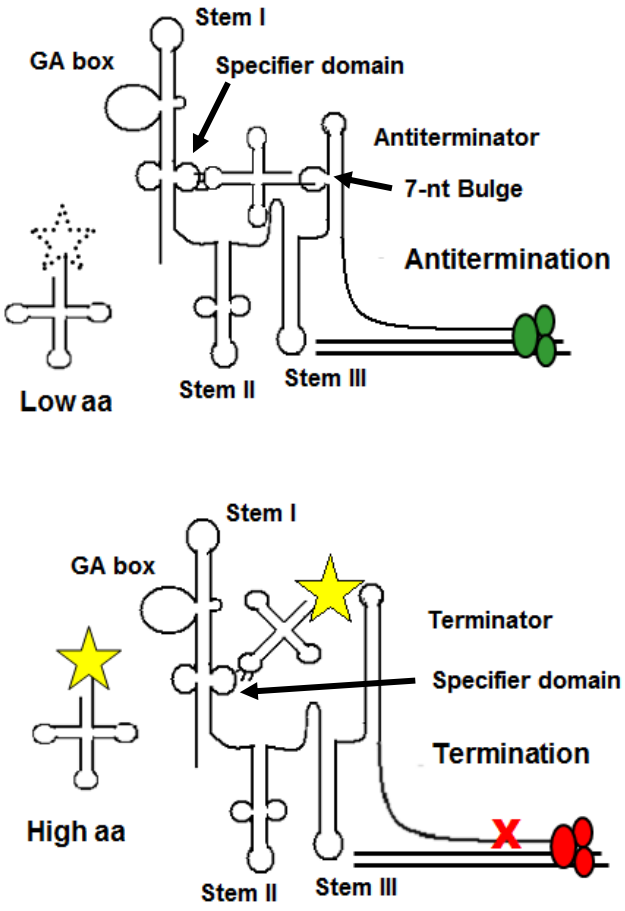

Figure 7. tRNA Mediated Transcriptional Regulation: The T Box Mechanism

When the level of charged tRNA is high, the 3' region of the tRNA is unable to bind to the 7 nt-bulge of the antiterminator, thus the default terminator structure is formed. When the population of cognate uncharged tRNA is limited, the 3' region of the tRNA binds to the bulge region and stabilizes the thermodynamically unfavorable antiterminator secondary structure. Formation of the antiterminator results in transcriptional read-through of the gene by RNA polymerase. The yellow star represents an amino acid and the white star indicates no amino acid is bound. Read-through of the downstream gene is represented by a green RNA polymerase and inhibition of transcription is represented by a red RNA polymerase.

through of the transcription termination site occurs when uncharged cognate tRNA binds and stabilizes the antiterminator hairpin by pairing nucleotides in the 3' end of the tRNA with a seven-nucleotide (7-nt) bulge in the antiterminator helix (Figure 7) (Grundy and Henkin, 1994). The Specifier Loop domain of the T box leader contains the Specifier sequence: three nucleotides that are complementary to the anticodon nucleotides of the cognate tRNA, which is the primary specificity determinant of the T box mRNA leader-tRNA interaction (Grundy et al., 1997). Changing the specificity of the specifier codon sequence and/or the antiterminator base alters the specificity of the T box. This finding suggests that other elements such as tRNA structure, sequence, or base modification may play an important role in tRNA-mRNA leader interaction and, subsequently, T box function.

The importance of T box conserved structures is not limited just to the leader RNA, but is also important for tRNAs as well. Maintenance of the 3' end (5'-NCCA-3') of the tRNA is critical because this region binds to the complementary region of a 7-nt bulge found in the antiterminator structure of the leader (Figure 7) (Yousef et al., 2003). Additionally, the orientation or register of the 3' end is important in promoting antitermination. Introduction of a half turn in the acceptor stem results in a loss of transcriptional read-through, whereas incorporation of a full turn in the RNA helix restores T box function (Yousef et al., 2003). Interaction of the 3' end is thought to be important in stabilizing the thermodynamically unfavorable antiterminator structure. The tRNA anticodon must also be conserved to facilitate the binding of the tRNA to the cognate specifier region.

1.5.3 Function and Specificity of T box mRNA Leaders

1.5.3.1 *proBA* and *proI* mRNA Leaders

In *B. subtilis*, the amino acid proline plays important functions in regulating osmotic

stress and protein synthesis (Brill et al., 2011a, 2011b). Interestingly, there are two independent pathways that are responsible for regulating proline levels in *B. subtilis* (Brill et al., 2011b; Hahne et al., 2010). The ProJ-ProA-ProH pathway produces high concentrations of proline used to regulate osmotic stress, whereas the ProB-ProA-ProI pathway is responsible for creating a less concentrated reserve of proline specific for protein synthesis (Brill et al., 2011b). Interestingly, only the ProB-ProA-ProI pathway is regulated by the T box mechanism (Brill et al., 2011b).

The *proBA* and *proI* mRNA leaders possess canonical secondary structural elements that are necessary for tRNA-mediated transcriptional regulation (Brill et al., 2011b). Both the *proBA* and the *proI* mRNA leaders contain a CCU sequence in their specifier domains, resulting in the leaders being responsive to changes in $tRNA^{Pro}$ concentration (Brill et al., 2011b). When *B. subtilis* is starved for proline, there is an increase in full-length *proBA* and *proI*, indicating that the mRNA leader was able to stabilize the antiterminator structure and read-through of the downstream gene took place (Brill et al., 2011b). Interestingly, the specificity of the leader to $tRNA^{Pro}$ concentration can be manipulated by changing the CCU sequence in the specifier domain to UUC, which is specific for $tRNA^{Phe}$. Altering the specificity of the *proBA* mRNA leader results in a loss of specificity to proline, but yields a gain in sensitivity to phenylalanine (Brill et al., 2011b).

1.5.3.2 *lysS* and *lysK* mRNA Leaders

In Gram-positive bacteria, expression of aminoacyl tRNA synthetase (AARS) genes are typically controlled by tRNA mediated transcriptional regulation (Vitreschak et al., 2008). These enzymes are responsible for adding amino acids to their cognate tRNA molecule (Beuning and Musier-Forsyth, 1999). Although AARSs carry out similar functions,

the enzyme family is divided into two classes: class I, which adds the amino acid to the 2'-hydroxyl of the terminal residue of the acceptor stem of the tRNA molecule, and class II, which adds the amino acid to the 3'-hydroxyl position (Beuning and Musier-Forsyth, 1999). Both class I and class II enzymes are structurally distinct and unrelated phylogenetically (Ibba and Soll, 2000; O'Donoghue and Luthey-Schulten, 2003).

Although most AARSs fall into one category or another, the Lysyl-tRNA synthetase (LysRS) is found as both a class I and a class II enzyme (Ibba et al., 1994). Most bacteria contain a single copy of the class I or the class II LysRS gene. However, there are four species of bacteria that contain functional copies of both class I and class II LysRSs, with one of the LysRSs being T box regulated (Foy et al., 2010). These species include all *Bacillus cereus* strains except AH820, *Bacillus thuringiensis*, *Clostridium beijerinckii*, and *Symbiobacterium thermophilum* (Foy et al., 2010). In all four species, only one of the LysRS genes is T box regulated (Foy et al., 2010). Interestingly, in the phylogenetically related species *B. cereus* and *B. thuringiensis*, the class I gene is T box regulated, whereas the class II gene in *S. thermophilum* is T box regulated (Foy et al., 2010). The mRNA leader from *S. thermophilum* shows little similarity to the conserved sequence found in most *Bacillus* species (Foy et al., 2010). Notably, *C. beijerinckii* contains two class II LysRS genes, but only one of them is under T box control, sharing only 50% similarity to the consensus sequence (Foy et al., 2010).

Although *B. subtilis* is phylogenetically related to *B. cereus* and *B. thuringiensis*, it only contains a single class II LysRS, which is denoted as *lysS* and it is not regulated by tRNA-mediated transcriptional regulation. In *B. cereus* the class I LysRS gene, *lysK*, is expressed mainly during stationary phase and is less efficient at charging its cognate tRNA

(Foy et al., 2010). Although most genes that are T box regulated are sensitive to depletion of a specific amino acid and show little to no promiscuity to other amino acids, the *lysK* gene from *B. cereus* appears to be sensitive to depletion in asparagine concentrations (Foy et al., 2010).

1.5.3.3 *thrS* and *thrZ* mRNA Leaders

In contrast to the unique class I LysRS in *B. subtilis*, which is not T box regulated, *B. subtilis* contains two independent genes that produce two functional copies of the threonyl-tRNA synthetase (ThrRS), which is unusual because bacteria normally only possess a single copy of a specific AARS (Putzer et al., 1990). The *B. subtilis thrS* and *thrZ* are located in different sections of the chromosome and are expressed at different stages of growth, with *thrS* being the main product expressed during vegetative growth (Putzer et al., 1990). Additionally, the two genes share 51% sequence similarity, indicating that the two genes are phylogenetically distinct (Putzer et al., 1990). In contrast to the LysRS genes from *B. cereus*, *B. thuringiensis*, *S. thermophilum*, and *C. beijerinckii* where only one LysRS gene is T box regulated, both ThrRS genes in *B. subtilis* are T Box regulated (Putzer et al., 1992). Additionally, both mRNA leaders share a conserved sequence that is common to other T box mRNA leaders found in Gram-positive bacteria (Putzer et al., 1992).

Unlike most genes regulated by the T box mechanism, the 5'-untranslated mRNA leader of *thrZ* is comprised of three domains with each domain containing structural elements that are usually present in T box regulated genes (Putzer et al., 1992). Domains II and III are practically identical; however, domain I possesses an open reading frame that encodes for five threonine residues (Putzer et al., 1992). Despite the variation in the mRNA leaders, both the *thrS* and *thrZ* genes are sensitive to threonine concentrations and do not show any

promiscuity to other aminoacyl-tRNAs (Putzer et al., 1992).

1.5.3.4 *glyQS* mRNA Leader

Unlike the multiple copies of the LysRS and ThrRS genes in *B. cereus* and *B. subtilis*, respectively, *glyQS*, which codes for the glycyl-tRNA synthetase, is unique and T box regulated (Grundy and Henkin, 2004; Yousef et al., 2003). Although *glyQS* is T box regulated, its mRNA leader differs significantly from other mRNA leaders found in *Bacilli* that are regulated by the T box mechanism (Grundy and Henkin, 2004; Yousef et al., 2005). Typically, the mRNA leaders of genes that are controlled by tRNA-mediated transcriptional regulation contain three stem-loop motifs, which are identified as I, II, IIA/B, and III (Grundy et al., 2002, 2005; Luo et al., 1998). To date, only the *glyQS* leader from *B. subtilis* has been found to not have Stem II or the Stem IIA/B pseudoknot motifs (Yousef et al., 2005). Although there are variations in the secondary structure of the *glyQS* mRNA leader, the gene is tightly regulated by its cognate tRNA and does not show any promiscuity to other tRNAs. However, when the specifier codon of the *glyQS* mRNA leader is changed to UAC (specific for $tRNA^{Tyr}$) and the discriminator base is changed from an A to a U, $tRNA^{Tyr}$ is able to initiate antitermination of the tyrosyl-tRNA specific *glyQS* leader ($glyQS^{Tyr}$) (Grundy et al, 2002).

In vitro studies with unmodified $tRNA^{Gly}$ in the presence of the *glyQS* mRNA leader demonstrate that antitermination can occur without the aid of additional factors, suggesting that T box function was due to the RNA factors of the system (Grundy et al., 2002). Surprisingly, when unmodified $tRNA^{Tyr}$ was in the presence of the $glyQS^{Tyr}$ mRNA leader, antitermination was not observed. However, if $tRNA^{Tyr}$ was isolated from natural sources −and therefore fully modified− and used with $glyQS^{Tyr}$, antitermination was achieved, but the

response was not as robust as $tRNA^{Gly}$ with the *glyQS* leader (Grundy and Henkin, unpublished). Surprisingly, unmodified $tRNA^{Tyr}$ can be charged with tyrosine, indicating that the tertiary structure of the tRNA has not been compromised. Since native $tRNA^{Gly}$ is not modified in the anticodon loop, it is possible that the lack of modifications in the *in vitro* transcribed $tRNA^{Tyr}$ is preventing it from functioning in an *in vitro* antitermination assay. This implies that base modifications may be important in stabilizing the interaction between the tRNA and its cognate mRNA leader.

1.5.3.5 *tyrS* and *tyrZ* mRNA Leader

In *E. coli* it is uncommon to find two phylogenetically distinct genes that code for an AARS that shares the same function (LysRS is an exception). However, in *Bacilli* such as *B. subtilis* and *B. anthracis*, it is slightly more common to find a second gene that codes for a specific AARS. Nevertheless, ThrRS and tyrosine tRNA synthetase (TyrTS) genes appear to be the exception. In *B. subtilis* the two TyrTS genes are *tyrS* and *tyrZ.* Similar to the ThrRS genes, only one of the TyrTS genes from *B. subtilis*, *tyrS*, was expressed during vegetative growth (Henkin et al., 1992). In contrast to the *thrZ* gene, little is known about the mRNA leader from *tyrZ* or its regulation.

Similar to other genes that are T box regulated, *tyrS* expression was not sensitive to concentration changes of non-cognate tRNA, however, modification of the specifier codon promoted specificity for a non-cognate tRNA (Grundy and Henkin, 1993; Grundy et al., 1997). For example, *in vivo* studies using *B. subtilis* where the UAC specifier codon (specific to $tRNA^{Tyr}$) of the *tyrS* gene was mutated to UUC (specific for $tRNA^{Phe}$) resulted in a 5.7-fold induction of the $tyrS^{UUC}$ gene by limiting concentrations of phenylalanine (Grundy et al., 1997). However, mutation of the UAC specifier codon to the asparagine specific codon AAC

and the antiterminator base from U to C did not result in an induction of the *TyrS*^{AAC} gene (Grundy et al., 1997). Additionally, mutating the specifier codon to the threonine codon, ACC, in combination with the U222A mutation led to a weak 2.4 fold induction of the *TyrS*^{ACC} gene (Grundy et al., 1997), indicating that there must be a unique property about tRNA^{Tyr}, as the leader RNA shares similarity to other T box leaders found in Gram-positive bacteria.

Chapter 2

Materials and Methods

2.1 Chemical and Enzymatic Reagents

All enzymes were purchased from Sigma Chemical, except for T7 RNA polymerase and MiaA, which were prepared as described (Davanloo et al., 1984; Leung et al., 1997). Deoxyribonuclease I type II, pyruvate kinase, adenylate kinase, and nucleotide monophosphate kinase were obtained as powders, dissolved in 15% glycerol, 1 mM dithiothreitol, and 10 mM Tris-HCl, pH 7.4, and stored at -20 ˚C. Guanylate kinase and nuclease P1 were obtained as solutions and stored at -20 ˚C. Unlabeled 5' nucleoside triphosphates (5'-NTPs) were purchased from Sigma, phosphoenolpyruvate (potassium salt) was purchased from Bachem, and 99% [^{15}N]-ammonium sulfate and 99% [^{13}C]-methanol were purchased from Cambridge Isotope Labs. γ, γ-dimethylallyl diphosphate was purchased from Sigma.

2.2 Preparation of RNA

The RNA sequence for *B. subtilis* ASL^{Tyr} shown in Figure 8 was synthesized *in vitro* using T7 RNA polymerase and a synthetic DNA template. The nucleotide sequence of the stem corresponds to residues G_{27} to C_{43} of full-length *B. subtilis* ASL^{Tyr}. Unlabeled RNA molecules were prepared using 10 ml transcription reactions containing 4 mM 5'-NTPs. Isotopically labeled RNA molecules were prepared using 10 ml transcription reactions containing 3 mM uniformly [^{13}C-^{15}N]-enriched 5'-NTPs as described (Nikonowicz et al.

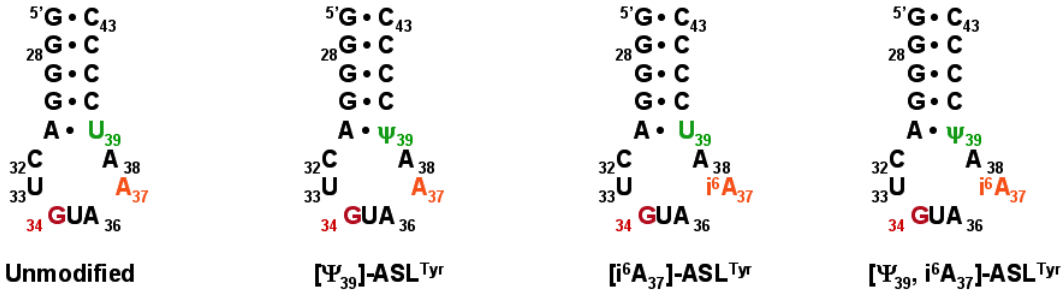

Figure 8. ASL^{Tyr} Hairpins Used in this Study

The hairpins used in this study were 17 nucleotides in length. The unmodified and [i^{6}A$_{37}$]-ASL^{Tyr} are isotipically labeled. The [Ψ$_{39}$]- and [Ψ$_{39}$, i^{6}A$_{37}$]-ASL^{Tyr} molecules are naturally abundant. The i^{6}A$_{37}$ modification was added enzymatically using the MiaA enzyme, which was expressed and purified. The Ψ$_{39}$ modification was chemically synthesized.

1992; Batey et al. 1992). After synthesis, RNA molecules were purified by passage through 20% (w/v) preparative polyacrylamide gels, electroeluted (Schleicher & Schuell), and precipitated with ethanol. The purified oligonucleotides were initially dissolved in 3 mL high salt NMR buffer (1 M NaCl, 20 mM potassium phosphate, pH 6.1, and 2 mM EDTA), and subsequently dialyzed against 1.5 mL low salt NMR buffer (10 mM KCl, 10 mM potassium phosphate, pH 6.1, and 0.02 mM EDTA) three times using a Centricon-3 concentrator (Amicon Inc.). The samples were diluted with the low salt NMR buffer to a volume of 300 μl and lyophilized to a powder. For experiments involving the non-exchangeable protons, the samples were exchanged twice with 99.9% D_2O and then dissolved in 300 μl of 99.96% D_2O. For experiments involving detection of the exchangeable protons, the samples were dissolved in 300 μl of 90% H_2O / 10% D_2O. The samples used for spectroscopic analysis contained 50-110 A_{260} OD units of RNA oligonucleotide in 300 μl (≈1.2–2.5 mM). The [Ψ_{39}]-ASL^{Tyr} oligonucleotide was chemically synthesized (Dharmacon, Boulder, CO), ethanol precipitated after deprotection, and dialyzed as described above to obtain material for spectroscopic analysis.

2.3 Preparation of the A_{37} (N^6)–Dimethylallyl Modified ASL^{Tyr}

The dimethylallyl group was introduced at position A_{37} of purified ASL^{Tyr} and [ψ_{39}]-ASL^{Tyr} oligonucleotides using the enzyme dimethylallyl diphosphate:tRNA transferase (MiaA) and dimethylallyl pyrophosphate (DMAPP) as reported (Cabello-Villegas et al, 2001.). Histidine-tagged MiaA was expressed in *E. coli* and purified using Ni^{2+} affinity resin as described (Leung et al., 1997). The modification reactions contained 50 μM oligonucleotide, 125 μM DMAPP, 50 mM Tris-HCl pH 7.6, 10 mM $MgCl_2$, 0.1 mg/ml BSA,

5mM β-mercapto-ethanol, and 26 μg/ml MiaA. The reactions were incubated overnight at 30 °C. Upon completion, the RNA was extracted with phenol:chloroform:isomayl alcohol (25:24:1) and chloroform, and the RNA precipitated with ethanol. Product formation was monitored using 20% denaturing PAGE, because the N6-modified oligonucleotides migrate slower than unmodified ASL^{Tyr}. The band shift is equivalent to that observed when 1 additional nucleotide is added to an oligonucleotide. The reaction was determined to be >98% complete by comparing CH-HSQC spectra.

2.4 NMR Spectroscopy

All spectra were acquired on Varian Inova 500 MHz (^{1}H-[^{13}C, ^{15}N, ^{31}P] probe) and 600 MHz (^{1} H-[^{13}C, ^{15}N] cryoprobe) spectrometers. Solvent suppression for ^{1}H homonuclear spectra collected in 90% H_2O was achieved using the binomial scheme. The data points were extended by 25% using linear prediction for the indirectly detected dimensions. NMR spectra were processed and analyzed using Felix 2007 (Felix NMR Inc., San Diego, CA).

Two-dimensional (2D) ^{13}C-^{1}H HSQC spectra were collected to identify ^{13}C-^{1}H chemical shift correlations. Sugar spin systems were assigned using 3D HCCH-TOCSY (16 ms and 24 ms DIPSI-3 spin lock) experiments collected in D_2O. A 3D HCCH-TOCSY (56 ms DIPSI-3 spin lock) was collected to establish the intra-base H2-C2-C8-H8 correlations in adenine residues. A 3D HCN experiment (Marino et al. 1997) was used to identify intra-residue base-ribose correlations.

Sequential assignments and distance constraints for the non-exchangeable resonances were determined at 25 °C from 2D ^{1}H -^{1}H NOESY spectra (τ_m = 120, 180, and 460 ms) and 3D ^{13}C-edited NOESY spectra (τ_m = 180 and 400 ms). Pyrimidine C2 and C4 resonances

were assigned from H6-C2 and H5-C4 correlations using 2D H(CN)C and 2D CCH-COSY experiments. 2D ^{15}N-^{1}H HSQC spectra optimized for 2-bond HN couplings were collected to identify purine N7 and adenine N1 and N3 resonances. For the exchangeable resonances, 2D ^{15}N-^{1}H HSQC spectra were collected to identify ^{15}N-^{1}H chemical shift correlations. 2D NOESY spectra (τ_m = 160 and 360 ms) were acquired in H_2O at 12 °C to obtain distance constraints involving exchangeable protons.

$^{3}J_{H-H}$ and $^{3}J_{P-H}$ coupling constants were estimated using DQF-COSY and ^{31}P-^{1}H HetCor experiments, respectively. $^{3}J_{C-P}$ coupling constants were estimated for ASL^{Tyr} and [$i^{6}A_{37}$]-ASL^{Tyr} using the ^{13}C-^{1}H ct-HSQC spin-echo difference method (Legault et al., 1995).

2.5 Distance and Torsion Angle Constraints

Interproton distance estimates were obtained from cross peak intensities in 2D NOESY and 3D ^{13}C-edited NOESY spectra. Using the covalently fixed pyrimidine H5-H6 distance (≈2.4 Å) and the conformationally restricted sugar H1'-H2' distance (2.8-3.0 Å) as references, peak intensities were classified as strong, medium, weak, or very weak and their corresponding proton pairs given upper bound distance restraints of 3.0, 4.0, 5.0, or 6.0 Å, respectively. Cross peaks observed only at mixing times ≥180 ms were classified as extremely weak and given 7.0 Å upper bound distance constraints to account for the possibility of spin diffusion. All distance restraints were given lower bounds of 0.0 Å to improve convergence of the calculations. Only the intra-residue sugar-to-sugar constraints involving H5' and H5" resonances included in the calculations are considered conformationally restrictive. Distance constraints involving exchangeable protons were estimated from 360 ms mixing time NOESY spectra and were classified as weak, very weak, or extremely weak.

Watson-Crick base pairs were identified by observation of a significantly downfield shifted NH or NH_2 proton resonance and the observation of strong G-C NH–NH_2 or A-U H2–NH NOEs. The C_{32}-A^+_{38} interaction was based on the A_{38} C2 upfield chemical shift (Simorre et al., 1996). Hydrogen bonds were introduced as distance restraints of 2.9 ± 0.3 Å between donor and acceptor heavy atoms and 2.0 ± 0.2 Å between acceptor and hydrogen atoms.

Ribose ring pucker and backbone dihedral constraints were derived from $^3J_{HH}$, $^3J_{HP}$, and $^3J_{CP}$ couplings (Varani et al., 1996). Ribose rings with $^3J_{H1'-H2'} > 7$ Hz and with C3' and C4' resonances between 76-80 and 85-86 ppm, respectively, were constrained to C2'-*endo*. Residues with $^3J_{H1'-H2'} < 5$ Hz and C3' resonances between 70-74 ppm were constrained to C3'-*endo*. Residues with intermediate $^3J_{H1'-H2'}$ couplings were left unconstrained. For residues 27-33 and 37-43, γ was constrained to the *gauche*$^+$ conformation (50 ± 40°) (Varani et al., 1996). The NOE intensities for these residues of ASL^{Tyr} and [i^6A_{37}]-ASL^{Tyr} with resolved H4'-H5' and H4'-H5" NOE cross peaks are consistent with the *gauche*$^+$ conformation. γ was left unconstrained for the anticodon residues. The conformations of the γ torsion angles of [Ψ_{39}]-ASL^{Tyr} and [i^6A_{37}, Ψ_{39}]-ASL^{Tyr} from G_{27}-C_{32} and A_{38}-C_{43} could not be confirmed as *gauche*$^+$ due to spectral overlap, but the conservation of ^1H chemical shifts between the corresponding structures, NOE patterns, and ^{31}P-^1H scalar couplings support regular A-form geometry. Dihedral angle restraints for the β and ε torsion angles were derived from $^3J_{P-H5'}$, $^3J_{P-H5"}$, and $^3J_{P-H3'}$ couplings estimated in 2D ^{31}P-^1H HetCor spectra and $^3J_{P-C2'/P-C4'}$ couplings measured in 2D ct-HSQC spin-echo difference spectra. For stem residues, β was constrained to the *trans* conformation (180 ± 40°). β was loosely constrained to the *trans* conformation (180 ± 70°) for loop residues except G_{34}-A_{37}. ε was constrained to the *trans* conformation (-

150 ± 50°) for residues with $^{3}J_{P\text{-}H3'} > 5$ Hz or $^{3}J_{P\text{-}C2'} > 5$ Hz. P–C2' couplings of ASL^{Tyr} and [$i^{6}A_{37}$]-ASL^{Tyr} indicate that the ε angles of G_{27}-C_{32} and A_{38}-C_{42} have the A-form *trans* conformation. α and ζ were constrained to -70 ± 30° for the stem residues (G_{27}-C_{32} and A_{38}-C_{43}). Because a down-field shifted ^{31}P resonance is associated with the *trans* conformation of α or ζ, and because no such shift is observed for any of the ^{31}P resonances in the RNA molecules, α and ζ were loosely constrained to exclude the *trans* conformation (0 ± 120˚) for residues U_{33}-A_{37}. No dihedral angle constraints were used for the glycosidic angle χ.

2.6 Structure Calculations and Refinement

An initial set of structures was calculated using a shortened version of the simulated annealing protocol (described below). A list of all proton pairs in the calculated structures closer than 5.0 Å (representing expected NOEs) was compared to the list of restraints. The NOESY spectra were then re-examined for predicted NOEs absent from the constraint list. In some cases, this allowed the unambiguous assignment of previously unidentified NOEs, but, in other cases, the predicted NOEs were unobservable due to spectral overlap or the broadening of resonances by exchange with solvent.

Structure refinement was carried out with simulated annealing and restrained molecular dynamics (rMD) calculations using Xplor-NIH v2.19 (Schwieters et al., 2003). Starting coordinates for ASL^{Tyr} were generated using Insight II (Accelrys, San Diego, CA) and were based on standard A-form helical geometry. Starting coordinates for the [Ψ_{39}]-ASL^{Tyr} model were created by atom replacement within the ASL^{Tyr} model coordinate file. Starting coordinates for the [$i^{6}A_{37}$]-ASL^{Tyr} and [Ψ_{39}, $i^{6}A_{37}$]-ASL^{Tyr} models were created by adding dimethylallyl groups to the A_{37} N6 atoms of the ASL^{Tyr} and [Ψ_{39}]-ASL^{Tyr} models,

respectively, using Insight II. Parameters for the Ψ_{39} and i^6A_{37} residues were obtained from (Charette et al. 2000). The structure calculations were performed in two stages. Beginning with the energy minimized starting coordinates, 50 structures were generated using 80 ps of rMD at 1200K with hydrogen bond, NOE-derived distance and base-pairing restraints. The system then was cooled to 25 K over 12 ps of rMD. Force constants used for the calculations were increased from 2 kcal mol^{-1} $Å^{-2}$ to 30 kcal mol^{-1} $Å^{-2}$ for the NOE and from 2 kcal mol^{-1} rad^{-2} to 30 kcal mol^{-1} rad^{-2} for the dihedral angle constraints. Each structure was then minimized with restraints at the end of the rMD. Ten structures were selected for the final refinement. The criteria for final structure selection included lowest energies, fewest constraint violations, and fewest predicted unobserved NOEs (^{1}H pairs less than 3.5 Å apart, but no corresponding cross peak in the NOE spectra). A second round of rMD was performed on these structures using protocols similar to those used in the first round of structure calculation. The major difference was the starting temperature of 300 K followed by cooling to 25 K over 28 ps of rMD. Ten refined structures for each model were analyzed using Xplor-NIH and Insight II.

2.7 Accession Numbers

Coordinates were deposited in the Protein Data Bank under accession numbers PDB ID: 2lac, 2la9, 2lbq, 2lbr. Chemical shifts have been deposited in the Biomolecular Magnetic Resonance Bank under accession numbers BMRB ID: 17517, 17520, 17572, and 17573.

2.8 UV Thermal Melting of Unmodified and Partially Modified RNA Hairpins

RNA stability was measured by monitoring the hyperchromic shift of the RNA hairpin bases using a Pharmacia Ultrospec 2000 UV-Visible spectrophotometer equipped with a peltier melting apparatus. UV melting studies were performed using 0.5 A_{260} units

RNA hairpin dissolved in low salt NMR buffer, pH 6.3. The samples were heated to 90°C for 90 s and cooled on ice before each melting experiment. A_{260} absorbance spectra from 10-92 °C were acquired (1.0 °C per minute). The melting curves were acquired in triplicate and are reported as the average value from all experiments.

2.9 Differential Scanning Calorimetry

Measurements were performed using a VP-DSC differential scanning microcalorimeter (MicroCAl, LLC, Northampton, MA) at a scan rate of 90°C h^{-1}. The RNA hairpin concentration was 10 μM in low salt NMR buffer at pH 6.3. Before measurements, the RNA hairpins were heated to 90°C for 90 s and snap cooled on ice. Following the cooling, the sample and buffer were degassed for 15 min at room temperature. During the heating cycles, a pressure of 2 atm was maintained in the cells to prevent degassing. A background scan collected with buffer in the sample and reference cells was subtracted from each scan. Data were analyzed with Origin 7.0 software (MicroCal) to obtain the melting transition temperature (T_m), the calorimetric enthalpy of thermal unfolding (ΔH), and the van't Hoff enthalpy. All DSC measurements were performed in triplicate and thermodynamic values represent the average from all three experiments.

2.10 Strains and Culture Conditions

The attenuated *Bacillus anthracis* Sterne strain 7702 ($pXO1^+$ $pXO2^-$) and isogenic mutants were employed for all functional and physiological studies (Table 1). Unless specified, *B. anthracis* strains were cultured at 37°C with shaking (225 rpm) in either Luria Bertani (LB) or RM (Leppla, 1988) medium. NovaBlue (Novagen) *Escherichia coli* K-12 strain was used as a host for cloning, and *E. coli* strain GM2163 was used to generate non-

Table 1 . *B. anthracis* Strains and Plasmids.

Name	Description	Reference
Strains		
7702	Sterne strain; $pXO1^{+}$ $pXO2^{-}$	Guillen et al., 1989
miaB–	*miaB*-null mutant, derivative of 7702	This study
tgt–	*tgt*-null mutant, derivative of 7702	This study
miaA–	*miaA*-null mutant, derivative of 7702	Kerri Thomason
Plasmids		
pHY304	Temperature-sensitive vector used for markerless deletion; Erm^{r}	Chaffin et al., 2005

methylated DNA. *E. coli* strains were cultured in LB at 37°C with shaking (250 rpm). When required, antibiotics were added at the following concentrations: ampicillin (100 μg/ml for *E. coli*), spectinomycin (100 μg/ml for *B. anthracis* and 50 μg/ml for *E. coli*), and erythromycin (5 μg/ml for *B. anthracis* and 300 μg/ml for *E. coli*).

2.11 Plasmid DNA Isolation and Manipulation

Cloning experiments employing *E. coli* were performed using standard protocols (Ausubel, F.M. 1993). Plasmid DNA was extracted from *E. coli* using a Wizard miniprep kit (Promega, Madison, WI) in accordance with the manufacturer's recommendations. After sequence verification, constructs were transformed into *E. coli* strain GM2163 to obtain nonmethylated plasmid. The nonmethylated plasmid was isolated and purified from GM2163 and used for electroporation of *B. anthracis* (Koehler et al., 1994).

2.12 Construction of *B. anthracis* Mutants

Null mutants were created by inserting stop codons near the 5' ends of the genes using pHY304, a temperature-sensitive vector containing an erythromycin resistance gene (Chaffin et al. 2005). The genes plus 0.2-kb to 1-kb of the flanking sequences was obtained by PCR (Table 2) and cloned into pGEM-T (Stratagene). A nonsense codon was introduced into the gene of interest after approximately 25 % of the coding region by primer-directed mutagenesis and amplified by PCR (Table 2). The genes containing the nonsense codon were cloned into pHY304 and electroporated into *B. anthracis* (Koehler et al., 1994). The electroporation mixture was plated on LB agar medium containing erythromycin and incubated at 30°C for 2 days to select colonies containing the plasmid. Clones were verified using PCR (*Taq* polymerase; NEB, Ipswich, MA), restreaked on the same medium, and

incubated at 30°C. An isolated colony was used to inoculate LB medium containing erythromycin, and was incubated at 30°C over night (O/N). To obtain an isolate with the pHY304 derivative integrated into the chromosome by a single crossover recombination event, the culture was passaged at a 1:1000 dilution into LB containing erythromycin and cultured at 41°C (the nonpermissive temperature for pHY304) O/N. Following a second passage at 1:1000 dilution under the same conditions, the culture was streaked onto selective LB agar and incubated at 41°C O/N. A single isolate was inoculated into LB medium without antibiotic, cultured at 30°C O/N, and then passaged at a 1:1000 dilution multiple times. Beginning with passage 3, serial dilutions of the culture were plated at 30°C O/N. Single colonies were streaked onto LB agar with and without erythromycin and incubated at 37°C O/N. Erythromycin-sensitive isolates were screened for loss of the plasmid and the nonsense mutation.

2.13 Growth Curves and Kinetics

Single isolates of the 7702 strain and isogenic mutant strains were grown to early stationary phase (3–4 OD_{600}) in LB medium and transferred to 25 ml fresh RM or RM^{-Tyr} medium at a starting OD_{600} of approximately 0.1. Cells were cultured at 37 ºC for 7 h and the OD_{600} was determined hourly. The doubling time was determined by the following equation: $(t_2\text{-}t_1)/3.3*\log(b/B)$ where $t_1\text{-}t_2$ = the duration of the exponential growth, b = the final culture concentration, and B = the initial culture concentration.

2.14 Minimum Inhibitory Concentration

Five isolates of either the 7702 strain or the isogenic mutant strain were picked and gown in LB medium for 4-6 h. The culture was diluted to OD_{600} = 0.08. Cells were further diluted 1:100 and 50 µl was used to inoculate 50 µl of the antibiotic dilution. Antibiotic

Table 2. Primers used for Gene Amplification, Mutagenesis, and qRT-PCR

Target Gene	Primers
miaB	5'-ACCGCTGCGCCCGTTTCACCCTTC
	5'-GGTAATGTTTATAGGGATAAAGCA
miaB	5'-GTGCAGTGAAAACTATACCCGCCATTACTTCTG
mutagenesis	5'-CAGAAGTAATGGCGGGTATAGTTTTCACTGCAC
tgt	5'-AAGCTTTGACGCTTTTGTTGCGGGCG
	5'-AAGCTTTTGCATCTCACGCTAAAATGGG
tgt	5'-CCTGCTTCACGAATCTAGATTTCGTGACCTGG
mutagenesis	5'-CCAGGTCACGAAATCTAGATTCGTGAAGCAGG

dilutions were prepared with LB and their concentrations decreased by a factor of two, with 64 μg/ml as the highest concentration tested and .125 μg/ml as the lowest concentration tested. The antibiotics used in this study were Tetracycline, Ampicillin, Spectenomycin, Erythromycin, Ciprofloxacin, Penicillin G, and Kanamycin. The cells were incubated in a 96-well plate without shaking at 37 ºC for 16 h.

2.15 RNA Purification

A single isolate was grown in LB medium to early stationary phase and was used to inoculate 25 ml of RM or RM^{-Tyr} medium to a starting OD_{600} = 0.08 to 0.1. The cultures were incubated until mid-exponential (OD_{600} = 0.5 to 0.6) growth phase. 6-ml samples were taken during exponential phase, and 2-ml samples were collected during the early stationary phase of growth. Cells were pelleted at 13,000 rpm for 2 min at room temperature. All subsequent centrifugation steps were done at 13000 rpm at 4 ºC, and samples were kept on ice except where noted. Cell pellets were resuspended in 500 μl of culture supernatant and transferred to a 1.5-ml screw-cap tube containing 500 μl of 0.1-mm zirconia/silica beads (BioSpec Products, Bartlesville, OK) and 500 μl of acid phenol warmed to 65°C (Sigma Aldrich, St. Louis, MO). The cell suspension underwent bead beating for 1 min using a Mini BeadBeater (BioSpec Products). The tube was placed at 65°C for 5 min, followed by a second round of bead beating. The cell suspension was centrifuged for 3 min and the aqueous phase was transferred to a new 2-ml tube. Acid phenol was added and the supernatants were vigorously vortexed for 15 s then put on ice for 5 min. The supernatants underwent centrifugation and the aqueous phase was transferred to a new 2-ml tube, 0.3 volumes of chloroform was added, and the contents were vortexed vigorously. The suspension was incubated for 10 min on ice and inverted every 2 min to avoid separation of phases. Samples were centrifuged for 15 min,

the aqueous phase was mixed with ½ of the starting volume (of the aqueous phase) of water and 1 volume of isopropanol. After a 10 min incubation on ice, RNA was pelleted using centrifugation for 15 min. Pellets were washed in 75% cold ethanol, air dried, and resuspended in 50 μl of water. The final concentrations of RNA ranged from 400 to 1000 ng/ul, as determined using a NanoDrop ND-1000 (NanoDrop Technologies, Wilmington, DE).

2.16 Quantitative Real-Time PCR

The quantitative Real-Time PCR (qRT-PCR) experiments were carried out by the Quantitative Genomics Core Laboratory at The University of Texas Health Science Center at Houston. Primers (sequences not shown) were designed for the 5′-UTR and coding sequences of *tyrS1* and *tyrS2* from the *B. subtilis* ames strain. Primers (sequences not shown) were also designed for *gyrB*, which served as an internal control. The reactions were carried out using 5 mM $MgCl_2$, 1X JumpStart PCR buffer, 200 μM dNTPs, 400 nM forward primer, 400 nM reverse primer, 100 nM fluorescence tagged reverse primer, and .25 U JumpStart Taq. The reactions were carried out in a total volume of 16 μl using a LC480 thermocycler and performed in triplicate.

*Sections 2.1 through 2.9 are courtesy of Denmon, et al., 2011

Chapter 3

Results

3.1 Structural and Stability Effects of Partial Modification of *B. subtilis* ASL^{Tyr}

Currently there are no structures available of a tRNA molecule from *B. subtilis*, which is one of the most studied Gram-positive bacteria. Aside from the limited information regarding tRNA structure (specifically $tRNA^{Tyr}$), there is even less knowledge regarding the contribution of individual base modifications on the known tRNA structures. Therefore, UV melting and DSC experiments were employed to elucidate the effects of base modification on the ASL^{Tyr} and heteronuclear NMR was used for structure determination of the unmodified and partially modified ASL^{Tyr} hairpins.

3.1.1 Enzymatic Modification of the Unmodified ASL^{Tyr} and $[\Psi_{39}]$-ASL^{Tyr}

The dimethylallyl group was introduced at position 37 in both the unmodified ASL^{Tyr} and $[\Psi_{39}]$-ASL^{Tyr} molecules enzymatically using MiaA and DMAPP. Upon completion of the *in vitro* reaction, the modified RNA gives the appearance of a molecule with a residue count of n + 1 when ran on a 20% Urea polyacrylamide gel (Figure 9).

3.1.2 Resonance Assignments of ASL^{Tyr} Molecules

The oligomeric states of the RNA molecules were examined to confirm formation of the hairpin secondary structure. The monomeric nature of the RNA is supported by moderate line widths (9-14 Hz ^{1}H) and the near identical cross peak patterns in NH spectra at low (20 μM) and high (1.4 mM) RNA concentrations. The RNAs also run as single bands on native PAGE (data not shown), consistent with a single form. The non-exchangeable ^{1}H and ^{13}C

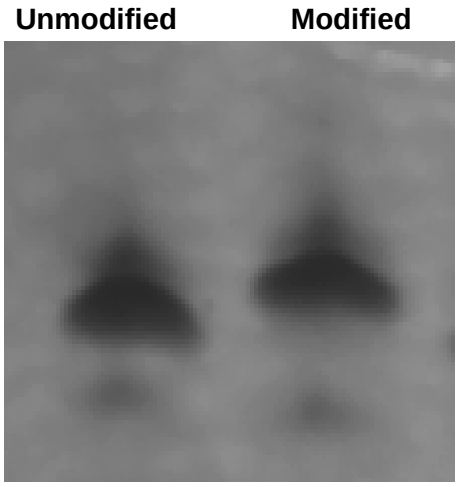

Figure 9. Enzymatic Modification of the [Ψ_{39}]-ASL^{Tyr} with MiaA

The modification reaction was carried out using 50 μM [Ψ_{39}]-ASL^{Tyr}, 125 μM DMAPP (dimethylallyl diphosphate), 50 mM Tris-HCl pH 7.6, 10 mM $MgCl_2$, 0.1 mg/ml BSA, 5 mM β-mercapto ethanol, and 26 μg/ml MiaA. The unmodified and modified samples were run on a 20% 7M Urea gel. The lower band is degraded RNA. The modified hairpin gives the appearance of a molecule with a residue count of n + 1.

resonances of ASL^{Tyr} and $[i^6A_{37}]$-ASL^{Tyr} (Figures 11 and 13) were assigned using standard heteronuclear techniques (Dieckmann and Feigon, 1997; Pardi, 1995). The $[i^6A_{37}]$-ASL^{Tyr} sample required 2.0 mM $Co(NH_3)_6^{3+}$ to achieve a conformationally homogeneous state and to reduce exchange broadening. For ASL^{Tyr} and $[i^6A_{37}]$-ASL^{Tyr}, most base and ribose ^1H and ^{13}C correlations are resolved (Figure 10). The A_{38} C2 resonance of unmodified ASL^{Tyr} is slightly broadened but has a chemical shift of 149.2 ppm indicative of protonation (Figure 10) (Legault and Pardi, 1994). For $[i^6A_{37}]$-ASL^{Tyr}, the A_{38} C2 resonance shifts downfield to 153.6 ppm, indicative of the non-protonated form of A. In the absence of $Co(NH_3)_6^{3+}$, the A_{38} C2 resonance is very broad (≈130 Hz) with a chemical shift centered at 151.8 ppm. Also for $[i^6A_{37}]$-ASL^{Tyr}, the A_{36} C8H8 resonance is absent from the ^{13}C-^1H HSQC spectrum in the absence of metal ions. All the ribose spin systems, except for the incompletely labeled 5'-terminal nucleotide, were identified using 2D or 3D HCCH-COSY and HCCH-TOCSY experiments. Three of the four adenine residues in ASL^{Tyr} yield intra-base H8-H2 correlations in the HCCH-TOCSY spectrum. The A_{38} H2-H8 correlation is not observed. Intra-residue base-to-sugar correlations were identified using 2D H(C)N experiments to obtain correlations H6-N1, H8-N9, and H1'-N1/N9. All pyrimidine correlations and all (ASL^{Tyr}) or six of eight ($[i^6A_{37}]$-ASL^{Tyr}) purine correlations were identified in these spectra. The A_{36} and i^6A_{37} correlations are not observed due to chemical exchange.

Sequential assignments for the non-exchangeable resonances were made using 2D NOESY and 3D ^{13}C-edited NOESY experiments to identify sequential H6/8-H1' NOE connectivities. The sequential base-1' NOE connectivities are continuous through all 17 nucleotides in the 180 ms NOESY spectrum (Figure 11), but the connectivity between nucleotides U_{33} and G_{34} is weak. The H6/8-H2' and H6/8-H6/8 inter-residue connectivities

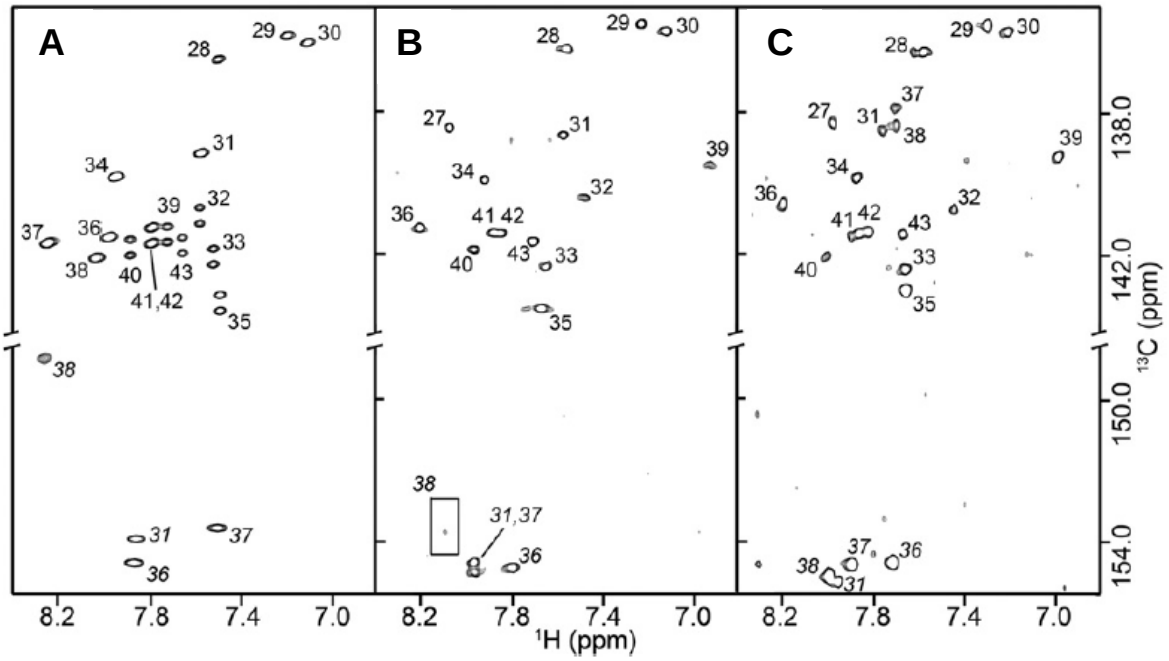

Figure 10. 2D ^{13}C–^{1}H HSQC Spectra

(a) unmodified ASL^{Tyr}, (b) [i^6A_{37}, Ψ_{39}]-ASL^{Tyr}, and (c) [i^6A_{37}, Ψ_{39}]-ASL^{Tyr} saturated with 2 mM $Co(NH_3)_6^{3+}$ RNA molecules at pH 6.3. Spectra (b and c) were acquired at natural abundance. The chemical shift of the A_{38} C2 resonance indicates the presence of a stable C_{32}–A_{38}^+ base pair. The A_{38} C2H2 cross peak is significantly weakened by chemical exchange upon modification (b) but appears with similar intensity (c). Addition of $Co(NH_3)_6^{3+}$ stabilizes the anticodon loop of [i^6A_{37}, Ψ_{39}]-ASL^{Tyr} and leads to the appearance of the A_{37} C8H8 resonance that is lost to exchange broadening with modification. (Image from Denmon et al., 2011)

also are continuous in the 180 ms spectrum except for the U_{35} H6 to A_{36} H8 step. The base-2' inter-residue connectivities from U_{33} to A_{37} are weak, consistent with the non-C3'-endo ribose ring conformations of these residues (described below).

The NH and NH_2 resonances of ASL^{Tyr} and [i^6A_{37}]-ASL^{Tyr} were assigned using ^{1}H-^{1}H NOESY and HNCCH experiments. Only the G_{28}-G_{30} NH resonances are sufficiently intense to yield NOE connectivities between neighboring base pairs. The G_{27} NH resonance of the terminal G-C base pair does not yield cross peaks in the NOESY spectrum. A broad G NH resonance, which has a chemical shift that corresponds to a non-base paired G (≈10.7 ppm), was assigned to G_{34}. The U_{39} NH resonance of ASL^{Tyr} is broadened by chemical exchange and is only observed in the 1D spectrum. The G_{34} and U_{39} NH resonances are further broadened by the i^6A_{37} modification and do not intensify with lower temperature. The cytidine and adenine NH_2 resonances were assigned via scalar correlations using HSQC and HNCCH experiments. The upfield chemical shifts (7.20 and 6.69 ppm) of the C_{32} H4 resonances are consistent with the lack of intra-molecular hydrogen bonding. A_{31} of ASL^{Tyr} is the only adenine residue from either molecule that has two resolved NH_2 ^{1}H resonances. The dimethylallyl modification of A_{37} causes the N6 resonance to shift downfield from 80.0 ppm to 92.3 ppm. This shift is similar to the shift observed upon dimethylallyl modification of A_{37} in *E. coli* $tRNA^{Phe}$ (Cabello-Villegas et al., 2002, 2004).

The [Ψ_{39}]-ASL^{Tyr} and [i^6A_{37}, Ψ_{39}]-ASL^{Tyr} molecules were not isotopically enriched and so resonances were assigned using 2D NOESY and natural abundance ^{13}C-^{1}H HSQC experiments (Figures 11 and 12). Many of the spectral features of these molecules parallel those of the ASL^{Tyr} and [i^6A_{37}]-ASL^{Tyr} molecules described above. The most substantial spectral difference between ASL^{Tyr} and [Ψ_{39}]-ASL^{Tyr} are the upfield shifts of the C6, H6, and

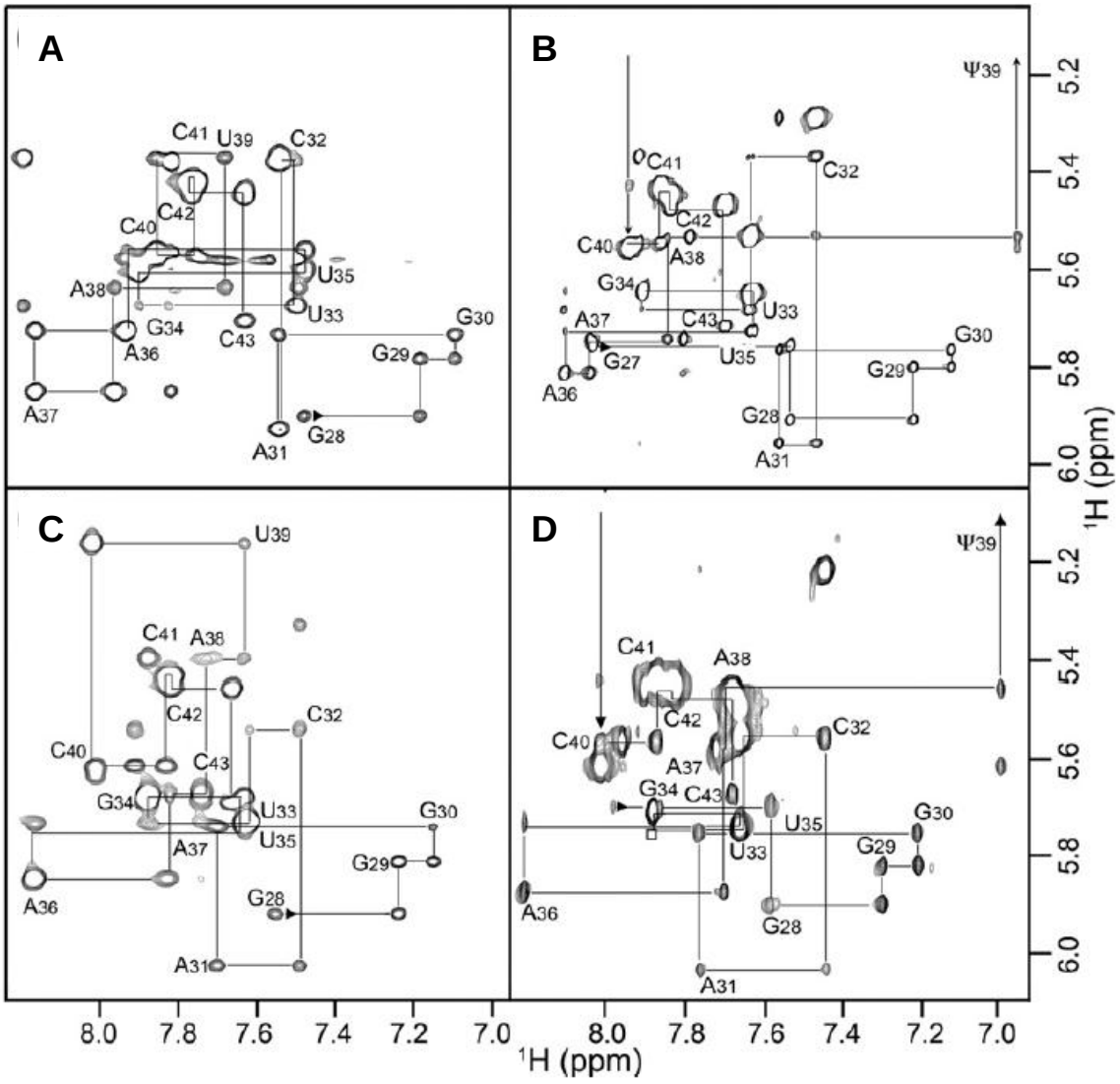

Figure 11. 2D NOESY Spectra from Unmodified and Partially Modified ASLs

(a) unmodified ASL^{Tyr}, (b) $[\Psi_{39}]$-ASL^{Tyr}, (c) $[i^6A_{37}]$-ASL^{Tyr}, and (d) $[i^6A_{37}, \Psi_{39}]$-ASL^{Tyr} molecules from *B. Subtilis*. (c) and (d) contain cobalt hexamine. The NOESY provides sequential assignment and structural information about the molecule. The H1' of the Ψ_{39} has a chemical shift of 4.47 ppm instead of a chemical shift in the range of 5-6 ppm like the uridine in the unmodified and $[i^6A_{37}]$-ASL^{Tyr} molecules. NOESY spectra represent unmodified and partially modified ASL^{Tyr} molecules in low salt NMR buffer (10mM Phosphate Buffer, 10 mM KCL, 0.02 mM EDTA) at pH 6.3. (Image from Denmon et al., 2011)

H1' resonances that correspond to Ψ_{39}. The A_{38} is not stably protonated in [Ψ_{39}]-ASL^{Tyr} (Figure 12), and deprotonates upon modification to [i^6A_{37}, Ψ_{39}]-ASL^{Tyr} (Figure 10), analogous to the deprotonation caused by introduction of the i^6A_{37} modification alone. The NOE cross peaks for [Ψ_{39}]-ASL^{Tyr} are continuous in the base-1' region of long mixing time NOESY spectra, but the G_{34} H8-U_{33} H1' cross peak is weak. This sequential NOE peak is missing from all [i^6A_{37}, Ψ_{39}]-ASL^{Tyr} NOESY spectra (Figure 11). The presence or absence of a non-sequential U_{35} H6-U_{33} H1' peak could not be determined due to spectral overlap. The addition of $Co(NH_3)_6^{3+}$ also was used to achieve conformational homogeneity with [i^6A_{37}, Ψ_{39}]-ASL^{Tyr}. It is notable that the cross peak patterns displayed by [i^6A_{37}, Ψ_{39}]-ASL^{Tyr} and [i^6A_{37}]-ASL^{Tyr} molecules with $Co(NH_3)_6^{3+}$ are very similar (Figure 11). The H1 imino resonance of Ψ_{39} is present in the ^{15}N-^{1}H HSQC spectrum at 10.6 ppm and is equally sharp in both of the Ψ-containing molecules. The presence of this resonance is consistent with the participation of the Ψ_{39} H1 in a water-mediated hydrogen bond with the phosphate backbone (Arnez and Steitz, 1994).

For all molecules, the inter-nucleotide phosphate ^{31}P resonances are clustered between -3.54 and -4.40 ppm and were assigned using HCP or ^{31}P-^{1}H hetero-TOCSY-NOESY spectra (Kellogg and Schweitzer, 1993). The sequential P–H6/8 and P–H1' correlations are continuous throughout the [Ψ_{39}]-ASL^{Tyr} (Figure 13). The P–H3' correlations and several P–H4' and P–H5'/H5" correlations are present in ^{31}P-^{1}H HetCor spectra and provide independent confirmation of the ^{31}P assignments. Notably, the ^{31}P resonances remain tightly grouped indicating that the i^6A_{37} and Ψ_{39} modifications have little effect on the phosphate backbone conformation (Figure 13). The most significant effect of the modifications occurs at the ^{31}P resonance of the phosphate 5' to Ψ_{39}. This resonance shifts

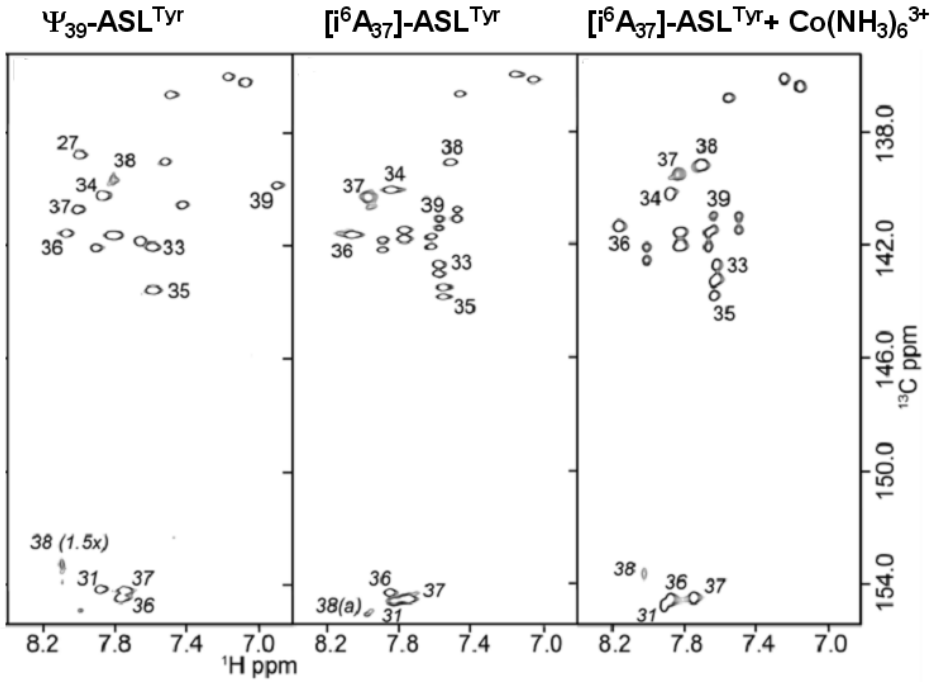

Figure 12. HSQC 2D [Ψ_{39}]- and [i^6A_{37}]-ASLs

The [Ψ_{39}]-ASL^{Tyr} spectra was collected at natural abundance, resulting in a loss of the C5 and C6 couplings. In all three panels the protonated C-A^+ base pair is disrupted upon modification. Additionally, the C2 peak is broadened by chemical exchange in all three spectra (Image from Denmon et al., 2011)

0.1 ppm upfield with the introduction of Ψ and is likely caused by the water-mediated hydrogen bond of the *pro-R* phosphoryl oxygen with the Ψ_{39} H1 imino.

The ^{1}H resonances of the dimethylallyl group were assigned using NOESY spectra. The ^{1}H chemical shifts of the dimethylallyl groups, CH 5.05 ppm, CH_2 4.04 ppm and 3.87 ppm, CH_3 1.53 ppm and 1.51 ppm, are nearly the same for [i^6A_{37}]-ASL^{Tyr} and [i^6A_{37}, Ψ_{39}]-ASL^{Tyr}. However, the CH and CH_2 resonances are shifted upfield to 4.96, 3.63, and 3.52, respectively, when $Co(NH_3)_6^{3+}$ is absent from the samples. The protons of the dimethylallyl group have NOE cross peaks to several base and 1' protons and are discussed below. A complete list of resonance assignments, including non-protonated positions of ASL^{Tyr} and [i^6A_{37}]-ASL^{Tyr}, is given in Table 3.

3.1.3 Effects of Metal Ions on the RNA Hairpins

Metal ions, most commonly Mg^{2+}, contribute to several aspects of RNA structure and function including RNA folding, tertiary structure stabilization, and catalysis. Mg^{2+} ions are crucial for maintaining the correct tertiary fold of tRNA and their binding sites within the molecule have been identified by multiple methods (Agris, 1996; Laing et al., 1994). In structure studies, Mg^{2+} and $Co(NH_3)_6^{3+}$ ions have been observed proximal to the loop-helix junction in the ASL of tRNA (Cabello-Villegas et al., 2004; Shi and Moore, 2000).

Therefore, the four ASL molecules were tested for their ability to bind Mg^{2+} and to examine possible Mg^{2+}-induced conformational effects. For unmodified ASL^{Tyr} and [Ψ_{39}]-ASL^{Tyr}, Mg^{2+} at concentrations between 5 and 10 mM slightly weaken the intensity of the U_{39} N3H ^{15}N-^{1}H cross peak and cause the ^{1}H resonance to shift upfield 0.2 ppm. The G_{28}-G_{30} NH resonances have small changes in chemical shift and intensity and the G_{34} resonances

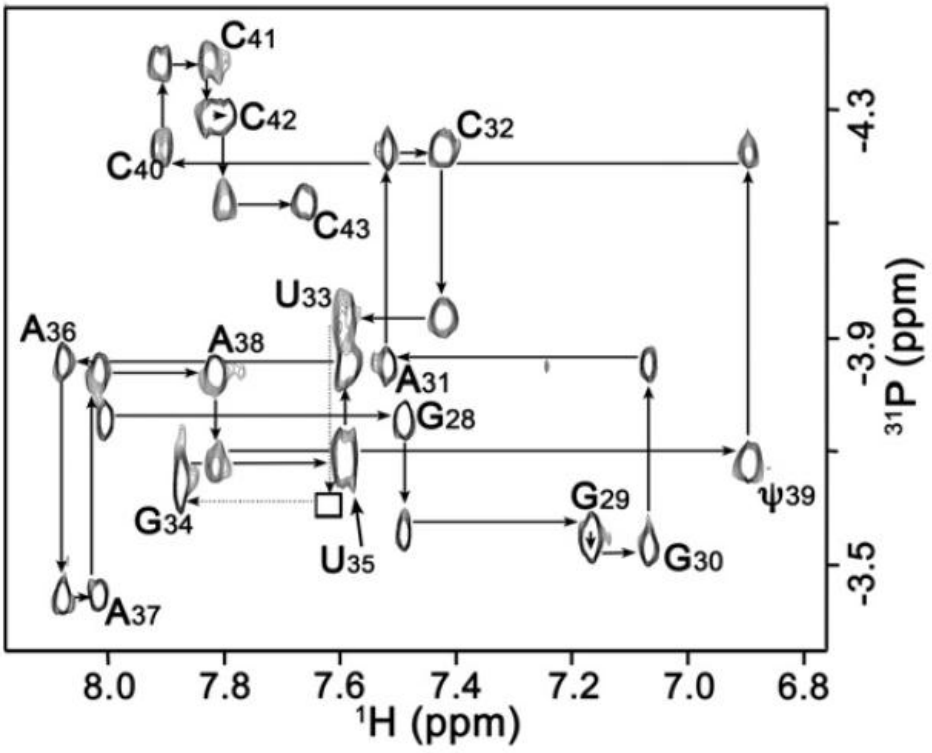

Figure 13. ^{31}P-^{1}H Hetero TOCSY-NOESY.

Sequential H6/8‑P connectivities in the 31P‑1H hetero-TOCSY‑NOESY spectrum of [Ψ39]-ASLTyr. The connectivity is disrupted between U33 and G34. This inter-residue step is also weak in the NOESY spectrum. (Image from Denmon et al., 2011)

become extremely broadened. The Ψ_{39} N1H resonance is broadened, but not shifted. The G_{28}-G_{30} chemical shift effects are consistent with binding of divalent metal ions to triplets of G-C base pairs (Allain and Varani, 1995). The non-exchangeable resonances also exhibit spectral changes. Most notably, the A_{38} C2 of unmodified ASL^{Tyr} shifts downfield ≈4.0 ppm, indicating deprotonation of the A_{38} base and loss of the C_{32}-A_{38}^{+} base pair. In [Ψ_{39}]-ASL^{Tyr}, the A_{38} H2C2 correlation appears and has a chemical shift indicative of the neutral base. The base 6 and 8 resonances of nucleotides U_{33}-A_{38} exhibit chemical shift changes and significant broadening with the base 8 resonances of A_{36} and A_{38} broadened beyond detection. The spectra could not be improved by increasing the Mg^{2+} concentration.

The effects of metal ions on the [i^6A_{37}]- and [i^6A_{37}, Ψ_{39}]-ASL^{Tyr} molecules are somewhat more variable. The imino ^1H resonances of the base paired G_{27}-G_{30} of both molecules broaden slightly with Mg^{2+} addition with the U_{39}/Ψ_{39} imino resonances exhibiting more substantial broadening, presumably caused by increased solvent exchange. The imino ^1H resonances of U_{33}, G_{34}, and U_{35}, already broad, exhibit small changes with Mg^{2+}. These effects on the imino resonances are independent of temperature from -3 °C to 15 °C. The non-exchangeable base and 1' resonances are more sensitive to Mg^{2+}. In the absence of metal ions, the stem (G_{27}-A_{31} and U/Ψ_{39}-C_{43}) resonances appear similar to the corresponding resonances of unmodified and [Ψ_{39}]-ASL^{Tyr} molecules, but resonances from the loop nucleotides are broadened by chemical exchange. The [i^6A_{37}]-ASL^{Tyr} exhibits the poorest spectral quality (absence of A_{37} C8 resonance and severe broadening of the A_{38} C8, A_{38} C2, and U_{39} C1' resonances), but shows modest improvement with addition of up to 5 mM Mg^{2+}. As the Mg^{2+} concentration was increased beyond 10 mM, the spectral quality again began to degrade. Although Mg^{2+} leads to sharpening of some loop nucleotide resonances, the general

Table 3. Resonance Assignments

Unmodified ASL^{Tyr}								
residue	H6/H8	H2/H5	H1'	H2'	H3'	H4'	H5'/5"	NH
G27	8.02							12.66
G28	7.51		5.90	4.65	4.58	4.50	4.49, 4.19	12.70
G29	7.19		5.78	4.64	4.48	4.46	4.47, 4.07	12.52
G30	7.11		5.74	4.68	4.42	4.46	4.39, 4.03	12.22
A31	7.58	7.83	5.93	4.63	4.44	4.47	4.51, 4.07	
C32	7.58	5.37	5.39	4.10	4.38	4.32	4.45, 4.03	
U33	7.52	5.63	5.69	4.21	4.41	4.31	4.28, 4.01	
G34	7.94		5.61	4.58	4.71	4.31	4.11, 4.00	10.76
U35	7.49	5.56	5.57	4.08	4.44	3.90	3.80, 3.53	
A36	7.98	7.83	5.73	4.67	4.73	4.41	4.10, 3.96	
A37	8.19	7.50	5.85	4.79	4.71	4.62	4.36, 4.31	
A38	8.01	8.22	5.64	4.51	4.32	4.54	4.36, 4.28	
U39	7.72	5.23	5.37	4.28	4.39	4.39	4.49, 4.06	14.18
C40	7.88	5.41	5.57	4.27	4.47	3.90	4.49, 4.05	
C41	7.79	5.41	5.43	4.34	4.46	4.38	4.50, 4.04	
C42	7.80	5.56	5.46	4.27	4.48	4.35	4.54, 4.02	
C43	7.66	5.42	5.71	3.97	4.14	4.14	4.44, 3.99	

Unmodified ASL^{Tyr} Continued								
residue	C6/C8	C2/C5	C1'	C2'	C3'	C4'	C5'	N
G27								
G28	136.32		92.83	75.68	72.74	82.25	69.60	147.00
G29	135.67		92.87	75.72	72.82	82.03	65.34	147.05
G30	135.83		93.17	75.81	73.08	82.21	65.90	146.53
A31	138.93	152.76	93.57	75.81	72.56	82.38	64.90	
C32	140.73		93.52	76.03	72.52	82.43	64.29	
U33	141.87		92.26	75.90	74.74	83.73	66.34	
G34	139.63		88.69	78.16	75.09	85.73	67.30	146.12
U35	143.22		89.17	75.72	77.59	84.69	67.82	
A36	141.31	154.41	89.95	75.81	76.77	84.51	68.21	
A37	141.50	153.46	90.35	75.76	75.50	84.25	68.08	
A38	141.94	148.65	93.44	75.68	73.56	83.16	67.47	
U39	141.31		93.44	75.09	72.44	82.18	64.08	
C40	141.19		93.87	75.72	72.17	84.69	66.76	
C41	141.24		94.13	75.46	72.17	81.86	64.51	
C42	141.24		94.39	75.57	71.82	81.99	64.16	
C43	141.61		92.96	77.59	74.16	83.56	65.03	

Unmodified ASL^{Tyr} Continued								
residue	YN1/ RN9	YC2	YC4	RN7	A N1	A N3	A/C N6/N4	NH_2	5'-P
G27								
G28	169.81			233.31				-3.72
G29	169.52			233.96				-3.56
G30	169.15			234.40				-3.54
A31	170.40			231.26	222.75	214.03	82.19	7.91,6.71	-3.90
C32	152.25	159.94	167.96				96.88	7.34,6.55	-4.23
U33	144.62	154.60	167.96						-3.95
G34	166.07			237.34					-3.72
U35	143.16	155.36	168.23						-3.68
A36	168.42			231.55	224.51	217.40	78.82	6.59	-3.84
A37	168.34			231.55	222.68	216.01	80.05	6.95	-3.45
A38	175.60			234.84	219.60	219.60	80.15	6.76	-3.86
U39	146.81	153.80	168.48						-3.79
C40	151.81	159.66	168.27				97.90	8.40,6.99	-4.22
C41	151.25	159.96	168.37				97.40	8.44,6.90	-4.40
C42	151.14	159.86	168.40				97.46	8.43,6.86	-4.31
C43	152.33	160.78	168.69				96.54	8.24,7.01	-4.12

$[i^6A_{37}]$-ASL^{Tyr}								
residue	H6/H8	H2/H5	H1'	H2'	H3'	H4'	H5'/5"	NH
G27	8.10		5.70					12.60
G28	7.54		5.89	4.60	4.63	4.49	4.52,4.11	12.69
G29	7.23		5.78	4.59	4.47	4.45	4.51,4.05	12.53
G30	7.13		5.72	4.50	4.41	4.28	4.43,4.02	12.35
A31	7.69	7.90	5.99	4.53	4.52/4.45	4.45	4.09, 4.02	
C32	7.47	5.32	5.52	4.01	4.00	4.33	4.28,4.02	
U33	7.60	5.58	5.70	4.22	4.44	4.22	4.05,3.94	
G34	7.87		5.66	4.71	4.68	4.37	4.11,4.02	
U35	7.62	5.58/5.52	5.71	4.22	4.36	4.45	4.43,4.15	
A36	8.15	7.73	5.81	4.82	4.69	4.47	4.23,4.11	
A37	7.82	7.88	5.64	4.78	4.68	4.45		
A38	7.71	8.02	5.70	4.50	4.25	4.25	4.11,4.02	
U39	7.62	5.22	5.15	4.23	4.40	4.35	4.43,4.04	13.95
C40	8.00	5.60	5.59	4.25	4.37	4.22	4.49,4.03	
C41	7.82	5.45	5.42	4.32	4.31	4.23	4.39,4.27	
C42	7.81	5.45	5.44	4.23	4.35	4.23	4.01,3.98	
C43	7.66	5.43	5.67	3.96	4.38	4.54	4.43,3.98	

$[i^6A_{37}]$-ASL^{Tyr} Continued								
residue	C6/C8	C2/C5	C1'	C2'	C3'	C4'	C5'	N
G27								
G28	136.54		92.66	74.53	71.08	81.62	65.81	147.05
G29	135.85		92.66	74.64	71.48	81.62	66.11	146.91
G30	136.15		93.04	74.35	72.80	83.86	66.80	146.47
A31	138.97	154.78	92.93	74.80	71.84	82.11	65.61	
C32	141.07	96.71	92.22	75.62	74.16	82.98	66.42	
U33	142.82	103.90	91.13	74.51	74.64	84.42	68.11	
G34	140.00		89.88	74.75	76.54	85.26	68.59	
U35	143.46		93.04	74.51	71.76	82.65	66.58	
A36		154.53	92.06	74.58	73.42	83.90	68.54	
A37	139.27	154.57	90.97	74.42	74.17	83.20	68.16	
A38	141.19	153.67	90.86	74.63	75.40	84.88	68.59	
U39	141.07		93.53	74.09	71.64	82.27	65.11	
C40	142.13	104.27	93.74	74.25		82.36	65.38	
C41	141.58	96.43	94.07	74.44	74.80	82.36	68.16	
C42	141.58	96.43	94.29	74.44	71.27			
C43	141.71	95.87	93.04	76.58	69.40	83.30	66.15	

$[i^6A_{37}]$-ASL^{Tyr} Continued								
residue	YN1/ RN9	YC2	YC4	RN7	A N1	A N3	A/C N6/N4	NH_2
G27								
G28	170.23			232.12				
G29	169.97			235.20				
G30	169.22			234.93				
A31	170.73			230.03	223.10	212.74	80.24	6.66
C32	151.12	158.70	167.38				96.12	7.20,6.69
U33	143.79	153.92	168.02					
G34	167.03			235.49				
U35	143.85	154.02	168.02					
A36	168.53			231.56	224.51	215.43	78.96	6.39
A37				229.83	220.81	212.25	92.32	6.78
A38				229.83		214.59	79.98	6.46
U39	145.98	152.38	168.53					
C40	152.06	158.63	168.53				97.98	8.40,7.01
C41	151.25	158.82	168.82				97.46	8.34,6.86
C42	151.12	158.82	168.50				97.60	8.36,6.86
C43	152.23	159.79	168.60				96.57	8.20,6.96

[Ψ_{39}]-ASL^{Tyr}							
residue	H6/H8	H2/H5	H1'	H2'	H3'	H4'	H5'/5"
G27	8.00		5.72	4.85	4.52	4.35	
G28	7.49		5.87	4.59	4.60	4.50	4.13
G29	7.17		5.76	4.61	4.44	4.47	4.04
G30	7.06		5.73	4.60	4.43	4.48	4.01
A31	7.51	7.88	5.93	4.59	4.45	4.47	4.06,4.02
C32	7.45	5.25	5.33	4.19	4.30	4.33	4.15, 4.02
U33	7.56	5.50	5.63	4.22	4.43	4.33	
G34	7.88		5.59	4.34	4.56		4.08,3.98
U35	7.55	5.61	5.64	4.18	4.49	4.18	
A36	8.05	7.77	5.78	4.44	4.74	4.47	4.17,4.08
A37	8.07	7.75	5.76	4.42	4.67	4.31	3.99
A38	7.88		5.53	4.45	4.47		
ψ39	6.87		4.47	4.41	4.34	4.33	4.17, 3.93
C40	7.91	5.52	5.51	4.26	4.49	4.39	
C41	7.83	5.40	5.42	4.34	4.48	4.38	
C42	7.80	5.41	5.44	4.24	4.48	4.36	
C43	7.66	5.52	5.68	3.98	4.15	4.14	

[Ψ_{39}]-ASL^{Tyr} Continued				
residue	C6/C8	C2/C5	C1'	5'-P
G27	138.40		91.79	
G28	136.34		93.02	-3.76
G29	135.73			-3.57
G30	135.98		92.92	-3.54
A31	138.66	153.84	93.69	-3.87
C32	140.26		93.80	-4.24
U33	141.70		91.22	-3.95
G34	139.89		89.47	-3.70
U35	143.24		90.19	-3.67
A36	140.41	154.20	91.02	-3.88
A37	141.23	153.89		-3.46
A38		154.61	93.13	-3.86
U39	139.59			-3.69
C40	141.75		94.16	-4.24
C41	141.34		94.26	-4.40
C42	141.34		94.57	-4.30
C43	141.54		93.18	-4.15

[i^6A_{37}, Ψ_{39}]-ASL^{Tyr}						
residue	H6/H8	H2/H5	H1'	H2'	H3'	H4'
G27	7.88		5.69	4.40		
G28	7.58		5.89	4.59	4.61	4.53
G29	7.30		5.81	4.59	4.53	4.48
G30	7.21		5.75	4.48	4.48	4.26
A31	7.76	7.95	6.03	4.42	4.43	
C32	7.44	5.21	5.56	4.04	4.06	4.39
U33	7.66	5.55	5.74	4.26	4.52	
G34	7.88		5.71	4.40	4.16	
U35	7.66	5.49	5.73	4.36	4.37	
A36	8.20	7.72	5.87	4.89	4.36	4.54
A37	7.70	7.89	5.58	4.37		4.57
A38	7.69	8.00	5.45	4.27	4.35	4.47
ψ39	6.99		4.35	4.14		
C40	8.01	5.61	5.56	4.24	4.39	4.27
C41	7.87	5.44	5.43	4.35	4.48	4.25
C42	7.82	5.45	5.45	4.39	4.24	4.35
C43	7.68	5.47	5.66	4.00	4.28	4.16

[i^6A_{37}, Ψ_{39}]-ASL^{Tyr} Continued			
residue	C6/C8	C2/C5	C1'
G27			92.22
G28	137.11		91.57
G29	136.35		91.53
G30	136.50		
A31	139.32	155.49	92.04
C32	141.55	96.89	91.74
U33	143.25	104.16	92.18
G34	140.64		90.41
U35	143.86	104.16	92.18
A36	141.43	155.45	90.41
A37	138.70	155.98	
A38	139.20	155.79	93.28
U39	140.08		
C40	142.89	96.49	94.16
C41	142.23	96.55	94.26
C42	142.23	96.55	94.57
C43	142.27	97.24	93.18

broadening of most other resonances that accompanied Mg^{2+} addition prevented complete resonance assignment. The [i^6A_{37}, Ψ_{39}]-ASL^{Tyr} spectrum also exhibits the effects of chemical exchange, but the effects differ slightly from those presented by [i^6A_{37}]-ASL^{Tyr}. Addition of 4 mM Mg^{2+} yielded only modest spectral improvement for loop resonances, but caused the base resonances of U_{32}, U_{33}, and A_{37} to be broadened beyond detection. Addition of Mg^{2+} to [i^6A_{37}, Ψ_{39}]-ASL^{Tyr} also leads to exchange broadening of the Ψ_{39} N3H resonance.

$Co(NH_3)_6^{3+}$ is more effective than Mg^{2+} at stabilizing the structure of the *E. coli* $tRNA^{Phe}$ anticodon loop (Cabello-Villegas et al., 2004). Thus, $Co(NH_3)_6^{3+}$ was tested for its ability to minimize the effects of chemical exchange among the loop nucleotide resonances of [i^6A_{37}]-ASL^{Tyr} and [i^6A_{37}, Ψ_{39}]-ASL^{Tyr} without deteriorating the overall spectral quality. The addition of $Co(NH_3)_6^{3+}$ (2.0 mM) produced conformationally homogeneous samples with excellent spectral properties. All base and ribose 1' resonances are present and only the A_{37} C8 and A_{38} C2 resonances are moderately broad in [i^6A_{37}]-ASL^{Tyr} (Figure 12). NOESY spectra (mixing time of 320 ms) were acquired in 90% ^1H_2O to locate the position of the $Co(NH_3)_6^{3+}$ ligands. The guanine NH and cytidine NH_2 resonances of the stem as well as H8 and H6 resonances have cross peaks with the $Co(NH_3)_6^{3+}$ protons. These peaks are consistent with coordination of $Co(NH_3)_6^{3+}$ in the major groove (Kieft and Tinoco, 1997). Although the spectral data defining the stem location of $Co(NH_3)_6^{3+}$ are very good, the cobalt hexamine complex cannot be uniquely positioned in the loop region and can only be restricted to the major groove. Very weak NOE cross peaks are observed between $Co(NH_3)_6^{3+}$ and the base protons of C_{32}, U_{33}, and A_{38} and a weak cross peak involving the CH_3 protons of the dimethylallyl modification. No evidence for coordination involving the loop nucleotide base atoms is reflected by the chemical shifts of the non-protonated ^{15}N resonances. Therefore,

coordination of the $Co(NH_3)_6^{3+}$ may involve bridging between phosphate groups across the major groove.

3.1.4 Structure Calculations

The structures of the ASL^{Tyr} molecules were calculated using a restrained molecular dynamics routine starting from 50 sets of coordinates with randomized backbone dihedral angles. The calculations used a total of 294-300 distance constraints and 60-70 dihedral angle constraints (Table 4) to produce eight converged structures for each molecule (Figure 14). Structures were classified as converged if they were consistent with the NMR data and maintained correct stereochemistry. The converged structures have an average of 7 distance constraint violations between 0.1 and 0.3 Å, most of these involving the loop region. All converged structures have no constraints violated by more than 0.3 Å. When the structures are arranged in order of increasing overall energy, the converged structures form a plateau with similarly low overall energies and constraint violation energies. The root mean square deviations (RMSDs) of the heavy atoms between the individual structures and the minimized mean structures are 0.36± 0.15 Å, 0.38± 0.05 Å, 0.55± 0.17 Å, and 1.09 ± 0.18 Å for ASL^{Tyr}, [Ψ_{39}]-ASL^{Tyr}, [i^6A_{37}]-ASL^{Tyr}, and [i^6A_{37}, Ψ_{39}]-ASL^{Tyr}, respectively. The global fold of ASL^{Tyr} is a hairpin composed of a six base pair stem and a three to five nucleotide loop (Figure 14). The overall fold of [i^6A_{37}]-ASL^{Tyr} (a five base pair stem with a five to seven nucleotide loop) is similar to ASL^{Tyr}, but the loss of some inter-residue NOEs among loop nucleotides and the loss of secondary structure proximal to the loop caused by the modification lead to a somewhat less precisely defined loop conformation (0.55± 0.17 Å RMSD compared to 0.36± 0.15 Å RMSD, respectively, for the heavy atoms). The Ψ_{39} modification does not alter the global fold of the anticodon arms, but destabilizes the C_{32}-A_{38}

Table 4. Summary of Experimental Distance and Dihedral Angle Constraints and Refinement Statistics for the Unmodified and Partially Modified ASL^{Tyr} Hairpins

Constraint		Co[i^{6}A$_{37}$, Ψ$_{39}$]-ASL^{Tyr}
NOE distance constraints		
Intraresidue[a]		109
Interresidue		164
mean number per residue		16
NOE constraints by category		
very strong	(1.8 - 3.0 Å)	9
Strong	(1.8 - 4.0 Å)	28
Medium	(1.8 - 5.0 Å)	163
Weak	(1.8 - 6.0 Å)	62
very weak	(1.8 - 7.0 Å)	22
Base pair constraints		
Total		28
Dihedral angle constraints		
ribose ring[b]		51
Backbone		70
mean number per residue		7.1
Violations		
average distance constraints > 0.5 Å[c]		5.8
average dihedral constraints > 0.5°[d]		1.6
RMSD from ideal geometry[e]		
Heavy Atoms (Å)		1.24
Backbone Atoms (Å)		1.27

Constraint		Co[i^{6}A$_{37}$]-ASL^{Tyr}
NOE distance constraints		
intraresidue[a]		110
interresidue		178
mean number per residue		16.9
NOE constraints by category		
very strong	(1.8 - 3.0 Å)	8
strong	(1.8 - 4.0 Å)	28
medium	(1.8 - 5.0 Å)	147
weak	(1.8 - 6.0 Å)	74
very weak	(1.8 - 7.0 Å)	18
Base pair constraints		
total		28
Dihedral angle constraints		
ribose ring[b]		51
backbone		70
mean number per residue		7.1
Violations		
average distance constraints > 0.5 Å[c]		5.8
average dihedral constraints > 0.5°[d]		1.6
RMSD from ideal geometry[e]		
Heavy Atoms (Å)		1.24
Backbone Atoms (Å)		1.27

Constraint		[Ψ_{39}]-ASL^{Tyr}
NOE distance constraints		
intraresidue[a]		109
interresidue		178
mean number per residue		16.8
NOE constraints by category		
very strong	(1.8 - 3.0 Å)	8
strong	(1.8 - 4.0 Å)	35
medium	(1.8 - 5.0 Å)	142
weak	(1.8 - 6.0 Å)	57
very weak	(1.8 - 7.0 Å)	15
Base pair constraints		
total		42
Dihedral angle constraints		
ribose ring[b]		51
backbone		70
mean number per residue		7.1
Violations		
average distance constraints > 0.5 Å[c]		5.8
average dihedral constraints > 0.5°[d]		1.6
RMSD from ideal geometry[e]		
Heavy Atoms (Å)		1.24
Backbone Atoms (Å)		1.27

Constraint		Unmodified ASL^{Tyr}
NOE distance constraints		
intraresidue[a]		110
interresidue		157
mean number per residue		15.7
NOE constraints by category		
very strong	(1.8 - 3.0 Å)	12
strong	(1.8 - 4.0 Å)	35
medium	(1.8 - 5.0 Å)	114
weak	(1.8 - 6.0 Å)	79
very weak	(1.8 - 7.0 Å)	16
Base pair constraints		
total		42
Dihedral angle constraints		
ribose ring[b]		51
backbone		70
mean number per residue		7.1
Violations		
average distance constraints > 0.5 Å[c]		5.8
average dihedral constraints > 0.5°[d]		1.6
RMSD from ideal geometry[e]		
Heavy Atoms (Å)		1.24
Backbone Atoms (Å)		1.27

[a]Only conformationally restrictive constraints are included.

[b]Three torsion angles within each ribose ring were used to constrain the ring to either the C2'-endo or C3'-endo conformation. The ring pucker of residues G_{11}, A_{13}, G_{26}, and A_{28} were not constrained.

[c]A distance violation of 0.5Å corresponds to 5.0 kcal energy penalty.

[d]A dihedral angle violation of 0.5° corresponds to 0.05 kcal energy penalty.

[e]Calculated against the minimized average structure.

base pair in ASL^{Tyr}.

3.1.5 Structures of the ASL^{Tyr} and $[\Psi_{39}]$-ASL^{Tyr} Loop Regions

The loops of unmodified ASL^{Tyr} and $[\Psi_{39}]$-ASL^{Tyr} are similar and are composed of nucleotides U_{33}-A_{37}. The stems of both molecules are closed by the C_{32}-A^{+}_{38} base pairs (Figure 15a), although exchange broadening of the A_{38} C2 resonance indicates weakening of the 38-32 base pair with the introduction of Ψ_{39}. In $[\Psi_{39}]$-ASL^{Tyr}, the base of G_{34} stacks against the base of U_{33} and is turned slightly away from the helix axis and towards the minor groove (Figure 15b). The base of A_{36} stacks against the base of A_{37} and is displaced toward the major groove. In the unmodified-ASL^{Tyr}, the base of G_{34} is parallel to the plane of the U_{33} base but does not stack against it and is turned out into the minor groove (Figure 15a). The base of A_{36} in the unmodified molecule stacks against the base of A_{37} as in $[\Psi_{39}]$-ASL^{Tyr} and also is displaced towards the major groove. The positions of the bases in the two molecules are in agreement with the observed H6-H8 and H5-H8 NOEs. The position of A_{36} is restricted by several NOEs involving its H2 resonance, including interactions with the H1' resonances of A_{36} and A_{37}, the H5'/5" of U_{35}, and the H2' of A_{37}. These NOEs position the base of A_{36} beneath the major groove edge of the A_{37} base (Figure 15a). The position of the U_{35} base in both molecules is more variable, but tends to partition to the major groove side of the helix and oriented parallel with the helix axis (Figure 15a). Although the U_{35} base is perpendicular to the neighboring bases, the ribose moiety of U_{35} also is rotated so that the configuration about the glycosidic bonds of all residues is *anti.* About 25% of the time, the base of U_{35} is positioned on the minor groove side of the helix. NOEs involving the U_{35} base do not exclude the later conformation, nor are NOE cross peaks predicted for that

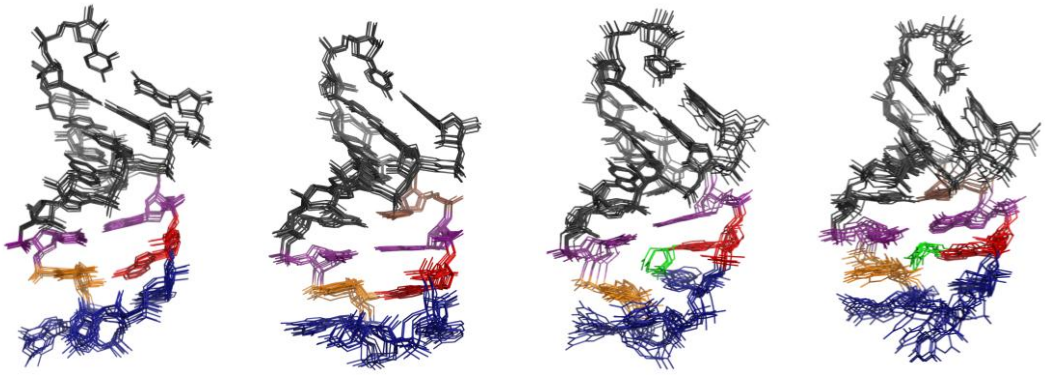

Figure 14. Overlay of Eight Converged Structures

(a) unmodified, (b) [Ψ_{39}]-ASL^{Tyr}, (c) [i^6A_{37}]-ASL^{Tyr}, and (d) [i^6A_{37}, Ψ^{39}]-ASL^{Tyr} RNA hairpins. Views are into the major grooves of the anticodon loops. The RMSDs between the individual structures and the average structure are listed below in figure 5. The greatest variability occurs among the anticodon bases and reflects the lower number of constraints for these residues, especially for G_{34} and U_{35}. Purple, residues 32 and 38; Gold, U_{33}; Blue, anticodon residues; Red, residue 37; Green, dimethylallyl; Brown, pseudouridine (Image modified from Denmon et al., 2011)

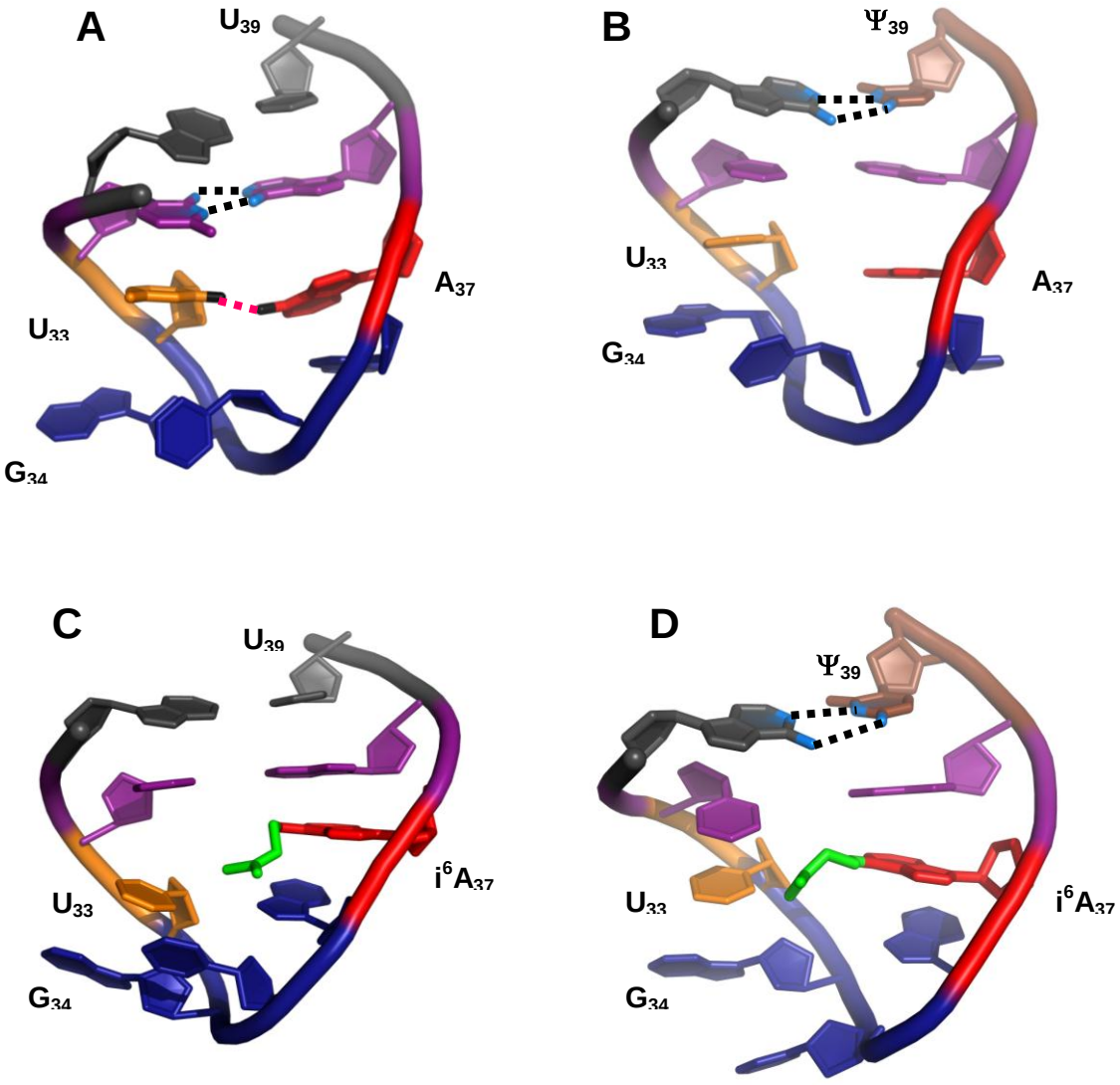

Figure 15. Structures of the Loop Regions

(a) unmodified, (b) [Ψ_{39}]-ASL^{Tyr}, (c) [i^{6}A$_{37}$]-ASL^{Tyr} and (d) [i^{6}A$_{37}$, Ψ_{39}]-ASL^{Tyr} *B. subtilis*. a) was solved using a low salt NMR buffer at pH 6.1 and structures (c) and (d) were solved using a low salt NMR buffer at pH 6.3 in the presence of cobalt hexamine. (a) and (b) formed a C-A$^+$ base pair, creating a 6 base pair stem. The C-A$^+$ base pair was also observed at pH 6.3. Structures a-d indicate that the hairpins do not adopt the canonical U-turn structure. Blue, anticodon; Brown, pseudouridine; Red, residue 37; Green, dimethylallyl; Purple, residues 32 and 38 (Modified image from Denmon et al., 2011).

conformations that are not observed in the NMR spectra. The structures of unmodified and Ψ_{39}-modified molecules suggest a cross-strand interaction between the A_{37} N6 and the U_{33} O2 atoms. For the [^{13}C, ^{15}N]-labeled ASL^{Tyr}, the chemical shifts of A_{37} N6 (80.1 ppm) and U_{33} C2 (153.6 ppm, Figure 16) lay between the chemical shift values observed for corresponding intra-molecular hydrogen bonded and non-hydrogen bonded atoms. The chemical shift range for adenine N6 in ASL^{Tyr} is 78.8 ppm (A_{36}) to 82.2 ppm (A_{31}). Intra-molecular hydrogen bonding of uridine O2 leads to a downfield shift of the C2 resonance with values ≈154.5 ppm for a G-U base pair, ≈153.5 ppm for a U-U base pair, and ≈152.5 ppm for an A-U base pair, and ≈152.5 ppm for a non-intra-molecular hydrogen bonded uridine base. These chemical shifts offer support for an A_{37}-U_{33} hydrogen bond interaction of moderate strength.

The sugar-phosphate backbone conformations of the loop nucleotides are surprisingly uniform (Figure 14). The majority of the nucleotides maintain the C3'-*endo* ring pucker, but the G_{34}, U_{35}, and A_{36} ribose groups have observable H1'–H2' couplings and ribose ^{13}C chemical shifts (C1' and C4') that indicate neither pure C2'- or C3'-*endo* ring pucker conformations. In addition, the uniformly small (<5 Hz) P–C2' coupling constants for the loop residues (unmodified ASL^{Tyr}) place the ε torsion angles in the *trans* conformation characteristic of RNA. The phosphate backbone torsion angles β, γ, and ε of residues G_{34}-A_{36} were not constrained for the calculations, but most have values within the range common to RNA helices with most deviations from standard values centered around residue U_{35}. The ^{31}P chemical shifts for all inter-residue phosphorus atoms are tightly clustered between -3.2 and -4.8 ppm (Figure 13, Table 3), indicating that the α and ζ torsion angles throughout the loop and helix adopt a gauche conformation. The *trans* conformation of the α or ζ torsion angle

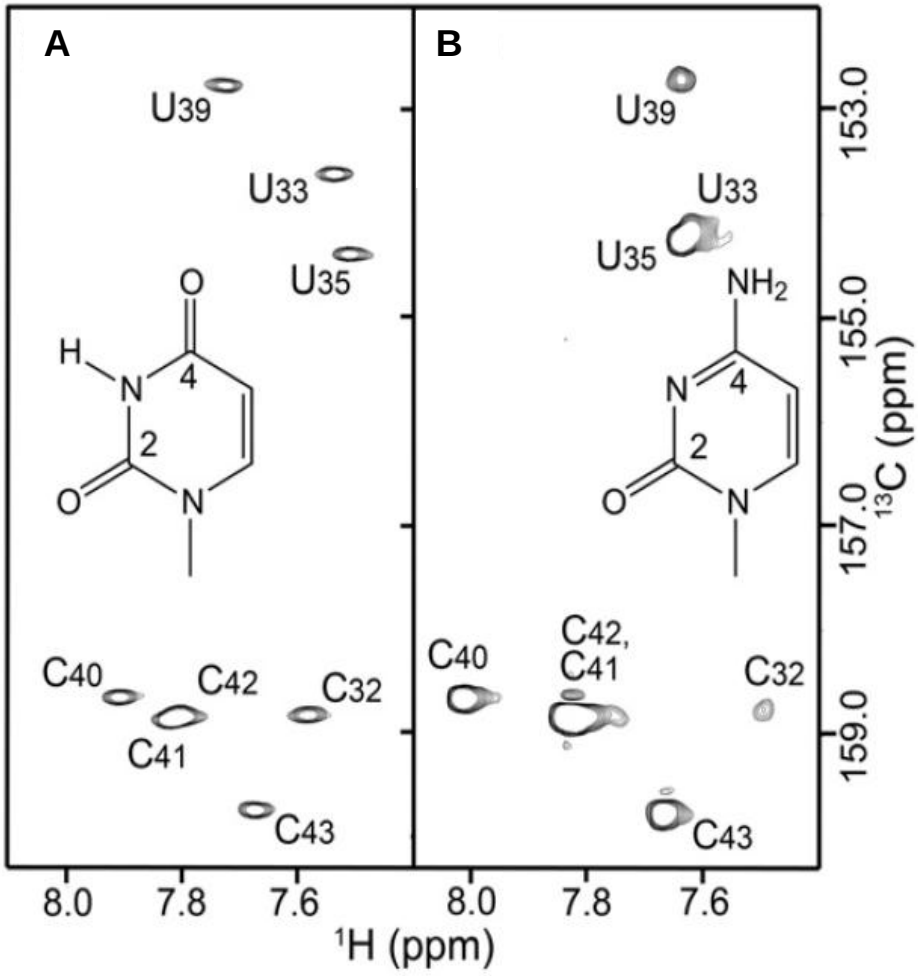

Figure 16. H6-C2 Regions of H(CN)C Spectra

(a) unmodified ASL^{Tyr} and (b) [i^6A_{37}]-ASL^{Tyr} and H5-C4 regions of CCH-COSY spectra of (c) unmodified ASL^{Tyr} and (d) [i^6A_{37}]-ASL^{Tyr}. (Image from Denmon et al., 2011)

causes a 2-3 ppm downfield shift of the corresponding ^{31}P resonance.

3.1.6 Structures of the [i^6A_{37}]-ASL^{Tyr} and [i^6A_{37}, Ψ_{39}]-ASL^{Tyr} Loop Regions

The loop conformations of the [i^6A_{37}]-ASL^{Tyr} and [i^6A_{37}, Ψ_{39}]-ASL^{Tyr} molecules are similar and are dominated by the effects of the dimethylallyl group (Figure 15). In both molecules, the helical base stack is continuous along the 3' side of the loop from A_{36} through C_{43} and along the 5' strand from G_{27} through U_{33}. The H6-H6 and H6-H5 NOEs between residues C_{32} and U_{33} are weak and result in a greater than normal inter-base separation. The base of G_{34} is not stacked beneath U_{33}, but is displaced away from the helix axis on the major groove side of the loop. The relative positions of G_{34} and U_{33} are consistent with the absence of an H6-H8 NOE and the very weak ([i^6A_{37}]-ASL^{Tyr}) or absent ([i^6A_{37}, Ψ_{39}]-ASL^{Tyr}) H8-H1' NOE. It is also worth noting that no non-sequential U_{33} H1' to U_{35} H6 NOE could be identified for either molecule. As with ASL^{Tyr} and [Ψ_{39}]-ASL^{Tyr}, the U_{35} base resides on the major groove side of the helix. However, the orientation of this base ranges from perpendicular to the helix axis to nearly parallel with the helix axis.

In both i^6A_{37}-modified molecules, the base plane of residue 37 is between C_{32} and U_{33}, and the dimethylallyl group protrudes into the major groove (Figure 15). In [i^6A_{37}]-ASL^{Tyr}, the methyl groups point above the plane of the A_{37} base in 75% of structures. The NOEs predicted by this orientation are consistent with those observed in the NMR spectra. In the structures of [i^6A_{37}, Ψ_{39}]-ASL^{Tyr}, the methyl groups lie below the plane of the A_{37} base as often as they lie above the base plane. The former orientation does not lead to a unique set of NOE cross peaks due to the sparseness of base and ribose protons that are near the dimethylallyl group and so excursions of the methyl groups below the base plane cannot be excluded by the experimental data. However, neither molecule displays evidence of multiple

conformations or dynamics for the dimethylallyl protons or loop nucleotide resonances. The conformation of the dimethylallyl group is restricted by NOEs to C_{32}, U_{33}, G_{34}, A_{37}, and A_{38}. The CH_3 groups produce strong NOE cross peaks with the U_{33} H4' and A_{38} H2 and both resonances of the CH_2 have strong cross peaks with the A_{38} H2. The CH_3 proton resonances have medium cross peaks with the C_{32} H1' and H5 and A_{37} H2 resonances and very weak cross peaks with the U_{32} and G_{34} H1', G_{34} H8, and A_{36} H2 resonances.

Although the i^6A_{37}-modified molecules share several structural features with the unmodified and Ψ_{39}-modified molecules, the ribose ring puckers differ significantly. All residues of the i^6A_{37}-modified molecules have the 3'-endo sugar pucker except G_{34} which displays a mixed 2'-*endo*/3'-*endo* conformation. This ribose conformation may favor the major groove residency of the U_{35} base. The torsion angles of the phosphate backbone are largely within the range common for RNA helices. The greatest variability centers on the phosphate backbone angles α, β, and ε in the i^6A_{37}-modified molecules. In [i^6A_{37}]-ASL^{Tyr}, α and ε of G_{34} are *trans* and *gauche*, respectively, and α, β, and ε of U_{35} are not typical of A-form helical geometry. In [i^6A_{37}, Ψ_{39}]-ASL^{Tyr}, β of U_{33} approaches the *trans* configuration whereas α and ε of G_{34} and α and γ of U_{35} are outside the standard A-form values.

3.1.7 Structure of the ASL^{Tyr} Stems

The conformations of the stems of the four forms of ASL^{Tyr} are very similar. The geometry of the hairpins from base pairs G_{27}-C_{43} to C_{32}-A_{38} is primarily A-form (Figure 14). H6/8-H6/8 and H6/8-H1',H2' NOEs from long and short mixing time NOESY spectra, respectively, are continuous (where not overlapped in [Ψ_{39}]-ASL^{Tyr}). The A_{31}-U_{39}/Ψ_{39} base pairs are sufficiently stable so that clear cross-strand NH–H2 NOEs can be observed,

although the imino H3 resonances are weakened by solvent exchange in the presence of $Co(NH_3)_6^{3+}$. While spectra for only the unmodified ASL^{Tyr} demonstrate the presence of a stable protonated C_{32}-A^{+}_{38} base pair, NOEs involving C_{32} and A_{38} and the exchange broadened A_{38} C2 in [Ψ_{39}]-ASL^{Tyr} suggest that pseudouridylation does not fully disrupt the base pair. The torsion angles of the sugar-phosphate backbones of all molecules are within the limits of A-form geometry and are supported by chemical shift, J-coupling, and NOE data.

3.1.8 Comparison of the ASL Structures

The anticodon loops of the ASL^{Tyr} molecules range in size from three to seven nucleotides. Surprisingly, the global conformations of the anticodon nucleotides are not dramatically altered by the Ψ_{39} and i^6A_{37} modifications. The A_{36} base is positioned on the minor groove side of the helix and stacks beneath the A_{37} base. The U_{35} base is positioned on the major groove side of the helix and is approximately co-planar with the base of G_{34}, which also resides on the major groove side of the helix (Figure 15). The ribose puckers of the anticodon nucleotides do change with base modification, especially U_{35} and A_{36} of the i^6A_{37}-modified molecules that adopt of the C3'-*endo* conformation common to the A-form helix. To examine the range of loop structure effects that result from the ribose ring pucker, simulations were performed for each of the molecules while restraining the ribose rings of U_{35} and A_{36} to C2'-*endo* and C3'-*endo* conformations. The C2'-*endo* pucker results in migration of the U_{35} base to the minor groove side of the helix in approximately 25% of the unmodified ASL^{Tyr} and [Ψ_{39}]-ASL^{Tyr} structures. The U_{35} base was found not to occupy the minor groove in either of the i^6A_{37}-modified molecules. Although only ASL^{Tyr} contains the well-defined C_{32}-A_{38}^{+} base pair the C_{32} and A_{38} bases remain largely coplanar and show

minimal lateral displacement in the modified molecules. The loops appear to be stabilized primarily by stacking and hydrophobic interactions because there is no spectral evidence of hydrogen bonding among the anticodon bases, although the ASL^{Tyr} may contain an A_{37} $N6H_2$-U_{33} O2 interaction.

Although the four ASL molecules each adopt well-ordered structures, the loops do not contain the signature U-turn motif (Figure 1a and 18a-c). In a U-turn, the sequential U_{33} H1' to G_{34} H8 distance is ≥6 Å and would lead to a break of H1'-base NOE connectivities whereas the non-sequential U_{33} H1' to U_{35} H6 distance is ≈3.8 Å and should give rise to a moderately intense NOE. For three of four ASL^{Tyr} molecules, the sequential H1'-base NOEs are continuous, albeit weak at the U_{33}-G_{34} step, and none contain the non-sequential U_{33}-U_{35} interaction. Many of the NOEs predicted for a molecule containing a U-turn are a subset of the NOEs observed for the ASL^{Tyr} molecules and do not conflict with the refined structures. However, key NOEs present in the spectra of the ASL^{Tyr} molecules (U_{33} H1' to A_{38} H2, G_{34} H1' to A_{37} H2, and U_{35} H1' to A_{36} H2) are not compatible with the U-turn motif. These NOEs lead to a loop structure in which the phosphate backbone does not turn abruptly between U_{33} and G_{34}, as observed in the crystalline forms of yeast and *E. coli* $tRNA^{Phe}$ (Byrne et al., 2010; Kim et al., 1974; Robertus et al., 1974; Shi and Moore, 2000) (Figure 17), but instead turns between G_{34} and U_{35}.. The turn of the phosphate backbone is maintained even when the unusual α and ζ torsion angles observed for the U-turn motif were applied during a separate set of constrained MD simulations. Another feature characteristic the U-turn motif is the *trans* conformation of backbone torsion angle a between U_{33} and G_{34}. The ^{31}P resonance corresponding to this phosphate is located in the main cluster of ^{31}P peaks (Figure 13), a position not consistent with the *trans* conformation of torsion angle α. Notably, the α or ζ

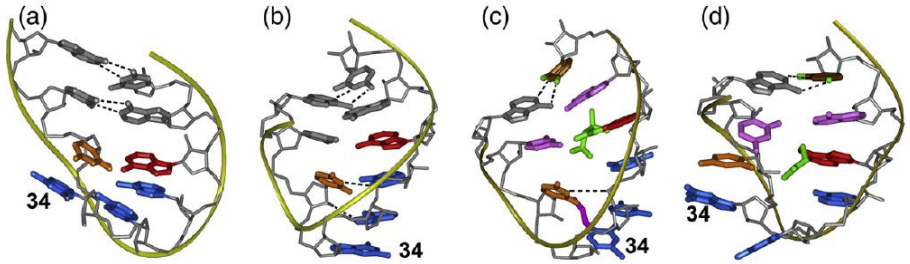

Figure 17. Comparison of the Anticodon Loop Regions
(a) Solution NMR structure of unmodified E. coli $tRNA^{Phe}$ (PDB 1KKA), (b) X-ray crystal structure of *E. coli* $tRNA^{Phe}$ (PDB 1IBL), (c) solution NMR structure of fully modified human $tRNA^{Lys,3}$ (PDB 1FL8), and (d) solution NMR structure of *B. subtilis* [i^6A_{37}, Ψ_{39}]-ASL^{Tyr}. The U-turn fold is present in (b) and (c) and is characterized by stacking of the anticodon bases (blue) along the minor groove side of the helix and the NH‑P hydrogen bond from U_{33} (orange). Molecules (a) and (d) do not form this same fold and maintain minor groove positions for residues 34 and 35 with stacking of U_{33} and G_{34} bases. Fully modified *E. coli* $tRNA^{Phe}$ contains $ms^2i^6A_{37}$ and Ψ_{32} (Image from Denmon et al. 2011).

angles in all of the converged structures occupy the *gauche*$^-$ conformation.

3.1.9 Effects of Modification on RNA Thermal Stability

The thermal stabilities of the ASL^{Tyr} RNA hairpins (Figure 1) were investigated using UV-monitored thermal melting experiments and differential scanning calorimetry (DSC) experiments. The normalized UV thermal denaturation curves indicate that the hairpins melt in two stages (Figure 18a). The lower temperature (<50 ˚C) transitions presumably correspond to the destacking of the loop nucleotides. At pH 6.3 the [Ψ_{39}]-ASL^{Tyr} and the unmodified ASL^{Tyr} hairpins have a protonated C-A$^+$ base pair, which contributes to the stability of the molecules by forming a six base pair stem instead of the five base pair stem observed in the [i^{6}A$_{37}$]-ASL^{Tyr} molecule. The increased absorbance of [i^{6}A$_{37}$]-ASL^{Tyr} relative to ASL^{Tyr} and [Ψ_{39}]-ASL^{Tyr} below 70 ˚C suggests that the dimethylallyl modification decreases base stacking in the modified hairpins. The percent hyperchromcity observed with melting is greatest for ASL^{Tyr} and [Ψ_{39}]-ASL^{Tyr} (10%-11%) and is least for the dimethylallyl-modified RNAs (7% and 5% for [i^{6}A$_{37}$]-ASL^{Tyr} and [i^{6}A$_{37}$, Ψ_{39}]-ASL^{Tyr}, respectively). The enhanced thermal stability of the stems of the [i^{6}A$_{37}$]-modified RNA hairpins is consistent with the stabilization conferred by the dimethylallyl modification in the context of the *E. coli* ASL^{Trp} (Kierzek and Kierzek, 2003), but differs from the destabilizing effect observed for the *E. coli* ASL^{Phe} (Cabello-Villegas et al., 2002).

The DSC curves (Figure 18b) indicate that the RNA hairpins undergo a single-step melting process. The unmodified RNA hairpin appears to contain a slight heat capacity change near 50 °C that is not observed in the other three molecules, but is small relative to the change that occurs in the multi-step melting of a tetraloop receptor homodimer complex (Vander Meulen et al., 2008). This small change could reflect melting of the C$_{32}$-A$^+_{38}$ base

pair that is present only in the unmodified RNA molecule (described below). The Ψ modification increased the T_m of the RNA hairpin by 5.7 °C, indicating that Ψ improves the stability of the stem. This finding is consistent with other studies that show Ψ improves the stability of a duplex when located at or near the end of the stem (Bilbille et al., 2009; Durant and Davis, 1999; Hall and McLaughlin, 1991). The enthalpy (ΔH) of melting for [Ψ_{39}]-ASL^{Tyr} is 5.24 ± 0.06 kcal/mol/bp, which suggests additional hydrogen bonding is not present in the unmodified molecule (ΔH = 4.17 ± 1.20 kcal/mol/bp). The dimethylallyl modification also confers stability to the ASL^{Tyr} stem, but the effect is not as robust as the Ψ modification (Figure 18). i^6A_{37} increases the T_m of the RNA hairpin by 3.7 °C and the ΔH by 1.39 kcal/mol/bp. The addition of Ψ_{39} and i^6A_{37} increases the T_m by 5.0 °C and the ΔH by 0.40 kcal/mol/bp, indicating that the i^6A_{37} modification interferes slightly with the stabilizing effects of the Ψ modification.

3.2 Characterization of Partial Modification on $tRNA^{Tyr}$ Function in *B. anthracis*

Although there have been many studies that highlight the role of tRNA molecules in translation and in the context of the ribosome, very little is known about the role of tRNAs in tRNA-mediated transcriptional regulation in Gram-positive bacteria or how base modifications affect their ability to regulate gene expression. Therefore, to determine the repercussions that partial modification has on physiology and tRNA mediated transcriptional regulation in *B. anthracis*, growth curves, antibiotic sensitivity tests, and quantitative real-time polymerase chain reaction (qRT-PCR) were employed.

3.2.1 Effects of $tRNA^{Tyr}$ Partial Modification on Growth Rates

When cultured in rich medium (LB), the parent strain exhibits a doubling time of 28.9

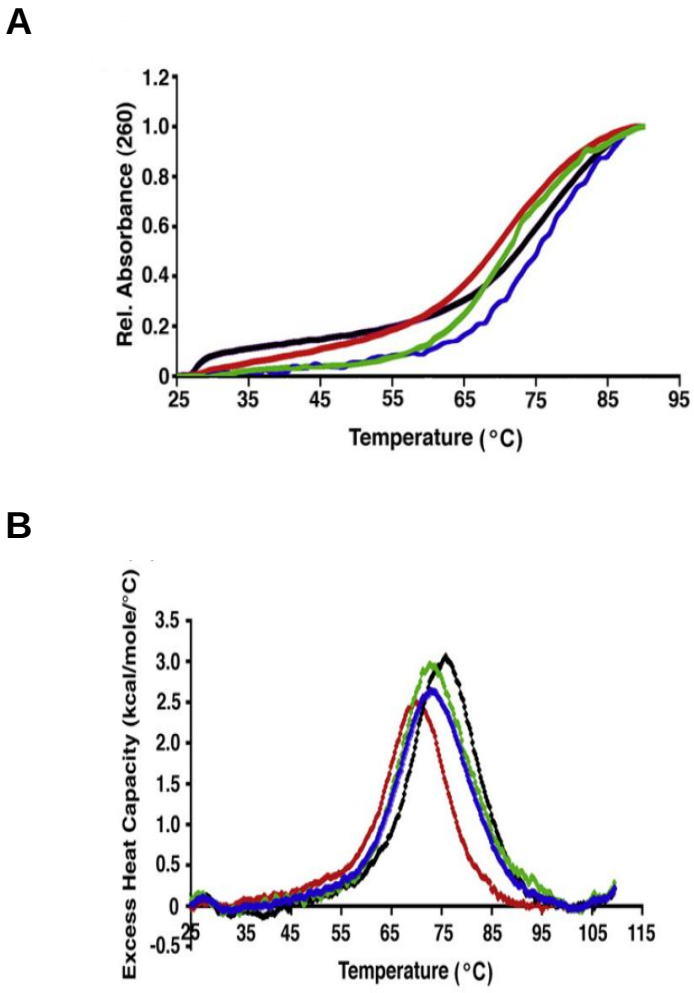

Figure 18. Thermal Melting of RNA Hairpins

A) UV Melting and B) Differential Scanning Calorimetry Data. Addition of Ψ to the *B. subtilis* ASL^{Tyr} improves the thermostability of the RNA molecule by ~5 °C. Interestingly, the addition of the dimethylallyl group did not decrease the stability of the molecule. Experiments were done in triplicate in low salt NMR buffer (10 mM Phosphate Buffer, 10 mM KCL, and 0.02 mM EDTA) at pH 6.3. The baseline was subtracted to obtain the melting temperature (T_m), enthalpy (ΔH), and the van't Hoff enthalpy (ΔH_V) for each molecule. The entropy (ΔS) was calculated using the formula $\Delta G = \Delta H - T\Delta S$, where $\Delta G=0$ at the T_m. Unmodified ASL^{Tyr}, red; $[\Psi_{39}]$-ASL^{Tyr}, black; $[i^6A_{37}]$-ASL^{Tyr}, green; $[\Psi_{39},i^6A_{37}]$-ASL^{Tyr}, blue. (Image from Denmon et al., 2011)

minutes, with the exponential phase lasting approximately 120 minutes. There appears to be no significant difference between the *tgt*⁻ strain, which presumably lacks Q at position 34 in its tRNAs, and the parent strain (Table 5). Interestingly, the *miaB*⁻ strain, which possesses tRNAs deficient in the ms^2 modification at position 37, has a doubling time that differs significantly from both the parent and *tgt*⁻ strains. Loss of ms^2 results in a faster doubling time (21.4 minutes) and the duration of the exponential growth phase (60 minutes) is shorter than the parent and *tgt*⁻ strains. Notably, all strains reached similar terminal densities.

In addition to LB medium, the parent and null mutant strains were also cultured in RM medium. RM is a defined medium that has been shown to support increased toxin production in B. anthracis (Leppla, 1988; Ristroph and Ivins, 1983). Previous studies using different strains of Bacilli cultured in RM medium showed an increase in the doubling times of the parent strain (Ristroph and Ivins, 1983). Unlike the doubling time observed in rich medium, the parent strain has a doubling time of 48.2 minutes and the *miaB*⁻ and *tgt*⁻ strains have doubling times of 54.6 minutes and 55.0 minutes, respectively. The increases observed in the doubling times of the null mutant strains compared to the parent strain suggests that partial modification at either position 34 or 37 negatively effects the growth rates of B. anthracis. Additionally, the duration of the exponential phase of the parent and null mutant strains is 180 minutes when grown in RM medium. Although the parent strain maintains a higher density through most of the study, the *miaB*⁻ strain eventually reaches a similar terminal density by the end of the growth experiment (Figure 19). Despite the *tgt*⁻ strain having a doubling time similar to the *miaB*⁻ null mutant, the *tgt*⁻ strain has a terminal density that is ~2-fold lower than both the parent and *miaB*⁻ strains.

The composition of the RM medium was modified slightly by omitting tyrosine to

Table 5. Doubling Times of the Parent and the Null Mutant Strains

Medium	Strain	Doubling Time (minutes)	Duration of Exponential Growth (minutes)
LB			
	Parent	28.9 ± 0.47	120
	miaB⁻	21.3 ± 1.37	60
	tgt⁻	29.5 ± 1.05	120
RM			
	Parent	48.2 ± 8.62	180
	miaB⁻	54.6 ± 11.93	180
	tgt⁻	55.0 ± 2.34	180
RM (without Tyrosine)			
	Parent	57.8 ± 11.55	180
	miaB⁻	63.7 ± 6.17	180
	tgt⁻	57.4 ± 6.34	120

determine if the parent and null mutant strains would be viable and to potentially stimulate one or both tyrosine tRNA synthetase genes via the T box mechanism. Both the mutant and parent strains grow in the modified RM medium; however, there was an increase in the doubling times compared to when the strains were grown in RM medium containing tyrosine (Table 5). Both the parent and *tgt*⁻ strains are in exponential phase for 120 minutes whereas, the *miaB*⁻ strain has a longer doubling period of 180 minutes. Unlike the parent and *miaB*⁻ strains, the *tgt*⁻ strain has a short lag phase and does not begin to show signs of doubling until 60 minutes into the growth study. Although the *tgt*⁻ strain has a short lag phase, once in exponential phase the doubling time is faster than the parent and *miaB*⁻ strains (Table 5). However, the terminal density is ~5-fold lower than the parent and ~4-fold lower than the *miaB*⁻ strains. Interestingly, even though the duration of the exponential phase is longer for the *miaB*⁻ strain, the doubling time is longer than that of the parent and the *tgt*⁻ strains, resulting in a lower density than the parent throughout the study (Figure 19).

3.2.2 Effects of Partial Modification on Antibiotic Sensitivity

To test what affect the loss of MiaA or TGT has on antibiotic sensitivity in *B. anthracis*, increasing dilutions of antibiotics were used to determine the Minimum Inhibitory Concentration (MIC) values of each strain in seven different antibiotics known to target different bacterial functions. When the parent, *miaA*⁻, and *tgt*⁻ strains are cultured in the presence of ampicillin, which inhibits cell wall synthesis by affecting peptidoglycan crosslinking, the MIC value was ≤ .125 μg/ml. Similar MIC values are observed with tetracycline, which binds reversibly to the 30 S subunit and inhibits protein synthesis and cell growth. The MIC value for benzylpenicillin (commonly referred to as penicillin G), which is a penicillin derivative that disrupts β-Lactam activity, is ≤ 0.6 μg/ml for the parent, *miaA*⁻,

A) LB Medium

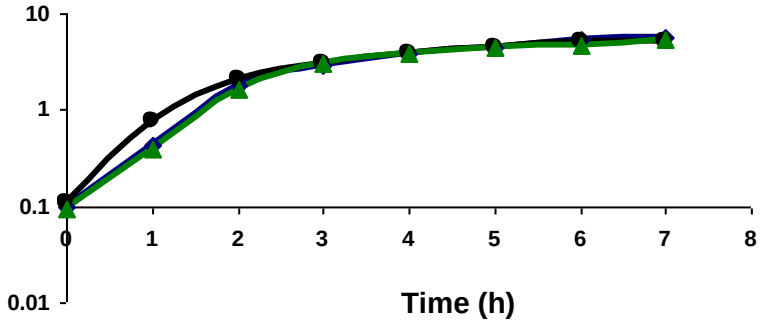

B) RM Medium

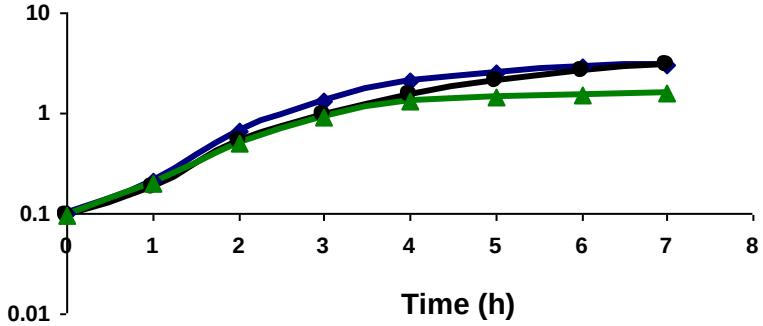

C) RM Medium without Tyr

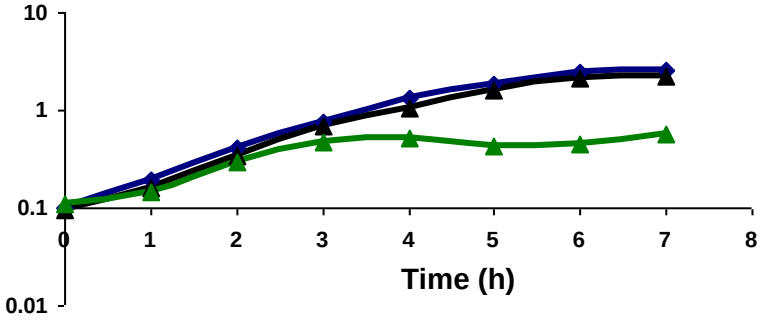

Figure 19. Growth Curves

(a) LB medium, (b) RM medium, and (c) RM medium without tyrosine. Strains were cultured at 37ºC in LB medium or in RM media in the presence (144 mg/ml) or absence (0 mg/ml) of tyrosine. All strains grew in the absence of tyrosine. Parent, blue; *miaB*⁻, black; *tgt*⁻, green.

and *tgt*⁻ strains (Table 6).

Interestingly, when cultured in the presence of spectenomycin, which inhibits translation by binding to the 30S subunit, the *miaA*⁻ strain appears to be more resistant to the antibiotic than the parent and *tgt*⁻ strains (Table 6). When the parent strain is treated with spectenomycin, the MIC value is 64 μg/ml, whereas the MIC value is greater than 64 μg/ml used in the presence of the *miaA*⁻ strain. The loss of $ms^2i^6A_{37}$ also appears to confer antibiotic resistance when cultured in ciprofloxacin, which is currently used to kill *B. anthracis* by interfering with the DNA gyrase. The MIC value for ciprofloxacin of both the parent and the *tgt*⁻ strain is ≤ .06 μg/ml but the MIC value increases to .125 μg/ml in the presence of the *miaA*⁻ strain.

When the parent and null mutant strains are cultured in the presence of erythromycin, which affects translation by binding to the 50 S subunit, the *tgt*⁻ strain appears to be more sensitive to the antibiotic. Loss of the Q base at position 34 in the *tgt*⁻ strain confers an increased sensitivity to erythromycin, which is evident by an MIC value of 1 μg/ml, whereas the parent and the *miaA*⁻ strains, which do not have tRNAs deficient in Q_{34}, the MIC value is 4 μg/ml.

3.2.3 Effects of Partial Modification on tRNA Mediated Transcriptional Regulation

To analyze the effects of partial modification on transcriptional regulation, qRT-PCR was employed to assess the transcript levels of the *tyrS1* and *tyrS2* tyrosyl-tRNA synthetase genes. Total RNA was harvested during mid-exponential phase from the parent, *miaA*⁻, and *tgt*⁻ strains grown in saturating (144 μg/ml) and limiting (0 μg/ml) concentrations of tyrosine. The ratio of T box leader to full-length transcript is represented as a bar graph (Figure 20).

Table 6. Minimum Inhibitory Concentration Values

Antibiotic	Parent	*miaA-*	*tgt-*
Tetracycline	≤ .125	≤ .125	≤ .125
Ampicillin	≤ .125	≤ .125	≤ .125
Erythromycin	4	4	1
Spectinomycin	64	> 64	64
Kanamycin	4	Ω-KAN Cassette	4
Ciprofloxacin	≤ .06	.125	≤ .06
Penicillin G	≤ .06	≤ .06	≤ .06

Concentrations are in μg/ml
Orange- Increased sensitivity to the antibiotic
Red- Increased resistance to the antibiotic
Lavender- conferred resistance by insertion of an Ω-Kanamycin resistance cassette

Surprisingly, both genes possess the putative T box sequence with the *tyrS1* T box sequence sharing 93% sequence identity to the T box consensus sequence and the *tyrS2* T box sequence sharing 79% identity (Figure 21). Although *tyrS1* has a T box sequence that is most similar to the T box consensus sequence, it possesses a G 3' to the specifier codon, whereas *tyrS2* has an A at this position (Figure 21). Previous studies have suggested that an A 3' to the specifier codon is important for interacting with U_{33}, which is conserved in all tRNA molecules discovered thus far.

In the case of *tyrS1*, which contains a T box sequence that is most similar to the consensus sequence, the parent strain shows a 5-fold increase in antitermination when cultured in tyrosine limiting conditions. The *miaA*⁻ strain shows a 1.6-fold induction in T box activity and the *tgt*⁻ strain shows a 2-fold increase in antitermination when grown in tyrosine limiting conditions (Figure 20). This suggests that *tyrS1* is T box regulated in all strains when amino acid conditions are limiting.

As for *tyrS2*, the parent strain shows a 16-fold increase in antitermination when cultured in tyrosine limiting conditions (Figure 20), which is consistent with observations made with the *tyrS* gene in *B. subtilis* (Grundy et al., 1997). Interestingly, *tyrS2* is no longer T box regulated the *miaA*⁻ strain, but it remains T box regulated in the *tgt*⁻ strain (2.6-fold induction) when grown in tyrosine limiting concentrations. These observations indicate that *tyrS2* is T box regulated.

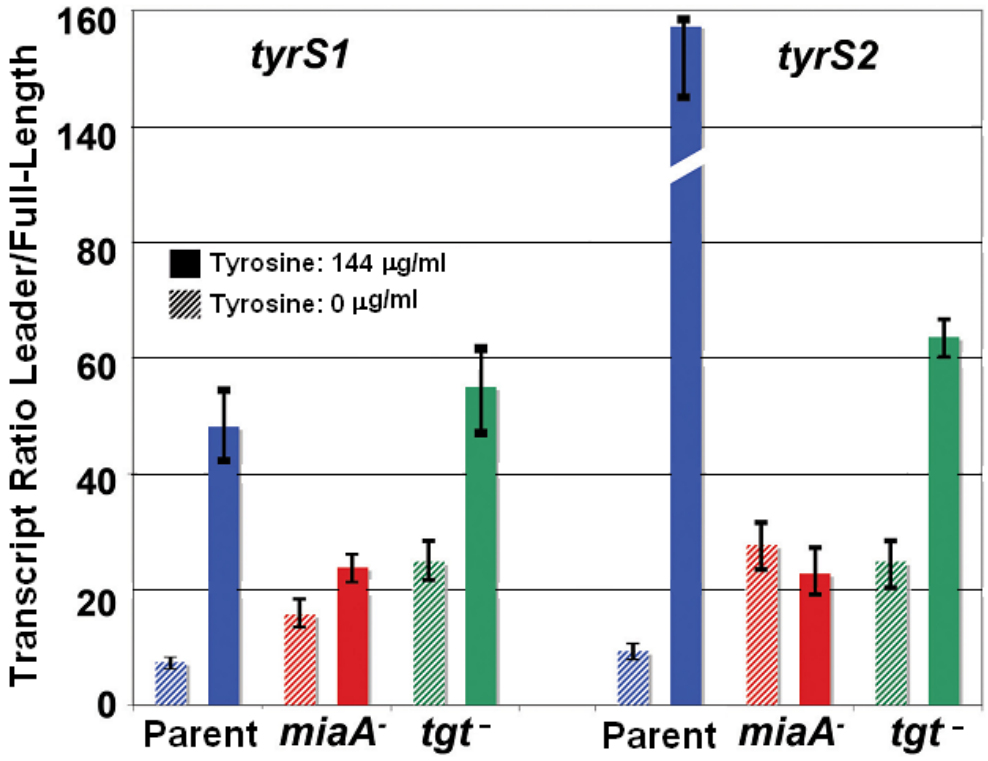

Figure 20. qRT-PCR of *tyrS1* and *tyrS2*

Parent, *miaA*–, and *tgt*– strains were grown at 37ºC on RM in the absence (0 mg/ml) and presence (144 mg/ml) of tyrosine. Total RNA was harvested during mid-log phase and analyzed by qRT-PCR at The University of Texas Health Science Center Quantitative Genomics Core Laboratory. Hashed bars indicate the absence of tyrosine and solid bars indicate tyrosine was present in the media. Parent, blue; *miaA*–, red; *tgt*–, green.

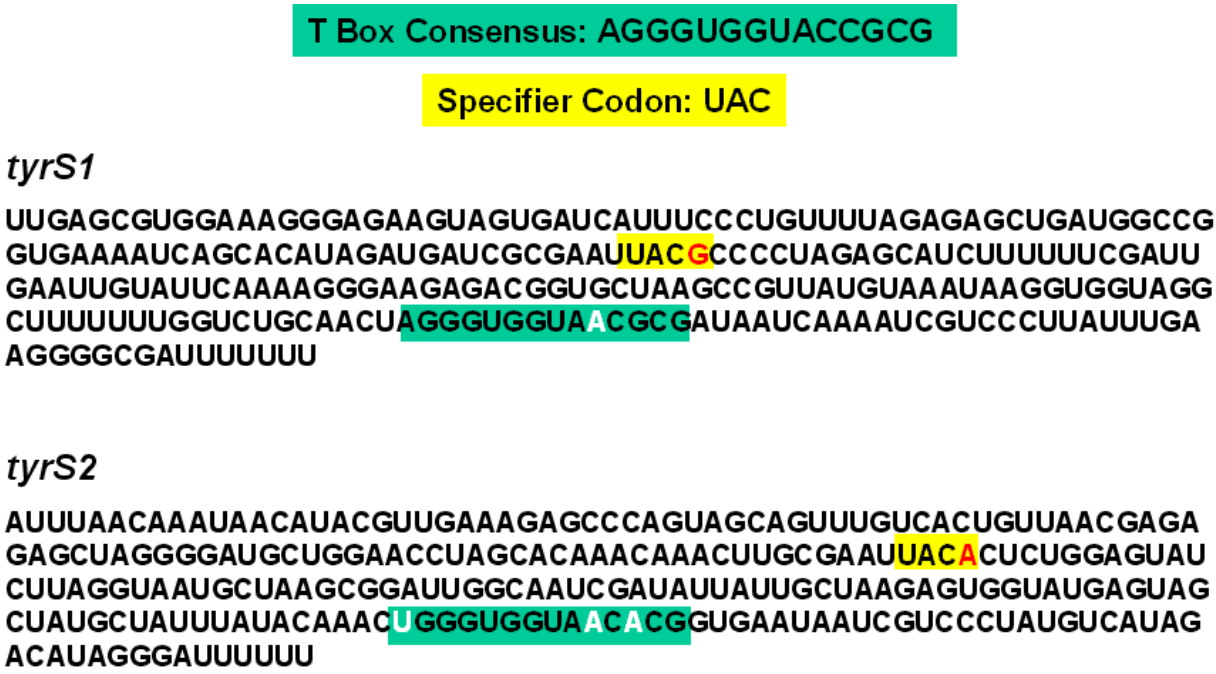

Figure 21. Comparison of the *tyrS1* and *tyrS2* mRNA Leader Sequences

The *tyrS1* gene shares 93% sequence identity to the consensus T box sequence and *tyrS2* shares 79% sequence identity to the consensus sequence. *tyrS1* and *tyrS2* share 71% sequence identity to each other. Teal rectangle, T box sequence; yellow rectangle, specifier codon; red text, conserved purine, white text, deviations from the consensus sequence.

*Sections 3.1 through 3.1.9 are courtesy of Denmon et al., 2011)

Chapter 4

Discussion

tRNAs from cells of all branches of life undergo base modification. However, there is limited information on how modification to the ASL affects the thermal stability, structure, and function of tRNA molecules. Through my dissertation work, I examined the effects of modification to positions 34, 37, and 39, which have been shown to play an important role in codon recognition, improving the base stacking on the 3' side of the stem, and stabilizing the loop-stem junction within the ASL. Through my dissertation work, the thermodynamic and structural contributions of the i^6A and Ψ modifications at positions 37 and 39 were examined using the *B. subtilis* ASL^{Tyr}. Additionally, I determined what role base modifications play in $tRNA^{Tyr}$ function by examining how Q_{34} and $ms^2i^6A_{37}$ contribute to the growth rate, antibiotic sensitivity, and transcriptional regulation in *B. anthracis*.

4.1 Comparison of ASL^{Tyr} Structures with other ASL Sequences

The U-turn motif and the functional significance of this conformation of the anticodon loop for translation was first revealed by the crystal structure of fully modified yeast $tRNA^{Phe}$ (Kim et al., 1974; Robertus et al., 1974; Shi and Moore, 2000). It has recently been shown that the anticodon arm of unmodified *E. coli* $tRNA^{Phe}$ adopts the same fold in the crystalline state (Byrne et al., 2010) (Figure 17). The nearly 180˚ reverse of the phosphate backbone between U_{33} and G_{34} and concomitant stacking of the anticodon nucleotide bases (residues 34, 35, and 36) on the 3' side of the loop, primes the tRNA for pairing with the mRNA codon on the ribosome (Weixlbaumer et al., 2007). The U-turn is stabilized in these molecules by the anticodon base stack and by hydrogen bonds from the U_{33} 2'-OH to the A_{35}

N7 and from the U_{33} N3H to the phosphoryl oxygen 5' to A_{36}. In the crystal structure of *E. coli* $tRNA^{Cys}$ (with the anticodon sequence 5'-GCA-3'), U_{33} and C_{35} form a hydrogen bond that stabilizes the U-turn. The exocyclic NH_2 group of C_{35} donates a proton to the U_{33} O2' while maintaining the ability of C_{35} to form Watson-Crick base pair interactions with the mRNA (Nissen et al., 1999). In modified *E. coli* $tRNA^{Lys}$ ASL (with the anticodon mnm^5s^2-UUU), the U_{33} NH-O1P hydrogen bond is maintained, but no interaction between U_{33} and U_{35} was identified (Sundaram et al., 2000).

Although the U-turn motif is prevalent in the anticodon arm of the crystal structures of tRNA molecules, in solution the *B. subtilis* unmodified and [Ψ_{39}]-, [i^6A_{37}]-, and [Ψ_{39}, i^6A_{37}]-ASL^{Tyr} molecules do not form this conserved structural motif. Our data indicate that the unmodified and partially modified molecules are composed of a five-base pair stem with a seven-nucleotide loop or a six-base pair stem with a five-nucleotide loop. Similar to the *B. subtilis* unmodified and [Ψ_{39}]-ASL^{Tyr}, the anticodon arms of the unmodified and Ψ_{39}-modified human $ASL^{Lys,3}$, the unmodified *E. coli* ASL^{Phe}, and the unmodified *E. coli* $tRNA^{Val}$ lack a defined U-turn structure (Cabello-Villegas and Nikonowicz, 2005; Durant and Davis, 1999; Vermeulen et al., 2005). However, the imino spectrum of the unmodified *E. coli* $tRNA^{Val}$ molecule in the presence of metal ion was similar to the native *E. coli* $tRNA^{Val}$, indicating that a U-turn was probably present (Vermeulen et al., 2005). Interestingly, the addition of i^6A_{37} and metal ion in the context of the *E. coli* ASL^{Phe} molecule resulted in the formation of a U-turn (Cabello-Villegas et al., 2004). Similarly, introducing N6-threonylcarbamoyl-A_{37} (t^6A_{37}) into the *E. coli* ASL^{Lys} in the presence of Ψ_{39} at pH 7 with metal ion promotes the structure toward the U-turn conformation (Sundaram et al., 2000). These data would suggest base modifications are critical for the formation of the archetypical

U-turn motif. However, this trend does not continue with the *B. subtilis* ASL^{Tyr} as the introduction of the i^6A_{37} modification alone or with Ψ_{39} in the presence or absence of metal ions does not lead to a U-turn (Figure 17). Similarly, the introduction of t^6A_{37} at pH 5.0 into the human $ASL^{Lys,3}$, which has the same nucleotide sequence as *E. coli* ASL^{Lys}, does not result in a U-turn (Stuart et al., 2000). Also analogous to the [i^6A_{37}]-ASL^{Tyr} and [i^6A_{37}, Ψ_{39}]-ASL^{Tyr} molecules, a C_{32}-A^+_{38} base pair is disrupted by the t^6A_{37} modification. Unlike the [i^6A_{37}]-ASL^{Tyr} and [i^6A_{37}, Ψ_{39}]-ASL^{Tyr} molecules, though, the human and *E. coli* ASL^{Lys} molecules have no cross-strand NOE's from the t^6A_{37} (Stuart et al., 2000; Sundaram et al., 2000). These results indicate that modification at residue 37 may be necessary to form the U-turn, but is not sufficient in all cases.

The structures of i^6A_{37}-modified *B. subtilis* ASL^{Tyr} and *E. coli* ASL^{Phe} demonstrate the sensitivity of the conformational effects of the i^6A_{37} modification to sequence context. The nucleotide sequences of these two molecules are very similar. The *E. coli* ASL^{Phe} anticodon sequence is 5'-GAA-3' and residue 32 is a uridine. The i^6A_{37} modification of *E. coli* ASL^{Phe} and metal ion binding lead to a stable U-turn fold (Cabello-Villegas et al., 2004), but these two elements are not sufficient to drive U-turn formation in the *B. subtilis* ASL^{Tyr}. Like the C_{32}-A^+_{38} base pair of ASL^{Tyr}, the U_{32}-A_{38} base pair of *E. coli* ASL^{Phe} is disrupted by the modification, and suggests the structural difference between the ASL^{Phe} and ASL^{Tyr} anticodon loops arises mainly from the base identity of nucleotide 35. The stacking energy for the purine base of ASL^{Phe} is more favorable than for the pyrimidine base of ASL^{Tyr}. Also, when paired with the adenine nucleotide of the codon, the O4 atom of U_{35} is not positioned to hydrogen bond with the U_{33} 2'-OH (Weixlbaumer et al., 2007), although this positional restriction may be relaxed outside the context of the ribosome. The lack of a U-turn

conformation with the i^6A_{37}-modification may offer a role for the Q modification at position 34 in ASL^{Tyr}. The Q_{34} base contains a dihydroxycyclopentene ring (Figure 6) that lends three hydrogen bond donors and substantial bulk to residue 34. Although the functional groups introduced by Q_{34} are not positioned to form additional hydrogen bonds with the Watson-Crick edge of the paired codon base, these attributes may increase the intra-loop base-sugar or base-base hydrogen bond network among the loop nucleotides. The bulkiness of the Q_{34} base also introduces additional stacking surface for the U_{35} base. Q_{34} at the 5' end of the anticodon loop may then function with the i^6A_{37} modification at the 3' end to stabilize stacking of the anticodon bases and re-mold the architecture of the loop.

Computational methods have been used to study the conformational features of N^6-dimethylallyl adenine. The methyl groups in the [i^6A_{37}]-ASL^{Tyr} and [Ψ_{39}, i^6A_{37}]-ASL^{Tyr} are oriented in a downward direction (Figure 15). This position of the methyl groups was found to be a low energy configuration of the dimethylallyl group in the absence of the ms^2 modification (Tewari, 1988). The addition of ms^2 results in an upward orientation of the methyl groups (Tewari, 1988). This may improve base stacking along the 3' side of the loop and along with Q_{34}, promote the formation of a U-turn.

4.2 Effects of Ψ_{39} and i^6A_{37} Modification on the Stability of the Anticodon Loop

Addition of Ψ_{39} to the ASL^{Tyr} molecule did not significantly alter the structure from the unmodified molecule. Residue U_{33} is stacked between C_{32} and G_{34} in both molecules and, unlike the *E. coli* ASL^{Phe} and human $ASL^{Lys,3}$ molecules that form compact tri-loop structures, the ASL^{Tyr} molecules form a five base loop that is well ordered.

The addition of Ψ to the ASL^{Tyr} RNA hairpin increased the stability of the stem by 5.7 ºC, which is similar to the effect observed in the human $ASL^{Lys,3}$ in low salt, acidic conditions. The ΔH of melting of the $[\Psi_{39}]$-ASL^{Tyr} hairpin obtained from DSC measurements was 1.07 kcal/mol per base pair higher than the unmodified molecule. The increase of the ΔH of melting is most likely due to the water-mediated hydrogen bond between the Ψ and the phosphate backbone (Arnez and Steitz, 1994). Additionally, Ψ_{39} increases the stability of the 31-39 base pair and contributes to the overall enthalpy (Durant and Davis, 1999). Although the transition event occurring at lower temperatures (<50ºC) in the UV curve is not as robust as in the unmodified ASL^{Tyr} hairpin, the $[\Psi_{39}]$-ASL^{Tyr} UV melting curve does suggest that the $[\Psi_{39}]$-ASL^{Tyr} has a well stacked loop. This finding is consistent with the structure of the $[\Psi_{39}]$-ASL^{Tyr} hairpin. However, the Ψ_{32} modification in the context of the *E. coli* ASL^{Phe} hairpin only increases the T_m of the molecule by 3.5 ºC, suggesting a Ψ at the stem-loop junction confers greater stability than when located in the loop proper with the water-mediated hydrogen bond to the phosphate backbone intact (Cabello-Villegas and Nikonowicz, 2005).

The dimethylallyl modification of A_{37} N6 opens up the helix proximal to the anticodon loop as evidenced by deprotonation of A_{38} and loss of the U_{39} H3 resonance. Broadening of base and sugar-phosphate backbone resonances of nucleotides in and near the loop indicate that i^6A_{37} destabilizes the structure of this region of the ASL^{Tyr} molecules and increases nucleotide mobility. The increased mobility in this region appears to be the result of steric clash between the modification and cross-strand nucleotides. The position of the dimethylallyl group in the helix leads to NOEs from dimethylallyl methyl protons to C_{32} and U_{33} base protons as well as disruption of the C_{32}-A^+_{38} base pair. While the i^6A_{37} modification

increases the dynamics of nucleotides within the loop region, the basic fold of the modified RNA hairpin in the presence of metal ion remains largely unchanged.

Although the dimethylallyl modification of A_{37} decreases the compact nature of the loop nucleotides, the DSC data indicate that the modification increases the stability of the hairpin stem by 3.7 °C and the ΔH by 1.39 kcal/mol. The absence of transitions at lower temperatures (< 50ºC) in the UV spectra confirms that the dimethylallyl modification is disrupting base stacking in the loop. A lower temperature transition is observed in the i^6 modified ASL^{Trp} molecule and the addition of the dimethylallyl group improved the stability of the hairpin compared to the unmodified form of the molecule (Kierzek and Kierzek, 2003). Interestingly, the t^6A_{37} modification in the human $ASL^{Lys,3}$ at pH 6.0 does not significantly affect the T_m or the thermal stability of the molecule compared to the unmodified molecule (Stuart et al., 2000). At pH 5.0, the T_m of the t^6A_{37} molecule was elevated ≈2 °C, but the thermal stability was comparable to the unmodified human $ASL^{Lys,3}$ (Stuart et al., 2000) which parallels the melting data obtained from the $[i^6A_{37}]$-ASL^{Tyr} molecule. Conversely, at pH 7.2 the t^6A_{37} modification decreases the T_m as well as the thermal stability, as does the i^6A modification in the *E. coli* ASL^{Phe} (Cabello-Villegas et al., 2004; Stuart et al., 2000).

4.3 Effect of Q_{34} Deficient and Hypomodified i^6A_{37} $tRNA^{Tyr}$ on Growth Rate in *B. anthracis*

To determine what role the loss of base modification at positions 34 (Q) and 37 (ms^2i^6A) play in *B. anthracis* growth rates, two null mutants deficient in either Q at position 34 or ms^2 at position 37 were created. The parent strain along with the two null mutants, *tgt*⁻ (deficient in Q) and *miaB*⁻ (deficient in ms^2), were cultured in three different medium

conditions: LB (rich medium), RM (defined medium), and RM lacking tyrosine (defined medium). When cultured in LB medium, no growth defects are observed in the *tgt*⁻ null strain and the doubling time and duration of the exponential phase is consistent with the parent strain (Table 5). Conversely, the *miaB*⁻ null strain shows a decrease in the doubling time and the duration of the exponential phase is shorter (Table 5). Despite the increased growth rate, the terminal density of *miaB*⁻ is within range of the parent and the *tgt*⁻ null strain (Figure 19). In *B. subtilis*, tRNAs that contain the ms^2i^6A modification at position 37 are found in two different forms. For example, both $tRNA^{Tyr}$ and $tRNA^{Phe}$ from *B. subtilis* are found in two modified states (Hoburg et al., 1979; McMillian and Arceneaux, 1975; Menichi and Heyman, 1976; Vold, 1978). The first form, which is the predominate species during exponential growth, is hypomodified with i^6A. The second species, which is the hypermodified form ($ms^2i^6A_{37}$), is the predominate form during stationary phase (McMillian and Arceneaux, 1975; Menichi and Heyman, 1976; Vold, 1978). The ratio of hypo- to hypermodified $tRNA^{Tyr}$ is 1:0.15 during exponential phase and 1:11.5 during stationary phase (McMillian and Arceneaux, 1975). These ratios suggest that the ms^2 modification plays a role in decreasing *B. subtilis* growth rates. Although the quantity of hypermodified $tRNA^{Tyr}$ is small during exponential growth, the ms^2 modification may play a role in keeping cellular growth rates in check. Therefore, the shorter doubling time observed in the *miaB*⁻ null mutant might be attributed to a loss in an unknown growth repressor activity that is normally provided by the ms^2 modification. The decrease in the duration of logarithmic growth might be attributed to the fact that the *miaB*⁻ strain is rapidly depleting the nutrient sources of the medium or other processes related to quorum sensing may support the transition into early stationary phase.

When the *tgt*⁻ and *miaB*⁻ null mutants are cultured in RM medium (defined), the duration of the exponential phase is the same as the parent strain. Although the *tgt*⁻ and *miaB*⁻ strains have similar doubling times (Table 5), the terminal density of the *tgt*⁻ strain is reduced compared to the parent and *miaB*⁻ strains (Figure 19). In addition to having tRNAs deficient in Q_{34}, the tRNAs from the *tgt*⁻ null mutant may also be deficient in ms^2. Previous studies have shown that *B. subtilis* grown in the presence of tyrosine show a decrease in the ratio (1:1.59) of hypo- to hypermodified $tRNA^{Tyr}$ species harvested from stationary phase cells (McMillian and Arceneaux, 1975). This suggests that tyrosine may play a role in delaying the exponential to stationary phase transition. Additionally, Horburg et al. showed that hypomodification at positions 34 and 37 in *B. subtilis* $tRNA^{Phe}$ resulted in fewer fMet-Phe dipeptides and the rate of polypeptide formation was also decreased (Hoburg et al., 1979). Modification at the wobble position (residue 34) has also been shown to contribute to enhance codon recognition. For example, in *E. coli* the 2'-O-methylcytosine (C_m) modification enhanced cognate codon recognition (Satoh et al., 2000). Therefore, the reduced terminal density observed in the *tgt*⁻ strain is likely attributed to a Q_{34} deficiency as well as hypomdification at position 37. The *miaB*⁻ strain's ability to reach a density comparable to the parent strain is likely due to the presence of Q_{34}.

Interestingly, all three strains (parent, *tgt*⁻, and *miaB*⁻) have slower doubling times when cultured in RM medium without tyrosine. When *B. subtilis* strains were cultured in Penassay Broth supplemented with or without tyrosine, the doubling times remained the same (McMillian and Arceneaux, 1975). It is possible that the Penassay Broth contains other nutrients that aid in maintaining the growth rate and supporting tyrosine biogenesis. The doubling time of both the parent and *miaB*⁻ strains increased by approximately 10 minutes

and the doubling time of the *tgt*⁻ strain showed a slight increase of approximately 2 minutes (Table 5). The reduced efficiency of growth in all three strains might be attributed to the inability of the RM medium without tyrosine to effectively support tyrosine biosynthesis. As previously mentioned, tyrosine may play an important role in delaying the exponential to stationary phase transition. The absence of tyrosine from the RM medium may facilitate a reduction in the growth rate and the exponential phase (Figure 19). In addition to a longer doubling time, the *tgt*⁻ strain was in lag phase for 1 hour (Table 5). Although the doubling time of the *tgt*⁻ strain was the same as the parent strain, the duration of the exponential phase was shorter and the density remained low (Figure 19). The low terminal density and lag phase may be attributed to an increase in an earlier and more robust production of ms^2 in the absence of tyrosine.

4.4 Effect of Q_{34}, and $ms^2i^6A_{37}$ Deficient $tRNA^{Tyr}$ on Antibiotic Sensitivity

To elucidate what role partial modification has on antibiotic sensitivity, the MIC values of the parent strain along with two mutants, *tgt*⁻ and *miaA*⁻ (deficient in ms^2i^6A), were determined (Table 6). The *tgt*⁻ and *miaA*⁻ strains have the same MIC values of four of the seven antibiotics tested. Surprisingly, when tested in the presence of the *miaA*⁻ strain, the MIC values increased for spectinomycin and ciprofloxacin, suggesting that cells containing tRNAs deficient in $ms^2i^6A_{37}$ might be more resistant to certain antibiotics (Table 6). Both antibiotics have different mechanisms of action. For example, spectinomycin binds to the 30S subunit and inhibits protein synthesis, whereas ciprofloxacin, which is currently used to kill *B. anthracis*, disrupts DNA gyrase function. A reduction in MIC for erythromycin when tested in the presence of *tgt*⁻, suggests that tRNAs deficient in Q_{34} might be sensitive to other antibiotics. Erythromycin inhibits translation by targeting the 50S subunit. Previous studies

have shown that *B. subtilis* treated with pactamycin, which inhibits protein synthesis by targeting the 70S ribosome, negatively affect SAM-dependent methylations (Kersten et al., 1968). Pectamycin treated *B. subtilis* were deficient in m^7G and ms^2 in $tRNA^{Tyr}$ and $tRNA^{Phe}$ (Arnold et al., 1976). Interestingly, *E. coli* treated with chloramphenicol, which affects peptide elongation by targeting the 50S subunit, have tRNAs that lack D, T, and ms^2 modifications (Mann and Huang, 1973; Waters et al., 1973). Therefore, the increased or decreased MIC values observed for the antibiotics tested with the *miaA*⁻ and *tgt*⁻ strains, respectively, might be the result of tRNAs deficient not only in $ms^2i^6A_{37}$ and Q_{34}, but other modifications as well.

4.5 Effect of Q_{34} and $ms^2i^6A_{37}$ Deficient $tRNA^{Tyr}$ on tRNA Mediated Transcriptional Regulation

To elucidate what role partially modified tRNAs have in tRNA mediated transcriptional regulation, T box regulatory function was examined in *miaA*⁻ and *tgt*⁻ strains by monitoring the transcription levels of the tyrosyl tRNA synthetase genes, *tyrS1* and *tyrS2*. In bacteria, it is rare to find a second gene that codes for a specific AARS. Nevertheless, certain strains of *Bacilli* appear to be the exception with three known tRNA synthetase genes (ThrRS, TyrTS, and LysRS) having two phylogenetically distinct copies within the cell (Foy et al., 2010; Grundy et al., 1997; Putzer et al., 1990). Unlike both of the ThrRS genes, which are T box regulated and expressed during different stages of growth, only one of the TyrTS genes (*tyrS*) and one LysRS gene (class I or class II synthetase) are T box regulated (Foy et al., 2010; Grundy et al., 1997; Putzer et al., 1990). Similar to the second ThrRS gene in *B. subtilis*, *thrZ*, the *tyrZ* gene is not expressed in vegetative growing cells (Henkin et al., 1992). In *B. anthracis*, both *tyrS1* and *tyrS2* appear to be T box regulated and expressed during logarithmic growth (Figure 20). Although the *tyrS1* T box sequence shares 93% sequence

identity to the consensus sequence, it does not show the same robustness in the induction of T box activity when the cells are starved for tyrosine (Figures 20 and 21). The modest induction rates of the parent (5-fold) and *tgt*⁻ (2.2-fold) strains as well as the low induction rate observed in the *miaA*⁻ strain (1.6-fold) are likely due to the presence of a G 3' to the specifier codon instead of an A (Figure 21). The conserved A may interact with U_{33}, which is conserved in all tRNA molecules. The loss of this conserved residue might impair the recognition of the specifier codon by $tRNA^{Tyr}$ or decrease the stability of the tRNA-specifier codon interaction. In contrast to *tyrS1*, the T box sequence found in the *tyrS2* leader mRNA is only 79% similar to the consensus sequence and the specifier codon is followed by an A (Figure 21). T box induction of the parent strain (16-fold) was comparable to that observed with *tyrS* from *B. subtilis* (Grundy et al., 1997). Interestingly, *tyrS2* was no longer T box regulated in the *miaA*⁻ strain. Additionally, there was no significant difference in T box induction in response to limiting concentrations of tyrosine in the *tgt*⁻ strain (Figure 20). The moderate and low T box induction ratios are similar to those observed by Grundy et al. when they mutated the specifier codon and discriminator base found in *tyrS*, which was specific to $tRNA^{Tyr}$, to respond to other tRNAs and the limiting concentrations of their cognate amino acids (Grundy et al., 1997). The reduction in T box induction suggested that other factors besides sequence, might contribute to tRNA mediated transcriptional regulation in *B. subtilis* (Grundy et al., 1997). Additionally, Means et al. suggest that additional factors, beyond nucleotide base pairing, may be important when designing tRNA analogs to disrupt T box activity (Means et al., 2007). Therefore, the moderate and low T box induction rates observed with *tyrS1* in the mutant strains and the obliteration of T box activity observed with *tyrS2* in the *miaA*⁻ strain strongly suggests that base modifications, in conjunction with nucleotide

interactions and sequence, are necessary to support tRNA mediated transcriptional regulation.

4.6 Significance of Ψ, ms^2i^6A, and Q Modifications in Translation

One of the most common modifications found in tRNA molecules is the Ψ modification. The pseudouridine synthase, TruA, catalyzes the isomerization of uridines 38, 39, and 40 in the anticodon arms of bacterial tRNA resulting in a $C_{1'}$-C_5 glycosidic bond and introduction of an additional NH functional group in the base (Hur and Stroud, 2007). When located in a helical stem, Ψ confers additional stability to the helix by forming a water-mediated hydrogen bond to the phosphate backbone through the N1 NH group. The addition of Ψ at position 39 leads to increased stability and stacking at the anticodon arm stem-loop junction (Cabello-Villegas and Nikonowicz, 2005; Durant and Davis, 1999). Presumably, the increased stability conferred by the Ψ at this location enhances translation efficiency and improves growth rate compared to tRNA molecules lacking the Ψ modification (Charette and Gray, 2000; Lecointe et al., 2002). In *S. cerevisiae*, loss of the $\Psi_{38/39}$ modifications in $tRNA^{Tyr}$, $tRNA^{Lys}$, and $tRNA^{Trp}$ impairs decoding of the amber UAG stop codon and decreases read-through efficiency during translation resulting in decreased growth rate (Lecointe et al., 2002). In *P. aeruginosa*, mutation of the *truA* gene leads to cells deficient in expressing functional type III secretion genes and are unable to sustain virulence (Ahn et al., 2004).

The importance of the dimethylallyl modification of A_{37} for tRNA function has been well-studied in *E. coli* (Björnsson and Isaksson, 1993; Bouadloun et al., 1986; Connolly and Winkler, 1989; Diaz et al., 1987; Ericson and Björk, 1991b; Hagervall et al., 1990) and

modification of A_{37} to i^6A_{37} is necessary to form the hypermodified base, $ms^2i^6A_{37}$ through the activity of MiaB (Björk, 1998). In *B. subtilis*, $tRNA^{Tyr}$ can exist in two forms, the hypomodified i^6A_{37} and the hypermodified $ms^2i^6A_{37}$ (Buu et al., 1981; Menichi and Heyman, 1976; Vold, 1978). In stationary-phase cells, the hypermodified form predominates whereas, in exponential growth phase cells, the single-modified form of $tRNA^{Tyr}$ is the dominant form (Menichi and Heyman, 1976). The hypermodified form is better able to decode the UAC codon (Menichi and Heyman, 1976) and the presence of the thiomethyl modification correlates with the onset of sporulation (Buu et al., 1981).

In *S. typhimurium*, modification of A_{37} to 2-methylthio-N^6-(4-hydroxyisopentenyl) adenosine (ms^2io^6A) can increase translational efficiency. Suppression of the amber codon by $tRNA^{Tyr}$, $tRNA^{Gln}$, and $tRNA^{Ser}$ containing $ms^2io^6A_{37}$ exhibited decreased codon context sensitivity, particularly when flanked on the 3' side by an A or a C (Ericson and Björk, 1991b). Readthrough of amber codons followed by an A increases in the absence of the hypermodified A_{37} (Ericson and Björk, 1991b). Interestingly, the loss of Ψ_{39} in suppressor $tRNA^{Tyr}$ and $tRNA^{Gln}$ decreases the translational efficiency of the molecules by two- and 10-fold, respectively (Ericson and Björk, 1991b). However, the absence of Ψ_{39} does not alter the codon context sensitivity of $tRNA^{Tyr}$ and $tRNA^{Gln}$ (Ericson and Björk, 1991b), indicating that the $ms^2io^6A_{37}$ and m^2A_{37} modifications are the principle forces in mitigating mistranslation caused by codon context but are not sufficient for maintaining translation efficiency.

Q, which is derived from guanine, is commonly found in $tRNA^{Asp}$, $tRNA^{Asn}$, $tRNA^{His}$, and $tRNA^{Tyr}$. Q is synthesized *de novo* by bacteria, but in vertebrates, Q must be supplemented through the diet. Loss of Q in mice and eukaryotic HepG2 cells results in an

inability to synthesize tyrosine from phenylalanine, which eventually leads to death (Rakovich et al., 2011). Loss of Q_{34} in *E. coli* $tRNA^{Tyr}$ and $tRNA^{His}$ resulted in frame shifting of $tRNA^{Pro}$ or $tRNA^{Phe}$ in the P-site when the UAU (Tyr) codon was in the A-site and frameshifting of $tRNA^{Phe}$ in the P-site when the CAU (His) codon was adjacent in the A-site (Urbonavičius et al., 2001). The slippage observed by the tRNA in the P-site is most likely caused by slow entry of the hypomodified (Q_{34} deficient) tRNAs into the A-site (Urbonavičius et al., 2001). Interestingly, both hypo- and fully modified tRNAs have a bias toward codons that have a C at the end position of the codon instead of a U (Urbonavičius et al., 2001).

4.7 Future Work and Applications

Prior to my thesis work, there was limited information regarding the effects of base modifications on tRNA structure, stability, and function. Currently, there are no crystal or solution structures available of tRNAs from Gram-positive bacteria or of the $tRNA^{Tyr}$ molecule from any organism. Through this work I have solved, to date, the first known structures of the unmodified, [Ψ_{39}]-, [i^6A_{37}]-, and [i^6A_{37}, Ψ_{39}]-ASL^{Tyr} hairpins from a Gram-positive organism. Determination of the solution structures of the unmodified and partially modified ASL^{Tyr} molecules will provide much needed information regarding the contribution of individual modifications on tRNA structure in the context of the $tRNA^{Tyr}$ ASL. Additionally, this information may provide new insight into $tRNA^{Tyr}$ interactions with the ribosome and other RNA molecules. To further our understanding of how the modifications within the ASL^{Tyr} affect the structure, the next step would be to see how the addition of the ms^2 and Q modifications contribute to the structure. The addition of the bulky modifications

may promote the formation of the canonical U-turn motif, which has been observed in all crystal structures known to date.

Although the structures, locations, or compositions of the known 107 base modifications have been well characterized, there are limited examples of how the known modifications affect the stability of RNA molecules, especially tRNAs. In addition to determining the contributions of base modification on ASL^{Tyr} structure, I also elucidated what effect partial modification has on the stability of the unmodified and partially modified molecules. Understanding what effect partial modification had on the stability of the ASL^{Tyr} hairpins might provide insight into the structure, binding interactions, and function of other tRNA molecules. To better our understanding of how base modifications affect the stability of $tRNA^{Tyr}$, the next step –in addition to seeing the effects of the ms^2 and Q modifications on stability– would be to test the stability of the various modified forms of the ASL^{Tyr} in different buffer conditions. NMR experiments can then be employed to examine any molecule or condition that showed a significant change in the enthalpy or melting temperature.

Even though there is substantial information regarding the roles that tRNAs play in translation, there is very little information on their involvement in tRNA-mediated transcriptional regulation via the T box mechanism. Moreover, the effects of base modification on T box function have never been studied. In addition to the lack of information regarding the importance of base modifications on tRNA-mediated transcriptional regulation, there was also limited information on the significance of ASL^{Tyr} modifications as it related to growth and antibiotic sensitivity in Gram-positive organisms. Through my work, I was able to elucidate what role base modifications play in T box

function, cellular growth, and antibiotic sensitivity. By understanding the importance of base modifications on transcriptional regulation and cellular physiology, new targets for antibiotics can be probed. For example, the Hines laboratory at Ohio State University is looking at tRNA derivatives that mimic full-length tRNAs to inhibit T box antitermination. Currently, they have discovered that sequence recognition is not enough as the rate of dissociation for the tRNA mimics is high. My work has shown that base modifications are important and have functional relevance. It is possible that the dissociation rates of these tRNA mimics can be improved by incorporating modified bases.

*Sections 4.1 through 4.2 are courtesy of Denmon et al., 2011

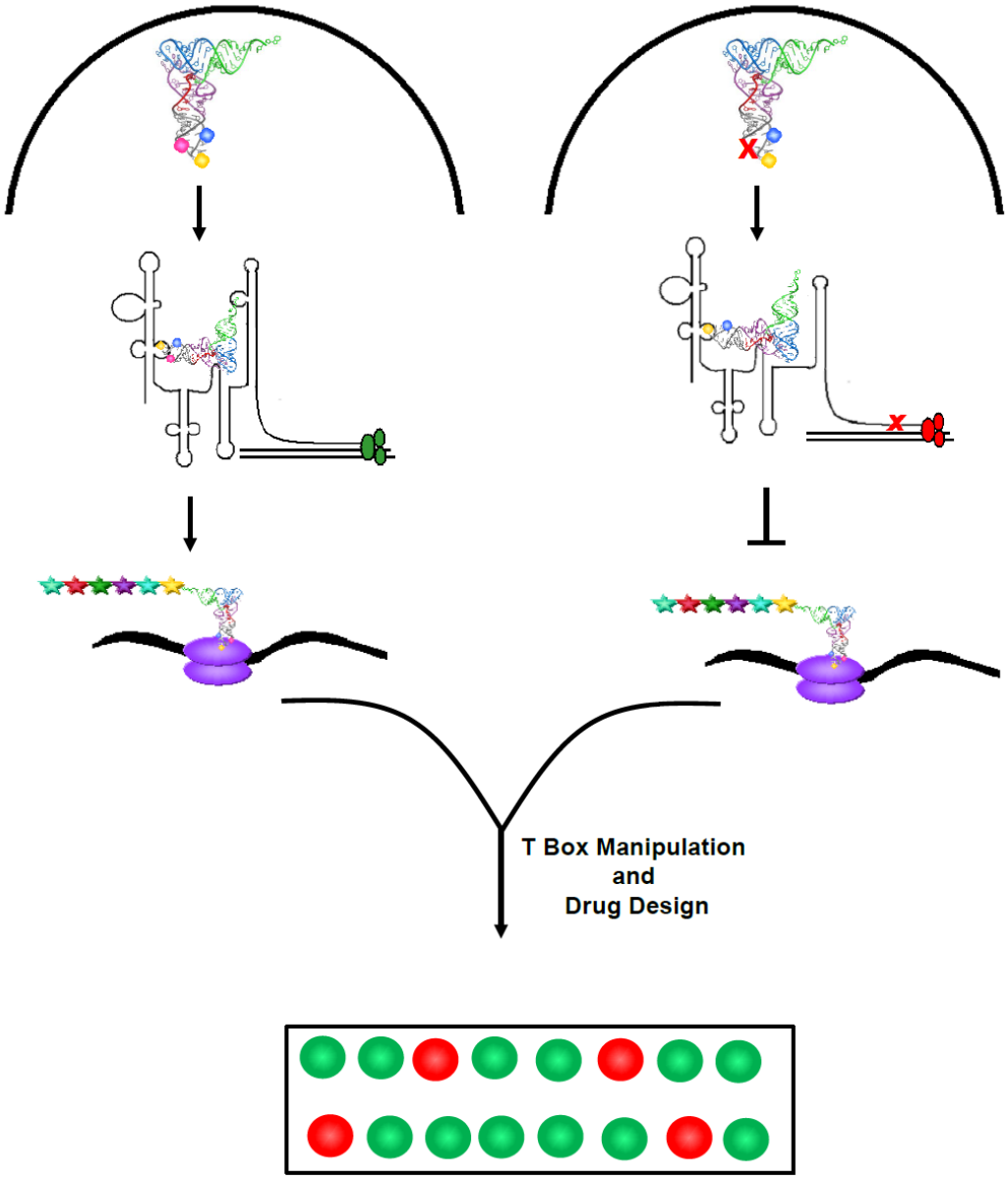

Figure 22. Base Modifications and Drug Design

Through my thesis work, I have shown that base modifications are important for tRNA structure, stability, and function. This figure illustrates the importance of understanding what role base modifications play in transcriptional regulation. The loss of a specific modification(s) (right) results in reduced T box activation, which causes a decrease in mRNA levels. Reduced mRNA levels may lead to insufficient protein production, resulting in decreased cellular viability or death. Using this information, future scientists will be able to design drugs that either inhibit base modifying enzymes or block the association of a tRNA molecule with its cognate mRNA. The green circles represent drugs that do not inhibit or significantly reduce T box function and do not promote cell death. The red circles represent drugs that reduce or inhibit T box function and promote cell death.

References

Agris, P.F. (1996). The importance of being modified: roles of modified nucleosides and Mg^{2+} in RNA structure and function. Prog. Nucleic Acid Res. Mol. Biol. *53*, 79–129.

Agris, P.F., Guenther, R., Sochacka, E., Newman, W., Czerwińska, G., Liu, G., Ye, W., and Malkiewicz, A. (1999). Thermodynamic contribution of nucleoside modifications to yeast tRNA(Phe) anticodon stem loop analogs. Acta Biochim. Pol. *46*, 163–172.

Ahn, K.S., Ha, U., Jia, J., Wu, D., and Jin, S. (2004). The *truA* gene of *Pseudomonas aeruginosa* is required for the expression of type III secretory genes. Microbiology (Reading, Engl.) *150*, 539–547.

Allain, F.H. and Varani, G. (1995). Divalent metal ion binding to a conserved wobble pair defining the upstream site of cleavage of group I self-splicing introns. Nucleic Acids Res. *23*, 431-350.

Arnez, J.G., and Steitz, T.A. (1994). Crystal structure of unmodified tRNA(Gln) complexed with glutaminyl-tRNA synthetase and ATP suggests a possible role for pseudo-uridines in stabilization of RNA structure. Biochemistry *33*, 7560–7567.

Arnold, H.H., Schmidt, W., Raettig, R., Sandig, L., Domdey, H., and Kersten, H. (1976). S-Adenosylmethionine and tetrahydrofolate-dependent methylation of tRNA in *Bacillus subtilis*. Incomplete methylations caused by trimethoprim, pactamycin, or chloramphenicol. Arch. Biochem. Biophys. *176*, 12–20.

Ashraf, S.S., Guenther, R.H., Ansari, G., Malkiewicz, A., Sochacka, E., and Agris, P.F. (2000). Role of modified nucleosides of yeast tRNA(Phe) in ribosomal binding. Cell Biochem. Biophys. *33*, 241–252.

Auffinger, P., and Westhof, E. (1999). Singly and bifurcated hydrogen-bonded base-pairs in tRNA anticodon hairpins and ribozymes. J. Mol. Biol. *292*, 467–483.

Babitzke, P. (2004). Regulation of transcription attenuation and translation initiation by allosteric control of an RNA-binding protein: the *Bacillus subtilis* TRAP protein. Curr. Opin. Microbiol. *7*, 132–139.

Baumann, U., Fischer, W., and Sprinzl, M. (1985). Analysis of modification-dependent structural alterations in the anticodon loop of *Escherichia coli* $tRNA^{Arg}$ and their effects on the translation of MS2 RNA. Eur. J. Biochem. *152*, 645–649.

Beuning, P.J., and Musier-Forsyth, K. (1999). Transfer RNA recognition by aminoacyl-tRNA synthetases. Biopolymers *52*, 1–28.

Bilbille, Y., Vendeix, F.A.P., Guenther, R., Malkiewicz, A., Ariza, X., Vilarrasa, J., and Agris, P.F. (2009). The structure of the human $tRNA^{Lys,3}$ anticodon bound to the HIV

genome is stabilized by modified nucleosides and adjacent mismatch base pairs. Nucleic Acids Res *37*, 3342–3353.

Björk, G.R. (1995). Biosynthesis and function of modified nucleosides. In tRNA: Structure, Biosynthesis, and Function, (Washington, DC: ASM Press), pp. 165–206.

Björk, G.R. (1998). Modified nucleosides at positions 34 and 37 of tRNAs and their predicted coding capacities. In Modification and Editing of RNA, (Washington, DC: ASM Press), pp. 577–582.

Björk, G.R., Jacobsson, K., Nilsson, K., Johansson, M.J., Byström, A.S., and Persson, O.P. (2001). A primordial tRNA modification required for the evolution of life? EMBO J. *20*, 231–239.

Björnsson, A., and Isaksson, L.A. (1993). UGA codon context which spans three codons. Reversal by $ms^2i^6A_{37}$ in tRNA, mutation in *rpsD*(S4) or streptomycin. J. Mol. Biol. *232*, 1017–1029.

Bossi, L., and Ruth, J.R. (1980). The influence of codon context on genetic code translation. Nature *286*, 123–127.

Bouadloun, F., Srichaiyo, T., Isaksson, L.A., and Björk, G.R. (1986). Influence of modification next to the anticodon in tRNA on codon context sensitivity of translational suppression and accuracy. J. Bacteriol. *166*, 1022–1027.

Brill, J., Hoffmann, T., Bleisteiner, M., and Bremer, E. (2011a). Osmotically controlled synthesis of the compatible solute proline is critical for cellular defense of *Bacillus subtilis* against high osmolarity. J. Bacteriol. *193*, 5335–5346.

Brill, J., Hoffmann, T., Putzer, H., and Bremer, E. (2011b). T-box-mediated control of the anabolic proline biosynthetic genes of *Bacillus subtilis*. Microbiology (Reading, Engl.) *157*, 977–987.

Buck, M., and Griffiths, E. (1982). Iron mediated methylthiolation of tRNA as a regulator of operon expression in *Escherichia coli*. Nucleic Acids Res. *10*, 2609–2624.

Buu, A., Menichi, B., and Heyman, T. (1981). Thiomethylation of tyrosine transfer ribonucleic acid is associated with initiation of sporulation in *Bacillus subtilis*: effect of phosphate concentration. J. Bacteriol. *146*, 819–822.

Byrne, R.T., Konevega, A.L., Rodnina, M.V., and Antson, A.A. (2010). The crystal structure of unmodified tRNAPhe from *Escherichia coli*. Nucleic Acids Res. *38*, 4154–4162.

Cabello-Villegas, J., and Nikonowicz, E.P. (2005). Solution structure of psi32-modified anticodon stem-loop of *Escherichia coli* $tRNA^{Phe}$. Nucleic Acids Res. *33*, 6961–6971.

Cabello-Villegas, J., Winkler, M.E., and Nikonowicz, E.P. (2002). Solution conformations of unmodified and A(37)N(6)-dimethylallyl modified anticodon stem-loops of *Escherichia coli* tRNA(Phe). J. Mol. Biol. *319*, 1015–1034.

Cabello-Villegas, J., Tworowska, I., and Nikonowicz, E.P. (2004). Metal ion stabilization of the U-turn of the A_{37} N^6-dimethylallyl-modified anticodon stem-loop of *Escherichia coli* $tRNA^{Phe}$. Biochemistry *43*, 55–66.

Cantara, W.A., Crain, P.F., Rozenski, J., McCloskey, J.A., Harris, K.A., Zhang, X., Vendeix, F.A.P., Fabris, D., and Agris, P.F. (2011). The RNA Modification Database, RNAMDB: 2011 update. Nucleic Acids Res. *39*, D195–201.

Cantara, W.A., Bilbille, Y., Kim, J., Kaiser, R., Leszczyńska, G., Malkiewicz, A., and Agris, P.F. (2012). Modifications modulate anticodon loop dynamics and codon recognition of *E. coli* tRNA(Arg1,2). J. Mol. Biol. *416*, 579–597.

Carlson, B.A., Mushinski, J.F., Henderson, D.W., Kwon, S.Y., Crain, P.F., Lee, B.J., and Hatfield, D.L. (2001). 1-Methylguanosine in place of Y base at position 37 in phenylalanine tRNA is responsible for its shiftiness in retroviral ribosomal frameshifting. Virology *279*, 130–135.

Charette, M., and Gray, M.W. (2000). Pseudouridine in RNA: what, where, how, and why. IUBMB Life *49*, 341–351.

Chimnaronk, S., Forouhar, F., Sakai, J., Yao, M., Tron, C.M., Atta, M., Fontecave, M., Hunt, J.F., and Tanaka, I. (2009). Snapshots of dynamics in synthesizing N(6)-isopentenyladenosine at the tRNA anticodon. Biochemistry *48*, 5057–5065.

Connolly, D.M., and Winkler, M.E. (1989). Genetic and physiological relationships among the miaA gene, 2-methylthio-N^6-(delta-2-isopentenyl)-adenosine tRNA modification, and spontaneous mutagenesis in *Escherichia coli* K-12. J. Bacteriol. *171*, 3233–3246.

Crick, F.H. (1966). Codon--anticodon pairing: the wobble hypothesis. J. Mol. Biol. *2*, 548-555.

Davanloo, P., Rosenberg, A.H., Dunn, J.J., and Studier, F.W. (1984). Cloning and expression of the gene for bacteriophage T7 RNA polymerase. Proc. Natl. Acad. Sci. U.S.A. *81*, 2035–2039.

Denmon, A.P., Wang, J., Nikonowicz, E.P. (2011). Conformation effects of base modification on the anticodon stem-loop of *Bacillus subtilis* $tRNA^{Tyr}$. J. Mol. Biol. *412*, 285-303.

Diaz, I., Pedersen, S., and Kurland, C.G. (1987). Effects of miaA on translation and growth rates. Mol. Gen. Genet. *208*, 373–376.

Dieckmann, T., and Feigon, J. (1997). Assignment methodology for larger RNA oligonucleotides: application to an ATP-binding RNA aptamer. J. Biomol. NMR *9*, 259–272.

Dineshkumar, T.K., Thanedar, S., Subbulakshmi, C., and Varshney, U. (2002). An unexpected absence of queuosine modification in the tRNAs of an *Escherichia coli* B strain. Microbiology (Reading, Engl.) *148*, 3779–3787.

Dönmez, G., Hartmuth, K., and Lührmann, R. (2004). Modified nucleotides at the 5' end of human U2 snRNA are required for spliceosomal E-complex formation. RNA *10*, 1925–1933.

Durand, J.M., Okada, N., Tobe, T., Watarai, M., Fukuda, I., Suzuki, T., Nakata, N., Komatsu, K., Yoshikawa, M., and Sasakawa, C. (1994). *vacC*, a virulence-associated chromosomal locus of *Shigella flexneri*, is homologous to *tgt*, a gene encoding tRNA-guanine transglycosylase (Tgt) of *Escherichia coli* K-12. J. Bacteriol. *176*, 4627–4634.

Durant, P.C., and Davis, D.R. (1999). Stabilization of the anticodon stem-loop of $tRNA^{Lys,3}$ by an A^{+}-C base-pair and by pseudouridine. J. Mol. Biol. *285*, 115–131.

Ericson, J.U., and Björk, G.R. (1991a). tRNA anticodons with the modified nucleoside 2-methylthio-N^6-(4-hydroxyisopentenyl)adenosine distinguish between bases 3' of the codon. J. Mol. Biol. *218*, 509–516.

Ericson, J.U., and Björk, G.R. (1991b). tRNA anticodons with the modified nucleoside 2-methylthio-N^6-(4-hydroxyisopentenyl)adenosine distinguish between bases 3' of the codon. J. Mol. Biol. *218*, 509–516.

Esberg, B., Leung, H.C., Tsui, H.C., Björk, G.R., and Winkler, M.E. (1999). Identification of the *miaB* gene, involved in methylthiolation of isopentenylated A_{37} derivatives in the tRNA of *Salmonella typhimurium* and *Escherichia coli*. J. Bacteriol. *181*, 7256–7265.

Foy, N., Jester, B., Conant, G.C., and Devine, K.M. (2010). The T box regulatory element controlling expression of the class I lysyl-tRNA synthetase of *Bacillus cereus* strain 14579 is functional and can be partially induced by reduced charging of asparaginyl-$tRNA^{Asn}$. BMC Microbiol. *10*, 196.

Friedman, R.A., and Honig, B. (1995). A free energy analysis of nucleic acid base stacking in aqueous solution. Biophys. J. *69*, 1528–1535.

Garcia, G.., and Goodenough-Lashua, D.M. (1998). Mechanisms of modifying enzymes. In Modification and Editing of RNA: The Alteration of RNA Structure and Function, (Washington, DC: ASM Press),.

Gaston, K.W., Rubio, M.A.T., Spears, J.L., Pastar, I., Papavasiliou, F.N., and Alfonzo, J.D. (2007). C to U editing at position 32 of the anticodon loop precedes tRNA 5' leader removal in trypanosomatids. Nucleic Acids Res. *35*, 6740–6749.

Gefter, M.L. (1969). The in vitro synthesis of 2'-omethylguanosine and 2-methylthio N^6 (gamma, gamma, dimethylallyl) adenosine in transfer RNA of *Escherichia coli*. Biochem. Biophys. Res. Commun. *36*, 435–441.

Gelfand, M.S., Mironov, A.A., Jomantas, J., Kozlov, Y.I., and Perumov, D.A. (1999). A conserved RNA structure element involved in the regulation of bacterial riboflavin synthesis genes. Trends Genet. *15*, 439–442.

Grundy, F.J., and Henkin, T.M. (1993). tRNA as a positive regulator of transcription antitermination in *B. subtilis*. Cell *74*, 475–482.

Grundy, F.J., and Henkin, T.M. (1994). Conservation of a transcription antitermination mechanism in aminoacyl-tRNA synthetase and amino acid biosynthesis genes in gram-positive bacteria. J. Mol. Biol. *235*, 798–804.

Grundy, F.J., and Henkin, T.M. (1998). The S box regulon: a new global transcription termination control system for methionine and cysteine biosynthesis genes in gram-positive bacteria. Mol. Microbiol. *30*, 737–749.

Grundy, F.J., and Henkin, T.M. (2004). Kinetic analysis of tRNA-directed transcription antitermination of the *Bacillus subtilis glyQS* gene in vitro. J. Bacteriol. *186*, 5392–5399.

Grundy, F.J., Rollins, S.M., and Henkin, T.M. (1994). Interaction between the acceptor end of tRNA and the T box stimulates antitermination in the *Bacillus subtilis tyrS* gene: a new role for the discriminator base. J. Bacteriol. *176*, 4518–4526.

Grundy, F.J., Hodil, S.E., Rollins, S.M., and Henkin, T.M. (1997). Specificity of tRNA-mRNA interactions in *Bacillus subtilis tyrS* antitermination. J. Bacteriol. *179*, 2587–2594.

Grundy, F.J., Collins, J.A., Rollins, S.M., and Henkin, T.M. (2000). tRNA determinants for transcription antitermination of the *Bacillus subtilis tyrS* gene. RNA *6*, 1131–1141.

Grundy, F.J., Moir, T.R., Haldeman, M.T., and Henkin, T.M. (2002). Sequence requirements for terminators and antiterminators in the T box transcription antitermination system: disparity between conservation and functional requirements. Nucleic Acids Res. *30*, 1646–1655.

Grundy, F.J., Lehman, S.C., and Henkin, T.M. (2003). The L box regulon: lysine sensing by leader RNAs of bacterial lysine biosynthesis genes. Proc. Natl. Acad. Sci. U.S.A. *100*, 12057–12062.

Grundy, F.J., Yousef, M.R., and Henkin, T.M. (2005). Monitoring uncharged tRNA during transcription of the *Bacillus subtilis glyQS* gene. J. Mol. Biol. *346*, 73–81.

Guillen, N., Weinrauch, Y., Dubnau, D.A. (1989). Cloning and characterization of the regulatory *Bacillus subtilis* competence genes *comA* and *comB*. J. Bacteriol. *171*, 5354-5361.

Gustafsson, C., and Persson, B.C. (1998). Identification of the rrmA gene encoding the 23S rRNA m^1G_{745} methyltransferase in Escherichia coli and characterization of an m^1G_{745}-deficient mutant. J. Bacteriol. *180*, 359–365.

Hagervall, T.G., Ericson, J.U., Esberg, K.B., Li, J.N., and Björk, G.R. (1990). Role of tRNA modification in translational fidelity. Biochim. Biophys. Acta *1050*, 263–266.

Hahne, H., Mäder, U., Otto, A., Bonn, F., Steil, L., Bremer, E., Hecker, M., and Becher, D. (2010). A comprehensive proteomics and transcriptomics analysis of *Bacillus subtilis* salt stress adaptation. J. Bacteriol. *192*, 870–882.

Hall, K.B., and McLaughlin, L.W. (1991). Properties of a U1/mRNA 5' splice site duplex containing pseudouridine as measured by thermodynamic and NMR methods. Biochemistry *30*, 1795–1801.

Harrington, K.M., Nazarenko, I.A., Dix, D.B., Thompson, R.C., Uhlenbeck, O.C. (1993). In vitro analysis of translational rate and accuracy with an unmodified tRNA. Biochemistry *32*, 7617-7622.

Henkin, T.M., and Yanofsky, C. (2002). Regulation by transcription attenuation in bacteria: how RNA provides instructions for transcription termination/antitermination decisions. Bioessays *24*, 700–707.

Henkin, T.M., Glass, B.L., and Grundy, F.J. (1992). Analysis of the *Bacillus subtilis tyrS* gene: conservation of a regulatory sequence in multiple tRNA synthetase genes. J. Bacteriol. *174*, 1299–1306.

Hernández, H.L., Pierrel, F., Elleingand, E., García-Serres, R., Huynh, B.H., Johnson, M.K., Fontecave, M., and Atta, M. (2007). MiaB, a bifunctional radical-S-adenosylmethionine enzyme involved in the thiolation and methylation of tRNA, contains two essential [4Fe-4S] clusters. Biochemistry *46*, 5140–5147.

Hoburg, A., Aschhoff, H.J., Kersten, H., Manderschied, U., and Gassen, H.G. (1979). Function of modified nucleosides 7-methylguanosine, ribothymidine, and 2-thiomethyl-N^6-(isopentenyl) adenosine in procaryotic transfer ribonucleic acid. J. Bacteriol. *140*, 408–414.

Horie, N., Hara-Yokoyama, M., Yokoyama, S., Watanabe, K., Kuchino, Y., Nishimura, S., and Miyazawa, T. (1985). Two $tRNA^{Ile,1}$ species from an extreme thermophile, Thermus thermophilus HB8: effect of 2-thiolation of ribothymidine on the thermostability of tRNA. Biochemistry *24*, 5711–5715.

Hur, S., and Stroud, R.M. (2007). How U38, 39, and 40 of many tRNAs become the targets for pseudouridylation by TruA. Mol. Cell *26*, 189–203.

Ibba, M., and Soll, D. (2000). Aminoacyl-tRNA synthesis. Annu. Rev. Biochem. *69*, 617–650.

Ibba, M., Kast, P., and Hennecke, H. (1994). Substrate specificity is determined by amino acid binding pocket size in *Escherichia coli* phenylalanyl-tRNA synthetase. Biochemistry *33*, 7107–7112.

Jäger, G., Leipuviene, R., Pollard, M.G., Qian, Q., and Björk, G.R. (2004). The conserved Cys-X1-X2-Cys motif present in the TtcA protein is required for the thiolation of cytidine in position 32 of tRNA from *Salmonella enterica* serovar Typhimurium. J. Bacteriol. *186*, 750–757.

Johansen, S.K., Maus, C.E., Plikaytis, B.B., and Douthwaite, S. (2006). Capreomycin binds across the ribosomal subunit interface using tlyA-encoded 2'-O-methylations in 16S and 23S rRNAs. Mol. Cell *23*, 173–182.

Jovine, L., Djordjevic, S., and Rhodes, D. (2000). The crystal structure of yeast phenylalanine tRNA at 2.0 A resolution: cleavage by Mg(2+) in 15-year old crystals. J. Mol. Biol. *301*, 401–414.

Jühling, F., Mörl, M., Hartmann, R.K., Sprinzl, M., Stadler, P.F., and Pütz, J. (2009). tRNAdb 2009: compilation of tRNA sequences and tRNA genes. Nucleic Acids Res. *37*, D159–162.

Kawai, G., Yamamoto, Y., Kamimura, T., Masegi, T., Sekine, M., Hata, T., Iimori, T., Watanabe, T., Miyazawa, T., and Yokoyama, S. (1992). Conformational rigidity of specific pyrimidine residues in tRNA arises from posttranscriptional modifications that enhance steric interaction between the base and the 2'-hydroxyl group. Biochemistry *31*, 1040–1046.

Kellogg, G.W., and Schweitzer, B.I. (1993). Two- and three-dimensional ^{31}P-driven NMR procedures for complete assignment of backbone resonances in oligodeoxyribonucleotides. J. Biomol. NMR *3*, 577–595.

Kersten, H. (1988). The nutrient factor queuine: biosynthesis, occurrence in transfer RNA and function. Biofactors *1*, 27–29.

Kersten, H., Chandra, P., Tanck, W., Wiedemhöver, W., and Kersten, W. (1968). Effect of pactamycin on methylation of RNA and protein synthesis. Hoppe-Seylers Z. Physiol. Chem. *349*, 659–663.

Kieft, J.S., and Tinoco, I., Jr (1997). Solution structure of a metal-binding site in the major groove of RNA complexed with cobalt (III) hexammine. Structure *5*, 713–721.

Kierzek, E., and Kierzek, R. (2001). Influence of N^6-isopentenyladenosine (i(6)A) on thermal stability of RNA duplexes. Biophys. Chem. *91*, 135–140.

Kierzek, E., and Kierzek, R. (2003). The thermodynamic stability of RNA duplexes and hairpins containing N^6-alkyladenosines and 2-methylthio-N^6-alkyladenosines. Nucleic Acids Res. *31*, 4472–4480.

Kim, S.H., Suddath, F.L., Quigley, G.J., McPherson, A., Sussman, J.L., Wang, A.H., Seeman, N.C., and Rich, A. (1974). Three-dimensional tertiary structure of yeast phenylalanine transfer RNA. Science *185*, 435–440.

Kobitski, A.Y., Hengesbach, M., Helm, M., and Nienhaus, G.U. (2008). Sculpting an RNA conformational energy landscape by a methyl group modification--a single-molecule FRET study. Angew. Chem. Int. Ed. Engl. *47*, 4326–4330.

Koehler, T.M., Dai, Z., and Kaufman-Yarbray, M. (1994). Regulation of the *Bacillus anthracis* protective antigen gene: CO_2 and a trans-acting element activate transcription from one of two promoters. J. Bacteriol. *176*, 586–595.

Kowalak, J.A., Dalluge, J.J., McCloskey, J.A., and Stetter, K.O. (1994). The role of posttranscriptional modification in stabilization of transfer RNA from hyperthermophiles. Biochemistry *33*, 7869–7876.

Krishna, P.S., Rani, B.R., Mohan, M.K., Suzuki, I., Shivaji, S., and Prakash, J.S.S. (2013). A novel transcriptional regulator, Sll1130, negatively regulates heat-responsive genes in Synechocystis sp. PCC6803. Biochem. J. *449*, 751–760.

Kumagai, I., Watanabe, K., and Oshima, T. (1980). Thermally induced biosynthesis of 2'-O-methylguanosine in tRNA from an extreme thermophile, *Thermus thermophilus* HB27. Proc. Natl. Acad. Sci. U.S.A. *77*, 1922–1926.

Laing, L.G., Gluick, T.C., and Draper, D.E. (1994). Stabilization of RNA structure by Mg ions. Specific and non-specific effects. J. Mol. Biol. *237*, 577–587.

Lecointe, F., Simos, G., Sauer, A., Hurt, E.C., Motorin, Y., and Grosjean, H. (1998). Characterization of yeast protein Deg1 as pseudouridine synthase (Pus3) catalyzing the formation of psi 38 and psi 39 in tRNA anticodon loop. J. Biol. Chem. *273*, 1316–1323.

Lecointe, F., Namy, O., Hatin, I., Simos, G., Rousset, J.-P., and Grosjean, H. (2002). Lack of pseudouridine 38/39 in the anticodon arm of yeast cytoplasmic tRNA decreases in vivo recoding efficiency. J. Biol. Chem. *277*, 30445–30453.

Lee, C.H., and Tinoco, I., Jr (1977). Studies of the conformation of modified dinucleoside phosphates containing 1, N^6-ethenoadenosine and 2'-O-methylcytidine by 360-MHz 1H nuclear magnetic resonance spectroscopy. Investigation of the solution conformations of dinucleoside phosphates. Biochemistry *16*, 5403–5414.

Legault, P., and Pardi, A. (1994). ^{31}P chemical shift as a probe of structural motifs in RNA. J Magn Reson B *103*, 82–86.

Legault, P., Jucker, F.M., and Pardi, A. (1995). Improved measurement of ^{13}C, ^{31}P J coupling constants in isotopically labeled RNA. FEBS Lett. *362*, 156–160.

Leppla, S.H. (1988). Production and purification of anthrax toxin. Meth. Enzymol. *165*, 103–116.

Leung, H.C., Chen, Y., and Winkler, M.E. (1997). Regulation of substrate recognition by the MiaA tRNA prenyltransferase modification enzyme of *Escherichia coli* K-12. J. Biol. Chem. *272*, 13073–13083.

Li, J., Esberg, B., Curran, J.F., and Björk, G.R. (1997). Three modified nucleosides present in the anticodon stem and loop influence the in vivo aa-tRNA selection in a tRNA-dependent manner. J. Mol. Biol. *271*, 209–221.

Luo, D., Condon, C., Grunberg-Manago, M., and Putzer, H. (1998). In vitro and in vivo secondary structure probing of the *thrS* leader in *Bacillus subtilis*. Nucleic Acids Res. *26*, 5379–5387.

Mack, M., Loon, A.P.G.M. van, and Hohmann, H.-P. (1998). Regulation of Riboflavin Biosynthesis in *Bacillus subtilis* is Affected by the Activity of the Flavokinase/Flavin Adenine Dinucleotide Synthetase Encoded byribC. J. Bacteriol. *180*, 950–955.

Mann, M.B., and Huang, P.C. (1973). Behavior of chloramphenicol-induced phenylalanine transfer ribonucleic acid during recovery from chloramphenicol treatment in *Escherichia coli*. Biochemistry *12*, 5289–5294.

Maus, C.E., Plikaytis, B.B., and Shinnick, T.M. (2005). Mutation of *tlyA* confers capreomycin resistance in *Mycobacterium tuberculosis*. Antimicrob. Agents Chemother. *49*, 571–577.

Maynard, N.D., Macklin, D.N., Kirkegaard, K., and Covert, M.W. (2012). Competing pathways control host resistance to virus via tRNA modification and programmed ribosomal frameshifting. Molecular Systems Biology *8*.

McMillian, R.A., and Arceneaux, J.L. (1975). Alteration of tyrosine isoaccepting transfer ribonucleic acid species in wild-type and asporogenous strains of *Bacillus subtilis*. J. Bacteriol. *122*, 526–531.

Means, J.A., Wolf, S., Agyeman, A., Burton, J.S., Simson, C.M., and Hines, J.V. (2007). T box riboswitch antiterminator affinity modulated by tRNA structural elements. Chem Biol Drug Des *69*, 139–145.

Meier, F., Suter, B., Grosjean, H., Keith, G., and Kubli, E. (1985). Queuosine modification of the wobble base in $tRNA^{His}$ influences “in vivo” decoding properties. EMBO J. *4*, 823–827.

Menichi, B., and Heyman, T. (1976). Study of tyrosine transfer ribonucleic acid modification in relation to sporulation in *Bacillus subtilis*. J. Bacteriol. *127*, 268–280.

Miranda-Ríos, J., Navarro, M., and Soberón, M. (2001). A conserved RNA structure (thi box) is involved in regulation of thiamin biosynthetic gene expression in bacteria. Proc. Natl. Acad. Sci. U.S.A. *98*, 9736–9741.

Motorin, Y., and Helm, M. (2010). tRNA stabilization by modified nucleotides. Biochemistry *49*, 4934–4944.

Motorin, Y., Bec, G., Tewari, R., and Grosjean, H. (1997). Transfer RNA recognition by the *Escherichia coli* delta-2-isopentenyl-pyrophosphate:tRNA delta-2-isopentenyl transferase: dependence on the anticodon arm structure. RNA *3*, 721–733.

Newby, M.I., and Greenbaum, N.L. (2001). A conserved pseudouridine modification in eukaryotic U2 snRNA induces a change in branch-site architecture. RNA *7*, 833–845.

Nissen, P., Thirup, S., Kjeldgaard, M., Nyborg, J. (1999). The crystal structure of Cys-tRNA^{Cys}-EF-Tu-GDPNP reveals general and specific features in the ternary complex and in tRNA. Structure *7*, 143-156

Niu, Y., Zhao, X., Wu, YS., Li, M.N., Wang, X.J., Yang, Y.G. (2013). N^6-methyl-adenosine (m^{6}A) in RNA: An old modification with a novel epigenetic function. Genomics Proteomics Bioinformatics *11*, 8-17.

O'Donoghue, P., and Luthey-Schulten, Z. (2003). On the evolution of structure in aminoacyl-tRNA synthetases. Microbiol. Mol. Biol. Rev. *67*, 550–573.

Palmer, D.T., Blum, P.H., and Artz, S.W. (1983). Effects of the *hisT* mutation of *Salmonella typhimurium* on translation elongation rate. J. Bacteriol. *153*, 357–363.

Pan, T. (2013). N^6-methyl-adenosine modification in messenger and long non-coding RNA. Trends Biochem. Sci.

Pardi, A. (1995). Multidimensional heteronuclear NMR experiments for structure determination of isotopically labeled RNA. Meth. Enzymol. *261*, 350–380.

Pierrel, F., Björk, G.R., Fontecave, M., and Atta, M. (2002). Enzymatic modification of tRNAs: MiaB is an iron-sulfur protein. J. Biol. Chem. *277*, 13367–13370.

Pierrel, F., Douki, T., Fontecave, M., and Atta, M. (2004). MiaB protein is a bifunctional radical-S-adenosylmethionine enzyme involved in thiolation and methylation of tRNA. J. Biol. Chem. *279*, 47555–47563.

Putzer, H., Brakhage, A.A., and Grunberg-Manago, M. (1990). Independent genes for two threonyl-tRNA synthetases in *Bacillus subtilis*. J. Bacteriol. *172*, 4593–4602.

Putzer, H., Gendron, N., and Grunberg-Manago, M. (1992). Co-ordinate expression of the two threonyl-tRNA synthetase genes in *Bacillus subtilis*: control by transcriptional antitermination involving a conserved regulatory sequence. EMBO J. *11*, 3117–3127.

Rakovich, T., Boland, C., Bernstein, I., Chikwana, V.M., Iwata-Reuyl, D., and Kelly, V.P. (2011). Queuosine deficiency in eukaryotes compromises tyrosine production through increased tetrahydrobiopterin oxidation. J. Biol. Chem. *286*, 19354–19363.

Reddy, R. (1989). [35] Compilation of small nuclear RNA sequences. In Methods in Enzymology, J.N.A. James E. Dahlberg, ed. (Academic Press), pp. 521–532.

Ristroph, J.D., and Ivins, B.E. (1983). Elaboration of *Bacillus anthracis* antigens in a new, defined culture medium. Infect. Immun. *39*, 483–486.

Robertus, J.D., Ladner, J.E., Finch, J.T., Rhodes, D., Brown, R.S., Clark, B.F., and Klug, A. (1974). Structure of yeast phenylalanine tRNA at 3 A resolution. Nature *250*, 546–551.

Romier, C., Reuter, K., Suck, D., and Ficner, R. (1996). Crystal structure of tRNA-guanine transglycosylase: RNA modification by base exchange. EMBO J. *15*, 2850–2857.

Rosenberg, A.H., and Gefter, M.L. (1969). An iron-dependent modification of several transfer RNA species in *Escherichia coli*. J. Mol. Biol. *46*, 581–584.

Rosner, A. (1975). Control of lysine biosynthesis in *Bacillus subtilis*: inhibition of diaminopimelate decarboxylase by lysine. J. Bacteriol. *121*, 20–28.

Satoh, A., Takai, K., Ouchi, R., Yokoyama, S., and Takaku, H. (2000). Effects of anticodon 2'-O-methylations on tRNA codon recognition in an *Escherichia coli* cell-free translation. RNA *6*, 680–686.

Schwieters, C.D., Kuszewski, J.J., Tjandra, N., and Clore, G.M. (2003). The Xplor-NIH NMR molecular structure determination package. J. Magn. Reson. *160*, 65–73.

Shi, H., and Moore, P.B. (2000). The crystal structure of yeast phenylalanine tRNA at 1.93 A resolution: a classic structure revisited. RNA *6*, 1091–1105.

Simorre, J.P., Zimmermann, G.R., Mueller, L., and Pardi, A. (1996). Correlation of the guanosine exchangeable and nonexchangeable base protons in ^{13}C-/^{15}N-labeled RNA with an HNC-TOCSY-CH experiment. J. Biomol. NMR *7*, 153–156.

Sprinzl, M., Horn, C., Brown, M., Ioudovitch, A., and Steinberg, S. (1998). Compilation of tRNA sequences and sequences of tRNA genes. Nucleic Acids Res. *26*, 148–153.

Stuart, J.W., Gdaniec, Z., Guenther, R., Marszalek, M., Sochacka, E., Malkiewicz, A., and Agris, P.F. (2000). Functional anticodon architecture of human tRNA^{Lys,3} includes disruption of intraloop hydrogen bonding by the naturally occurring amino acid modification, t^{6}A. Biochemistry *39*, 13396–13404.

Stuart, J.W., Koshlap, K.M., Guenther, R., and Agris, P.F. (2003). Naturally-occurring modification restricts the anticodon domain conformational space of tRNA(Phe). J. Mol. Biol. *334*, 901–918.

Sundaram, M., Durant, P.C., and Davis, D.R. (2000). Hypermodified nucleosides in the anticodon of tRNALys stabilize a canonical U-turn structure. Biochemistry *39*, 12575–12584.

Testa, S.M., Disney, M.D., Turner, D.H., Kirzek, R. (1999). Thermodynamics of RNA-RNA duplexes with 2- or 4-thiouridines: implications for antisense design and targeting a group I intron. Biochemistry *38*, 16652-16662

Tewari, R. (1988). Conformational Preferences of Modified Nucleic-Acid Bases N6-(delta-2-Isopentenyl) Adenine and 2-Methylthio-N^6-(delta-2-Isopentenyl) Adenine by the Quantum Chemical Pcilo Calculations. Int. J. Quantum Chem. *34*, 133–142.

Urbonavicius, J., Qian, Q., Durand, J.M., Hagervall, T.G., and Björk, G.R. (2001). Improvement of reading frame maintenance is a common function for several tRNA modifications. EMBO J. *20*, 4863–4873.

Vander Meulen, K.A., Davis, J.H., Foster, T.R., Record, M.T., Jr, and Butcher, S.E. (2008). Thermodynamics and folding pathway of tetraloop receptor-mediated RNA helical packing. J. Mol. Biol. *384*, 702–717.

Vermeulen, A., McCallum, S.A., and Pardi, A. (2005). Comparison of the global structure and dynamics of native and unmodified $tRNA^{Val}$. Biochemistry *44*, 6024–6033.

Vitreschak, A.G., Mironov, A.A., Lyubetsky, V.A., and Gelfand, M.S. (2008). Comparative genomic analysis of T-box regulatory systems in bacteria. RNA *14*, 717–735.

Vold, B.S. (1978). Post-transcriptional modifications of the anticodon loop region: alterations in isoaccepting species of tRNA's during development in *Bacillus subtilis*. J. Bacteriol. *135*, 124–132.

Wakeman, C.A., and Winkler, W.C. (2009). Analysis of the RNA backbone: structural analysis of riboswitches by in-line probing and selective 2'-hydroxyl acylation and primer extension. Methods Mol. Biol. *540*, 173–191.

Watanabe, H., Ohgi, K., and Irie, M. (1979). Modification of an arginine residue of a base-nonspecific ribonuclease from *Aspergillus saitoi*. J. Biochem. *85*, 1315–1320.

Waters, L.C., Shugart, L., Yang, W.K., and Best, A.N. (1973). Some physical and biological properties of 4-thiouridine- and dihydrouridine-deficient tRNA from chloramphenicol-treated *Escherichia coli*. Arch. Biochem. Biophys. *156*, 780–793.

Weixlbaumer, A., Murphy, F.V., 4th, Dziergowska, A., Malkiewicz, A., Vendeix, F.A.P., Agris, P.F., and Ramakrishnan, V. (2007). Mechanism for expanding the decoding capacity of transfer RNAs by modification of uridines. Nat. Struct. Mol. Biol. *14*, 498–502.

Wels, M., Groot Kormelink, T., Kleerebezem, M., Siezen, R.J., and Francke, C. (2008). An *in silico* analysis of T-box regulated genes and T-box evolution in prokaryotes, with emphasis on prediction of substrate specificity of transporters. BMC Genomics *9*, 330.

Winkler, M.E. (1998). Genetics and regulation of tRNA and rRNA modification. In Modification and Editing of RNA: The Alteration of RNA Structure and Function, (Washington, DC: ASM Press),.

Winkler, W.C., Cohen-Chalamish, S., and Breaker, R.R. (2002). An mRNA structure that controls gene expression by binding FMN. Proc. Natl. Acad. Sci. U.S.A. *99*, 15908–15913.

Xie, W., Liu, X., and Huang, R.H. (2003). Chemical trapping and crystal structure of a catalytic tRNA guanine transglycosylase covalent intermediate. Nat. Struct. Biol. *10*, 781–788.

Yang, H., and Lam, S.L. (2009). Effect of 1-methyladenine on thermodynamic stabilities of double-helical DNA structures. FEBS Lett. *583*, 1548–1553.

Yousef, M.R., Grundy, F.J., and Henkin, T.M. (2003). tRNA requirements for *glyQS* antitermination: a new twist on tRNA. RNA *9*, 1148–1156.

Yousef, M.R., Grundy, F.J., and Henkin, T.M. (2005). Structural transitions induced by the interaction between tRNA(Gly) and the *Bacillus subtilis glyQS* T box leader RNA. J. Mol. Biol. *349*, 273–287.